T.R.
VAN YUZUNCU YIL UNIVERSITY
INSTITUTE OF NATURAL AND APPLIED SCIENCE
ELECTRICAL ELECTRONICS ENGINEERING DEPARTMENT

DESIGN AND APPLICATION OF PLANAR TYPE FLYBACK TRANSFORMER

M. Sc. THESIS

PREPARED BY: Bestoon Ahmed MUSTAFA
SUPERVISOR: Asst. Prof. Dr. Ali MAMIZADEH

VAN - 2021

T.R.
VAN YUZUNCU YIL UNIVERSITY
INSTITUTE OF NATURAL AND APPLIED SCIENCE
ELECTRICAL ELECTRONICS ENGINEERING DEPARTMENT

DESIGN AND APPLICATION OF PLANAR TYPE FLYBACK TRANSFORMER

M. Sc. THESIS

PREPARED BY: Bestoon Ahmed MUSTAFA

VAN – 2021

ACCEPTANCE and APPROVAL PAGE

This thesis entitled "Design and Application of Planar Type Flyback Transformer" presented by Bestoon Ahmed MUSTAFA under supervision of Asst. Prof. Dr. Ali MAMIZADEH in the department of Electrical Electronics Engineering has been accepted as a M. Sc. thesis according to Legislations of Graduate Higher Education on 29/01/2021 with unanimity of votes members of jury.

President: Prof. Dr. Naci GENÇ Signature:

Member: Asst. Prof. Dr. Abdullah Oğuz KIZILÇAY Signature:

Member: Asst. Prof. Dr. Ali MAMIZADEH Signature:

This thesis has been approved by the committee of The Institute of Natural and Applied Science on …. /.... /…...... with decision number..................

Signature
Prof. Dr. Suat ŞENSOY
Director of Institute

THESIS STATEMENT

All information presented in the thesis obtained in the frame of ethical behavior and academic rules. In addition, all kinds of information that does not belong to me have been cited appropriately in the thesis prepared by the thesis writing rules.

Signature

Bestoon Ahmed MUSTAFA

ABSTRACT

DESIGN AND APPLICATION OF PLANAR TYPE FLYBACK TRANSFORMER

MUSTAFA, Bestoon Ahmed
M.Sc. Thesis, Department of Electrical Electronics Engineering
Supervisor: Asst. Prof. Dr. Ali MAMIZADEH

February 2021, 99 pages

Flyback converters are becoming more and more popular due to their simplicity and the few number of components that they require. One of the main challenges that face the design of Flyback converters is the design of the planar transformer which is vital to the operation of the converter. The transformer stores energy when the electronic switch is ON and transfers this energy through the secondary side when the switch is OFF. The most important part of the transformer is its core, the cores in the planar transformer have different shapes and are available in different sizes. A planar core that is optimized, when compared with the conventional core with similar properties, exhibit better properties. In planar winding, we have different configurations available and with the optimum configuration, the losses of the transformer can be efficiently reduced. For the magnetic components, operation at high frequencies leads to increased conductor losses due to skin and proximity effects. The use of planar transformers on printed circuit boards (PCB) can mitigate this problem. The thinner and wider conductors of PCBs assist in reducing high frequency losses. With larger surface areas, planar transformers also offer better thermal performance than conventional wire-wound magnetic core. This thesis presents the design of a Flyback planar transformer. The essential equations with calculations for Flyback PT are presented, transformer CU and core losses, efficiency, air gap length, number of turns on both sides of core is illustrated. Design of RCD clamping is presented. Topology circuit simulation has been conducted and discussed within the 50 watt Flyback converter employing the improved PT structure has been designed, more than 98% transformer efficiency is achieved.

Keywords: Flyback converter, Planar transformer (PT), Transformer losses.

ÖZET

DÜZLEMSEL TİP FLYBACK TRANSFORMATÖR TASARIMI VE UYGULAMASI

MUSTAFA, Bestoon Ahmed
Yüksek Lisans Tezi, Elektrik Elektronik Mühendisliği Bölümü
Tez Danışmanı: Dr. Öğr. Üyesi Ali MAMIZADEH
Şubat 2021, 99 sayfa

Flyback dönüştürücüler, kullanım kolaylığı ve ihtiyaç duydukları az sayıda devre elemanlarından dolayı giderek daha popüler hale gelmektedirler. Flyback dönüştürücülerin tasarımında karşılaşılan temel zorluklardan biri, dönüştürücünün çalışması için hayati önem taşıyan düzlemsel transformatörün tasarımıdır. Transformatör, anahtarlama elemanı iletim halinde olduğunda birincil sargıda enerji depolar, kapalı durumda olduğunda ise depolanan enerji ikincil sargıya aktarılır. Düzlemsel transformatörün en önemli kısmı, faklı şekilleri ve ebatları olan nüvesidir. Optimize edilmiş düzlemsel bir nüve, benzer özelliklere sahip geleneksel bir nüveye kıyasla daha iyi özellikler sergiler. Düzlemsel trafonun sargılarında farklı konfigürasyonlar mevcuttur ve optimum konfigürasyon ile transformatör kayıpları verimli bir şekilde azaltılabilir. Manyetik bileşenler için, yüksek frekanslarda çalışma, yüzeysel ve yakınlık etkilerinden kaynaklanan iletken kayıplarını artırır. Düzlemsel transformatörlerin baskılı devre kartlarında (PCB) kullanılması bu sorunu hafifletebilir. Daha geniş yüzey alanlarına sahip düzlemsel transformatörler ayrıca geleneksel sargılı manyetik nüveden daha iyi termal performans sağlar. Bu tez çalışmasında, Flyback düzlemsel transformatör (DT) tasarımını için gerekli olan temel denklemler ve Snubber RCD devresinin detaylı analiz sunulduktan sonra 50 W güce sahip Flyback DT tasarımı yapılmıştır. Yapılan tasarımın, MATLAB/Simulink ortamında benzetim çalışmaları gerçekleştirilmiştir. Yapılan benzetim çalışmalarının sonucunda önerilen topolojinin verimini %98 'ün üzerinde olduğu görülmüştür.

Anahtar Kelimeler: Düzlemsel trafo (DT), Flyback dönüştürücü, Trafo kayıpları.

ACKNOWLEDGMENTS

I would like to express my sincere gratitude to my supervisor Asst. Prof. Dr. Ali MAMIZADEH for his guidance, support and providing me an opportunity to work on this thesis. It is truly an honor to work with him. I am very fortunate to work with him due to his patience, consistent support and motivation over the past two years.

Thanks go to Prof. Dr. Naci GENC for helping me develop my background in power electronics.

My earnest gratitude to my parents, brothers, sisters and beloved family members for their continuous support and prayers during all the stages of my life. I am always thankful for their blessings which makes me to climb new heights. My deepest and heartfelt appreciation goes to my families for their unconditional love. Finally, I would like to thank Mr. Hasan ÜZMUŞ in Electrical Electronics Engineering department Van Yuzuncu Yıl university and all friends for their contributions and help.

2021

Bestoon Ahmed MUSTAFA

TABLE OF CONTENTS

Pages

pages

Pages

LIST OF TABLES

Table **Pages**

LIST OF FIGURES

Figure **Pages**

Figure **Pages**

Figure **Pages**

SYMBOLS AND ABBREVIATIONS

Along with descriptions. Some symbols used in this study are:

Symbols	Explanation
Ae	Effective Cross-sectional area
P_{in}	Input Power
B_{peak}	Peak Flux Density
P_o	Output Power
F_s	Switching Frequency
Vin_{min}	Minimum Input Voltage
I_{prms}	Primary Rms Current
V_o	Output Voltage
I_{srms}	Secondary Output Current
η	Efficiency of Transformer
D_{max}	Maximum Duty Cycle Signal
L_{pri}	Primary Self-Inductance
L_{sec}	Secondary Self-Inductance
G	Airgap Length
N_p	Primary Winding Turns
N_s	Secondary Winding Turns
Ds	Duty Cycle Secondary
μ_o	Permeability of Free Space.
n	Turn Ratio
I_{av}	Primary Average Current
K_{RP}	Ripple to Peak Current Ratio
I_{ppeak}	Primary Peak Current
I_R	Primary Ripple Current
I_{speak}	Secondary Peak Current

I_{sav}	Secondary Average Current
P_{tr}	Total losses in the transformer
ΔT	Temperature rise
R_{th}	Thermal resistance of the transformer
P_{core}(watt)	Maximum core loss in watt
T	Temperature
C_m, x, y, ct_0, ct_1 and ct_2	Curve fitting power loss data Parameters.
Ve	Effective Volume of the core,
P_{core}	Volumetric power losses in watts / cubic meter
MLT	Mean length copper traces per turn
P_{cu}	Copper loss in the windings
I	Rms current in the winding
ρ	Resistivity of the winding conductor
L	length of the winding
A	wire bare cross-sectional area
Rdc	DC resistance
$F(t)$ and $F(0)$	Magneto motive force (MMF)
m	Number of layers in winding
t	Thickness of conductor
δ	Skin depth at the switching frequency.
dx	Distance across the conductor
l_u	length of one turn
b_u	Width of each turn
N	Number of turns on the winding
M	Number of section interfaces between prim and sec.
$\sum x$	Sum of all section layer heights (windings)
$\sum x_\Delta$	Sum of all intersection layer heights (insulator)
PT	Planar transformer
Rp	Resistance of the primary winding.
Rs	Resistance of the secondary winding.

Cpo	Self-capacitance of the primary winding.
Cso	Self-capacitance of the secondary winding.
Cpso	Mutual capacitance between the two windings
ε_o	Permittivity in free space
ε_r	Relative permittivity of the insulating material
l	Length of the center leg cross-section
b	Conductor width
h_Δ	Distance between the conductive plates
u	Number of overlapping turns.
t_{ON}	Time for which the fly-back switch is ON
T	Time period of the switching cycle
t_{ON}/T	Duty cycle (D) of the switch
L_{lk}	Leakage inductance of the primary winding
V_{sn}	Snubber cap. voltage at Vin_{min} and full load.
V_{RO}	Reflected output voltage
R_{sn}	Snubber Resistor
P_{sn}	Power dissipation in the snubber circuit.
C_{sn}	Snubber Capacitor
ΔV_{sn}	Maximum ripple voltage of the snubber capacitor.
$R_{dc\ pri}$	Primary dc resistance
$R_{dc\ sec}$	Secondary dc resistance
$P_{pri\ cu}$	Primary cupper loss
$P_{sec\ cu}$	Secondary cupper loss
$P_{Tt\ cu}$	Total Cupper loss
$P_{Tt\ loss}$	Total loss in Transformer
N_t	number of turns per layer
sp	spacing between the turns
b_{wi}	available winding width
w_{track}	track width
T_s	Maximum allowable temperature

$\mathbf{T_a}$	Maximum ambient temperature
$\mathbf{V_c}$	Volume of the core
$\mathbf{V_w}$	Volume of the winding
$\mathbf{Q_{max\ dissipation}}$	Maximum power dissipation per volume
$\mathbf{J_{rms}}$	Maximum current density for the winding
$\boldsymbol{\rho}_{\mathbf{cu}}$	Resistance of copper
$\mathbf{K_{cu}}$	The copper fill factor
$\mathbf{A_{pricu}}$	Primary minimum winding conductor size
$\mathbf{A_{seccu}}$	Secondary minimum winding conductor size
$\mathbf{A_{wpri}}$	Area of the Primary winding
$\mathbf{A_{wsec}}$	Area of the Secondary winding
$\mathbf{A_{wtotal}}$	Total needed winding area
$\mathbf{J_{prms}}$	Actual current density in the Primary Winding
$\mathbf{J_{srms}}$	Actual current density in the Secondary Winding
$\mathbf{Q_{pri\ dissipation}}$	Power loss density in the primary winding
$\mathbf{Q_{sec\ dissipation}}$	Power loss density in the secondary winding
$\mathbf{P_{max\ loss}}$	Maximum allowable power dissipation of the transformer

LIST OF APPENDIX

Appendix **Pages**

1. INTRODUCTION

Characterized by their low cost and simplicity flyback converters are becoming more popular in low power applications. Two main factors control the design and operation of these converters the first, is the control circuit that produces the pulses (modulation techniques) for the static electric switch and the second is planar transformer design. The inductor-transformer for these converters play a major role during the ON period of the switch and during the OFF period. Energy handling capacity is a decisive factor in the performance behavior of these converters, therefore the design of the inductor- transformer is an active part of the overall design of the converter (Al-Jubory and Al-Khafaf., 2008).

Nowadays, the switching frequencies have gone higher based on the application and with higher frequencies, we can achieve smaller size which will be very helpful for high power densities. For high frequency switching operations, conventional wire wound magnetic materials are not compatible, which is the reason we move to planar magnetic technology (Venkatanarayanan., 2019). Comparing to the conventional wire wound magnetics, planar magnetic cores provide better performance, smaller in size, easy to design as the windings are mostly repeatable.

The growing need for smaller size and cost efficient DC/DC Converters has led to design engineers designing power converters able to work at highly efficient switching frequencies, however, magnetic core is still one of the major obstacles in achieving higher power density and greater performance, due to the important part of magnetic cores in the entire power structure even with new advanced topologies (Quinn et al., 2001). Two distinct trends in power electronics systems have been observed in recent years for magnetic design. The first trend relates to the use of planar structures (Rascon et al., 2001). Printed circuit boards (PCBs), planar magnetic core can be mass-manufactured with highly repeatable circuitry. Thinner and larger conductors often help to minimize losses relates to skin and proximity effects at high frequencies, which can be accomplished by much closer board spacing and a lower profile, easier processing because of the simplified conductor assembly methods makes planar structures predominant in the power converter industry.

The second trend is to shift constantly into higher frequencies in order to minimize the magnetic part size.

Figure 1.1 and 1.2 illustrates the typical structure of a traditional transformer and a planar transformer respectively. The height of the planar magnetic component (z-axis) is lower and it has more area than the traditional magnetic component, the planar windings stack in Z axis on top each other, while the traditional windings are wound in a manner close to that of a low-frequency transformer.

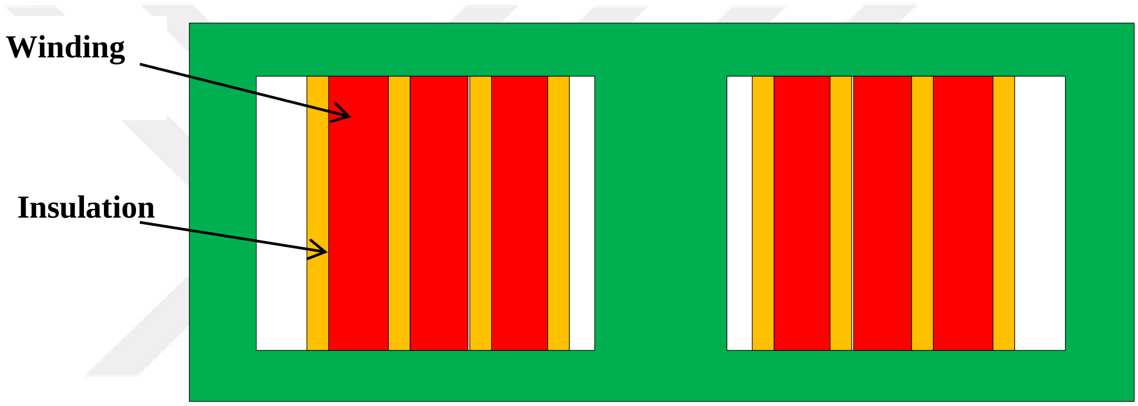

Figure 1.1. Typical conventional transformer.

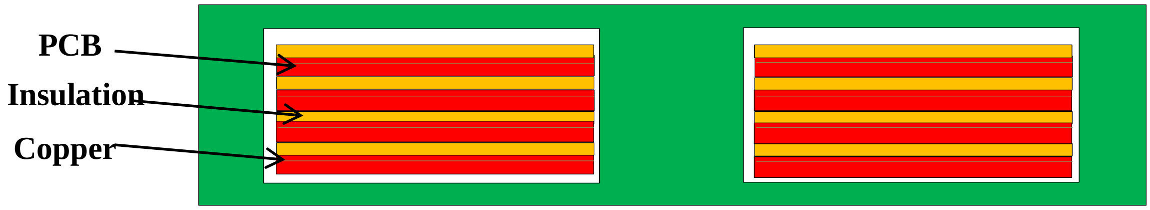

Figure 1.2. Typical planar transformer.

In this thesis, design concerns for planar transformers, PCB winding design, selection of the core, winding arrangements, the essential equations for flyback PT are presented, calculations of primary and secondary winding specifications is carried out. Including loss mechanism in copper and core losses, efficiency, air gap length, number of turns on both sides of core is illustrated. Design of RCD clamping is presented. Simulation of the circuit was performed and discussed within the 50 watt flyback converter using the improved PT was designed, more than 98% transformer efficiency is achieved.

2. LITERATURE REVIEW

İt's necessary to review the preceding documents and papers for better understanding the thesis background. This section of the thesis reviews numerous research's, documents, papers and investigations on flyback planar transformers.

Chen et al. (2003), studied the parallel winding in planar transformers, while this technique is assumed to be successful in improving the current handling ability of the windings, if the winding layers are not correctly organized and connected, the effect may be offset because of the disproportionate current sharing between parallel layers. The basic concerns resulting from parallel winding are discussed, modelled and based on a model of a one-dimensional field, the variables effecting winding losses with parallel connection are analyzed.

Arshak and Almukhtar (2000), presented step-by-step design procedure of planar transformer for Flyback (SMPS) DC-DC converter. The maximum dimensions of this transformer are 2cmx2cmx0.4cm. In order to achieve an efficiency of 99 percent with operating frequencies of 500 kHz, this planar transformer is particularly optimized for the development of thick film technolog.

Ropoteanu et al. (2017), the comparative study of winding losses in two forms of PCB stack configuration of planar transformers was studied. The research aimed to examine the effect of the winding arrangement on a planar step-up transformer dependent on the magneto motive force on the leakage inductance, the findings revealed the influence of losses in two FR4 structure embodiments on the complete converter, one with the secondary on a single inner layer and the second in multiple layers with the winding, for this method a planar core transformer was modelled for sub-MHz range study (0.4-1.0 MHz).

Zhang et al. (2013), the calculation technique for the transformer leakage inductance with magnetic shunt by means of magnetic energy stored on the transformer's primary and secondary side was studied by using the method of variation of the magetomotive force (MMF) and even shunt energy stored on the basis of the reluctance model, the comprehensive calculation method is defined.

Li et al. (2002), PCB planar transformer was presented, the model and the methods of calculation were verified by the simulation performance. The optimization modeling approaches are applied to reduce the bad effect of parasite components based on these data finally the drawback of this model is studied.

Ouyang et al. (2012), the most significant factors in the design of the planar transformer (PT) were analyzed, including core loss, winding loss, stray capacitance, and leakage inductance. In order to obtain optimum conditions, tradeoffs between these factors have to be evaluated. Combined with the application, the benefits and drawbacks of four standard winding arrangements have been compared, it suggests an improved interleaving layout, which builds the up layer parallel to the bottom layer, then in series with the other primary turns, in order to achieve a lower magneto motive force ratio of m, as well as reduced ac resistance, leakage inductance and even stray capacitance, about 96% efficiency is obtained and a 2.7 percent increase is achieved relative to the non-interleaving structure.

Gurusamy (2018), the design of such an optimized LLC planar transformer has been studied. Detailed discussions on design flow of integrated preparation magnetic cores. The main challenge of high frequency loss and the achievement of required leakage inductance. It addressed the cause behind the high frequency eddy current losses due to skin effect and proximity effect and offered a way to resolve the high frequency loss, the solutions for minimizing eddy current losses have been shown to minimize the leakage inductance that is good for converter system, in which only magnetizing transformer inductance plays a vital role and leakage inductance, a parasite parameter creates undesirable effects.

Magambo et al. (2018), presented the advantages and disadvantages of high frequency planar transformers, various models built for their design and various issues related to technology and planar specific geometry in the MEA context were discussed.

A. Razak et al. (2016), presented the new split-planar transformer for flyback topology. Simulation of the topology circuit was performed and discussed with the model parameters of 5 W power, 500 to 1.5 MHz operations, 15 V output-voltage of 80 percent efficiency and input from a single photo-voltaic module. The most appropriate micro power transformer pairs to be produced on a silicon wafer were found to be 6 pairs with a core gap of 100 μm at the operating frequency of 1 MHz.

Ahmad and Sonar (2020), A 120 watt flyback converter for DC-DC application was presented with a complete design. The analytical analysis of various related circuits is discussed. ETD39TH is an appropriate core for the design of the flyback transformer. The design is presented for RCD clamping. To justify the suitability of the suggested design, a protype is developed, results are introduced.

Miyan et al. (2013), the flyback transformer design for variable DC input (18V to 60V) to 12V DC output has been introduced and the wave shape was observed through the switch, transformer primary and secondary.

Dixon (2007), the magnetic fields and their influence on the distribution of high frequency currents in the windings is addressed within the planar system. Strategies are illustrated and presented with design examples, to optimize the flyback planar transformer design. The best suitable circuit topologies are discussed for high frequency applications.

Derkaoui et al. (2013), the square micro-transformer design and modeling for its integration in the flyback converter was presented. The geometric parameters of that micro transformer have been determined by the specifications of the switching power supply. A good geometrical parameter dimensioning effectively reduces the energy losses in the micro-transformer and allows the converter output voltage to achieve the desired value. Presented the equivalent electrical circuit of the converter containing the electrical circuit of the planar micro-transformer.

Choi (2003), presented instructions for the design of flyback off-line converters using FPS-(Fairchild Power Switch). The design with switched mode power (SMPS) is a time consuming task that requires multiple changes and iterations with a wide range of design variables. It explained the step-by-step design process, it allows engineers to quickly design SMPS. To make the design process more effective, FPS design assistants are also provided with all the equations mentioned in this article.

Ravelas (2017), presented a technology of planar PCB transformer. These research activities are aimed at improving the modelling, design and utilization for high-frequency power converters with planar PCB transformers. A new non-linear model of planar PCB magnetics was developed to model the winding loss, core loss and saturation characteristics. The developed model can be implemented in a circuit simulation package which can be used to predict the performance of the PCB transformer in a power converter system. The model was also used to derive the high-frequency electrical parameters of a PCB transformer, the model-derived parameters were proven to be comparable to LCR measurement and results obtained. Through the evaluated design guidelines, prototypes of multiple core transformers were designed and characterised in a power converter system. Result of the comparison of the different implementations showed that the trade-off is between high-frequency losses and thermal dissipation.

Venkatanarayanan et al. (2019), detailed the design of planar transformer for power electronics applications. In order to design a power planar transformer, all design requirements were considered and an optimal design method was developed. It further discusses the situation where the increase in temperature is more than what the PCB can withstand and tries to find a solution for that. The next step for the planar transformer is to transfer to the co-fired ceramic (LTCC) substrate that is being tried in this work. The key subject of this work is the planar transformer-based LTCC design technique.

Al-Jubory and Al-Khafaf (2008), presented an algorithm to design the inductor-transformer of a flyback converter. The essential equations for inductor-transformer are presented, calculations of primary and secondary winding specifications is also carried out. The algorithm adopts a method of optimizing the design by considering an optimal copper/core loss ratio. Several common cores configuration are considered and results for each type is presented numerical values such as optimum cupper and core losses, air gap length, efficiency, number of turns on both sides for each type of core is illustrated. Change of switching frequency and its effect on optimal efficiency and air gap length is carried out using two configurations only. Results show that some of the proposed cores have high optimal efficiency, reasonable weight and satisfactory performance. The proposed algorithm can be utilized for continuous and discontinuous modes of operation for a flyback converter.

Maswood and Song (2003), a high-frequency flyback transformer was designed to be incorporated into the dc/dc pulse width-modulated switch-mode power supplies using two separate technological approaches: a traditional wound-coil magnet with copper wires and a planar magnet with layered copper tracks on laminated printed circuit boards. Comparisons between the two approaches in terms of profile: surface area, mounting height and performance: power loss, quality. A suggested sandwiched arrangement for the planar type for primary and secondary windings. In particular, the dominant factor in cost-effectiveness, efficiency, or compactness of the circuit that limits the selection of an evaluated unique type.

Ebert (2008), concerned the study of planar transformers and inductors as well as presented the development of a methodology for designing these magnetic elements, which are used in power supplies operating at high frequencies (from 50 kHz to 100 kHz). The study included the materials used in the manufacture of a magnetic core structure, the design and its optimization. It was made an analysis of the effects due to operation at high frequencies. Among these factors, there are the core and winding losses, the leakage inductance and inter-winding capacitance.

3. MATERIALS AND METHODS

In this thesis, the design methodology of flyback planar transformer and simulation study of flyback converter has been done employing PT was designed. Firstly theoretical background of flyback planar transformer structure, materials, losses and flyback converter, principle of operation, design RCD snubber are mentioned. Then the topology circuit in the matlab simulation and the 50-watt flyback converter was modeled using the improved PT structure over 98% transformer efficiency obtained.

3.1. Planar Magnetic Technology Review

3.1.1. Structures of planar magnetic cores

The push to higher power density and lower profiles in switched power supplies has revealed a range of shortcomings in the use of traditional magnetic structures. However, this led to issues of increased loss due to skin and proximity effects in the round conductors for traditional wire wound magnetic components, especially at frequencies above 100 kHz. The use of flat large conductors to minimize skin and proximity losses in windings relative to circular wire was shown by the earlier applications of planar magnetic cores (Wallace., 1982; Estrov., 1986), it demonstrated the regulation of other parameters, such as leakage inductance. Also of great significance was the repeatability of component characteristics.

Windings of planar magnetic cores are formed mainly by common interconnection systems, such as PCBs, flex and thick film. Many early designs have used technologies for thick films (Gradski and Lee., 1988; Quirke et al., 1992; Barnwell and Jackson., 1993) the use of PCB, flex or stamped copper turns was by far the most common approach to the realization of the windings. Many experiments on the characteristics, simulation and optimization of planar magnetic cores were performed in the early 90s (Huljak et al., 2000). In the mid 90's, the drawbacks of using non-standard low-profile cores were addressed when core manufacturers incorporated common flat cores such as a planar EE core into their devices, which led to a wider adoption of planar magnetic cores. Figure 3.1 shows typical planar magnetic core systems compared with traditional wire wound magnetic cores used in power electronics.

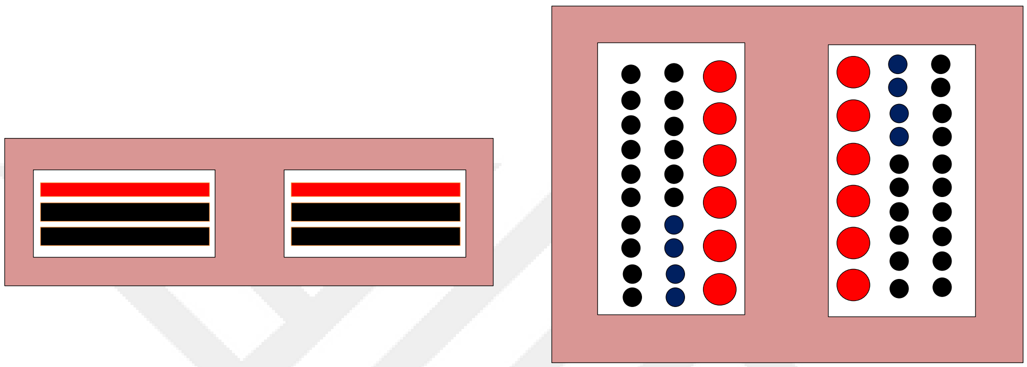

(a) (b)

Figure 3.1. Magnetics structures: (a) planar structure; (b) conventional structure.

The core of the planar structure has a clearly lower profile than the traditional. Furthermore, the windings on the traditional device are stacked such that they are successively farther from the middle of the body (center leg) windings are thus shaped horizontally. While stacked on the planar device in the vertical direction instead. For higher frequencies (Xiao., 2004). Due to its low electrical conductivity, MnZn ferrites are used.

3.1.2. Planar magnetic cores characteristics

Since multi-layer PCBs permit arbitrary layers to be interconnected, it’s much easier to implement interleaved primary and secondary windings than traditional magnetics. This gives a way to further reduce leakage and winding losses at high frequency (Dai et al., 1994), they have apparent benefits in terms of square wave switching at high frequency. The benefit of planar magnetic cores is that the greater surface area to volume will improve thermal performance, it thus provides more area for interaction with the heat sink. This is demonstrated by the smaller thermal resistance value cited for planar cores over traditional cores (Philip., 1997). The properties of planar magnetic cores are, of course, not always benefit. In particular, the planar format increases the footprint area, while it enhances thermal performance. The fact that windings may be put near together, thereby minimizing leakage inductance, has the generally undesirable effect of increasing parasitic capacitance. The repeatability of the characteristics obtained from the PCB windings often comes at the expense of making a larger portion of the winding window filled with dielectric materials, thereby decreasing the copper filling factor and limiting the number of turns.

3.1.3. Advantages of planar technology and drawbacks

The winding difference between the planar magnetic material and the conventional material can be seen in Figure 3.2 and Figure 3.3. As the figure shows, planar magnetic cores have low profile cores relative to the magnetic wire wound. The planar transformer's windings are also flat on the surface of PCBs, the planar transformer windings may have various shapes that influence the transformer's copper loss.

Figure 3.2. Conventional transformer winding. Image from Wikipedia.

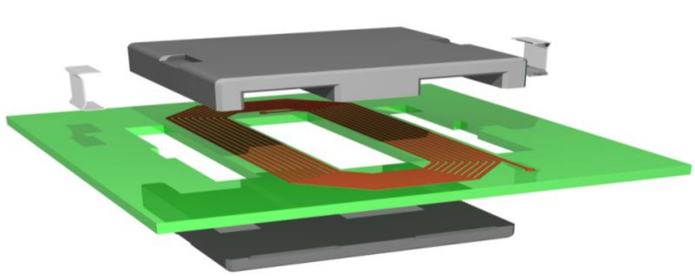

Figure 3.3. The winding layer of a planar transformer on the PCB. Image from Wikipedia.

3.1.3.1. The benefits of the planar magnetic core components over the traditional magnetic core include

3.1.3.1.1. Low profile

The low profile of the planar transformers is a significant feature. This function makes the use of planar transformers in on-board converters almost necessary. For planar magnetic cores, the term low profile is also used to describe it. Planar magnetic cores, being low-profile, help to miniaturize power supplies. A planar magnetic component's height is 25-50 percent smaller than its wire-wound component counterpart. (Ouyang and Andersen., 2014). In applications where weight and volume are a premium, it makes them appealing. Low profile over traditional structures due to greater design surface area with lower cubic volume this offers greater volumetric efficiency. As stated earlier, the low profile core structures of planar transformers suggest that the transformer volume has been efficiently used and also provides higher power densities.

3.1.3.1.2. Good repeatability

It is very easy to design windings as you have to repeat the same thing. The repetitiveness of the components not only helps a lot in the perspective of architecture but also in resonant topologies. The windings and isolators are precisely positioned as the planar magnetic structure is strictly controlled. This gives consistent and controlled parasitic parameters. Unlike wire wound magnetics, which are vulnerable to variance from operator to operator because they do not have firm control over the winding structure.

3.1.3.1.3. High power density

Since the surface area to volume ratio of planar magnetic components is considerably higher than that of the traditional structure, heat conduction is improved. This results in improved cooling, allowing higher power at the same temperature rise, thus improving the power density.

3.1.3.1.4. Lower leakage inductance

The simplicity with which interleaving can be applied in planar system enables leakage inductance inside the windings to be reduced and controlled. (Dai et al., 1994; Skutt et al., 1994).

Winding arrangements affect the leakage inductance. There are two types of configurations in planar transformers such as non-interleaving and interleaving. The P-S-P-S-P-S-P-S is an example of interleaving structure based on the number of boards.

In a planar transformer, this method of arrangement can easily be achieved, helping to reduce the leakage inductance. The transformer's leakage inductance depends on the relative location of the primary and secondary windings in the planar transformer core. The leakage inductance is also closely controlled as the winding location and distance between the windings are strictly controlled.

3.1.3.1.5. Improved thermal management

Planar magnetic cores appear to have better thermal conductivity for their bigger surface area than conventionally shaped cores. Planar magnetics tend to have more efficient heat dissipating properties due to their larger surface-to-volume ratio. The wide surface area also allows a greater contact area for heat sinks. Heat conduction is improved, this gives way to better cooling, higher power densities can be obtained by the improved thermal properties of planar magnetics.

3.1.3.1.6. Mitigating effects of high frequency

The effect of skin and proximity due to the high fréquences can be minimized by the use of wider and thinner conductors. In addition, multilayer PCBs permit layers to be interconnected, allow windings to interleave, minimizing leakage inductance and high frequency winding losses in the components of planar PCB transformers. (Ouyang et al., 2009).

3.1.3.2. Planar technology drawbacks (limitations)

3.1.3.2.1. Larger footprint

A planar structure's low-profile characteristic results in a greater surface area. Because of the rise in the main surface area, the component footprint area is more than equivalent traditional magnetic component.

3.1.3.2.2. Low copper fill factor

According to safety specifications and the capabilities of manufacturers, the insulators between conductors have a minimum thickness of 100-150 μm for multilayer PCB windings. (Ouyang and Andersen., 2014)

In comparison with traditional magnetic parts, this results in fewer conductors for the same winding area. PCB-based windings that have a low copper fill factor of about 0.25 are used in most planar magnetic parts, while conventional form has about 0.4. This is due to the greater inter turn spacing and PCB winding dielectric thickness. (Quinn et al., 2001)

3.1.3.2.3. Limited number of turns

The number of turns and number of layers are also reduced as a result of the low copper fill factor. The conductor width may be shortened to maximize the number of turns or layers, but this results in increased winding losses.

3.1.3.2.4. Increased parasitic capacitance

Since we stack windings on top of each other, there is often a certain air gap that contributes to an increase in parasitic capacitance. This is a very big drawback that will impact the transformer's efficiency. To eliminate this higher parasitic capacitance we would have to reduce the air gap to the lowest possible level.

3.2. Designing of Flyback Transformer

In this section, we study about the calculations that are required in order to design a flyback planar transformer, general design procedure, what is all the core materials available, basic construction of a planar transformer. There are 3 important parts in a planar transformer which include core material, windings on PCB and the insulation.

3.2.1. Formulas for flyback transformers

$$N_p = \frac{Vin_{min} \, . \, \mathrm{D}_{max}}{f_s \, . \, B_{peak} \, . \, Ae} \tag{3.1}$$

$$\mathrm{n} = \frac{Vin_{min}}{V_O} . \frac{\mathrm{D}_{max}}{(1 - \mathrm{D}_{max})} \tag{3.2}$$

$$\mathrm{Ns} = \frac{\mathrm{Np}}{\mathrm{n}} \tag{3.3}$$

$$I_{av} = \frac{P_o}{\eta \, . \, Vin_{min}} \tag{3.4}$$

$$I_{ppeak} = \frac{I_{av}}{\mathrm{D}_{max} \, . \, (1 - 0.5 * K_{RP})} = \frac{I_{av}}{0.5 \, . \, \mathrm{D}_{max}} \tag{3.5}$$

$$L_{pri} = \frac{2 \, . \, P_{in}}{f_s \, . \, {I_{ppeak}}^2} \tag{3.6}$$

$$\mathrm{G} = \frac{{N_p}^2 \, . \, \mu_o * \mathrm{Ae}}{L_{pri}} \tag{3.7}$$

$$K_{RP} = \frac{\mathrm{I}_R}{\mathrm{I}_{Ppeak}} \tag{3.8}$$

$$I_{prms=} \sqrt{\mathrm{D}_{max} \cdot \frac{{I_r}^2}{3}} \tag{3.9}$$

$$I_{speak} = I_{ppeak} . n \tag{3.10}$$

$$I_{srms=} I_{speak} \cdot \sqrt{\frac{\mathrm{D}_s}{3}} \tag{3.11}$$

$$I_{sav} = \frac{\mathrm{P}_o}{\mathrm{V}_o} \tag{3.12}$$

$$\mathrm{D}_s = \frac{I_{sav}}{0.5 * I_{speak}} \tag{3.13}$$

$$I_{srms=} I_{speak} \cdot \sqrt{\frac{\mathrm{D}_s}{3}} \tag{3.14}$$

$$\mathrm{P}_{in} = \frac{D_{max}}{2} . Vin_{min} . I_{ppeak} \tag{3.15}$$

$$\eta = \frac{P_o}{P_{in}} . 100\% \tag{3.16}$$

Where

Ae = effective cross-sectional area

B_{peak} = peak flux density

f_s = switching frequency

I_{prms} = primary rms current

P_{in} = input power

P_o = output power

Vin_{min} = minimum input voltage

V_o = output voltage

I_{srms}= secondary output current

I_{sav} = secondary average current

L_{pri} = primary self-inductance

N_p = primary winding turns

D_s = duty cycle secondary

n = turn ratio

K_{RP} = ripple to peak current ratio

I_R = primary ripple current

η = efficiency of transformer

D_{max} = max. Duty cycle signal

G = airgap length

N_s = secondary winding turns

μ_o = permeability of free space.

I_{av} = primary average current

I_{ppeak} = primary peak current

I_{speak} = secondary peak current

3.2.2. Basic construction of planar transformer

A planar transformer's basic construction is very similar to that of the traditional transformer. Although the basic transformer operation is also true for the planar transformer, both transformers are very similar in construction and components. Like a traditional transformer, planar transformer often involves core, windings and insulation. The core can be two halves, one at the top and the other at the bottom. Ferroxcube produces planar transformer cores mainly (Ferroxcube., 2013).

Windings are placed in between these core halves. Instead of Litz wire, windings are built over the PCB. The PCB dimensions differ depending on the dimensions of the core of the transformer that we select. There are primary and secondary windings. Based on the appropriate requirements, the number of turns will differ for each winding. If the winding turns higher on the secondary side of the PCB, it is a step-up transformer and if it is vice versa, a step-down transformer. Insulation between the windings is also provided. (Venkatanarayanan., 2019). Selection of materials based on our requirements is one of the transformer's greatest challenges.

The core of the planar structure has a clearly lower profile than the traditional. Furthermore, the windings on the traditional device are stacked such that they are successively farther from the middle of the body (center leg) windings are thus shaped horizontally. When stacked on the planar device in the vertical direction instead.

3.2.3. Planar cores

Cores for planar components, as shown in Figure 3.4.

(a)

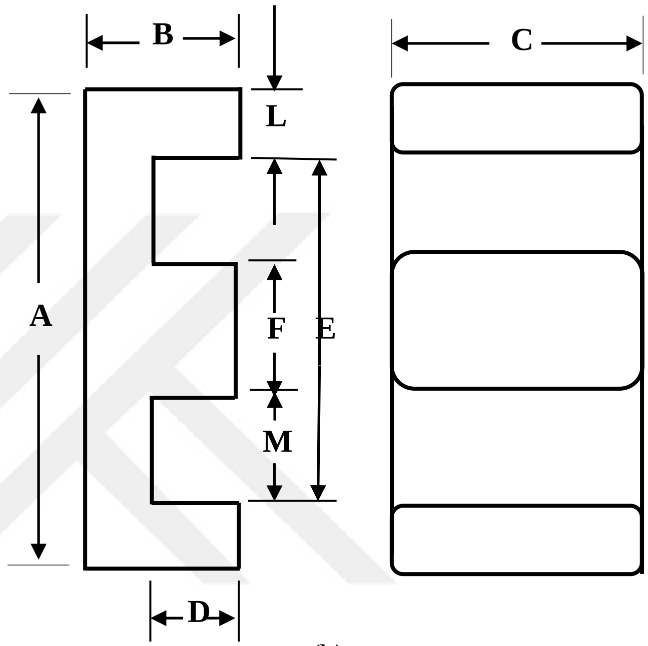

(b)

Figure 3.4. Typical planar core.

The planar EE and EPLT core, specifically designed for planar magnetic cores and now available to most manufacturers in many industry standard sizes and is currently the most common.

It is important to note that optimization experiments have shown that there is an optimum component height for any set of requirements that maximizes power density. (Ngo and Lai., 1992). And that the use of custom cores will achieve higher power densities. (Prieto et al., 1996). The limited selection of standard flat core systems would therefore unlikely provide the ideal solution for a specific design, so that custom solutions should be invesitaged if cost constraints allow, in order to maximize performance of a standard flat EE core details from ferroxcube planar cores are shown in Table 3.1. Dimension represents the all external and internal dimensions of the core dimensions reference to Figure 3.4. (b).

Table 3.1. Standard planar EE cores for industrial uses dimensions reference to figure 3.4 (b)

Core	A mm	B mm	C mm	D mm	E mm	F mm
E/E14	14.00	3.50	5.00	2.00	11.00	3.00
E/E18	18.00	3.98	10.00	1.98	14.00	3.98
E/E22	21.60	5.72	15.90	3.18	16.50	5.08
E/E32	31.75	6.35	20.32	3.28	25.40	6.35
E/E38	38.10	8.26	25.40	4.45	30.48	7.62
E/E43	43.18	9.53	27.90	5.46	35.05	8.13
E/E58	58.40	10.55	38.10	6.50	51.10	8.10
E/E64	64.00	10.20	50.80	5.10	53.60	10.20
E/E102	102.00	20.30	37.50	13.13	86.00	14.10

3.2.4. Planar core material

Magnetic cores are composed of soft magnetic materials. In comparison to hard magnetic materials that are widely used in permanent magnets, soft materials can attain high flux density with less coercive force. As seen in Figure 3.5. They have less hysteresis loop area that contributes to lower loss of hysteresis. Core materials such as soft ferrites, powdered iron core, amorphous alloys, nano crystalline materials, and so on are available. Many planar cores are built of soft ferrites because of their reduced core loss.

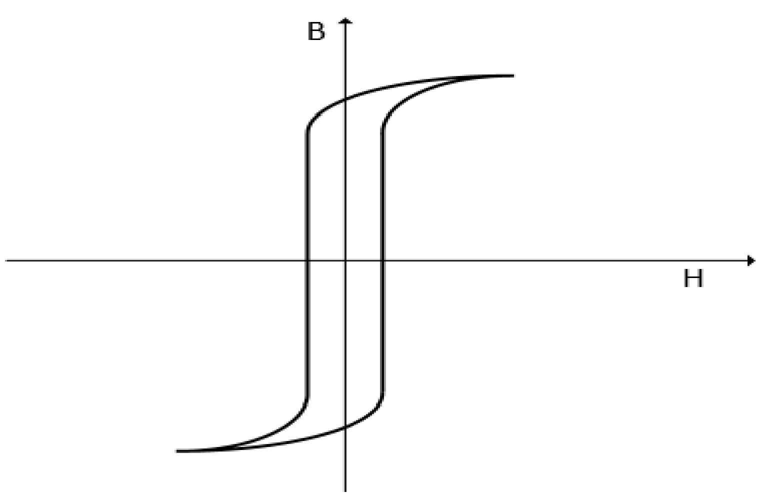

Figure 3.5. Soft ferrite hysteresis loop.

Ferrites are composed of iron oxide and metals such as cobalt, magnesium, nickel, silicon, manganese, or zinc are alloyed. Manganese-zinc (Mn-Zn) and nickel-zinc (Ni-Zn) ferrites are the most widely used. High electrical resistivity and less permeability are available for Ni-Zn ferrites. It is typically used for high frequency applications in the order of MHz. Ferrites of Mn-Zn have decreased electrical resistivity and greater permeability than ferrites of Ni-Zn. It is used in applications that have a frequency of a few hundred kHz. (Kumar et al., 2015).

Generally, the transformer's core material is ferrite. Nowadays, Ferroxcube provides core materials for transformers that are commonly used all over the world. For our transformer, there are several factors that contribute to determining the core material, such as the core dimensions, shape, ferrite quality and magnetizing length. From Ferroxcube, we get various shapes of core material. In figure 3.6. EE and EPLT types are shown, some of these core types are available. 3C80, 3C92, 3C94, 3C97, 3F3 and so on. We would only be able to design our PCB windings depending on the dimension of these core materials so that they fit perfectly between the cores. (Venkatanarayanan., 2019).

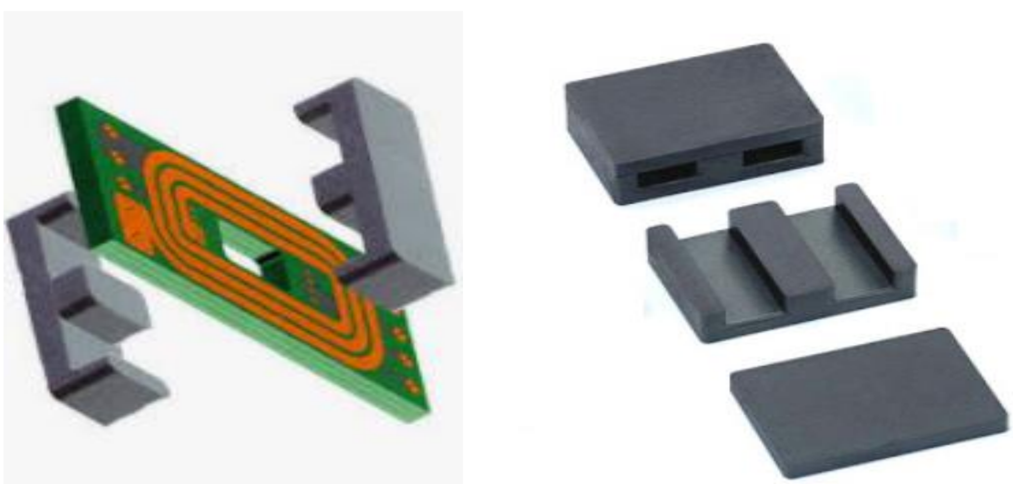

(a) (b)

Figure 3.6. Examples of Ferroxcube EE and EPLT type cores. Left Picture from Ferroxcube https://www.acalbfi.com/se/search/PMA and right picture from yeng tat electronics co., ltd.

3.2.5. Technologies for planar winding

Different technologies are available for the implementation of planar windings. The most famous ones compared in literature (Dai et al., 1994). The winding type used for a planar structure is determined by the core window area, operating frequency, production cost and application. The current density and switching frequency determine the conductor size. Printed circuit board (PCB), flex circuit and stamped copper are the different kinds of winding methods available for planar magnetic cores and the most common technologies.

Thick-film windings were also mainly used in lower- power applications. This thesis focuses mainly on PCB structures in the design of magnetic core. The use of PCBs offers an extremely repetitive way to implement planar windings. In general, the windings will form an integral part of the system interconnection substrate thus remove all terminations. In fact, however, the interconnection substrate seldom has enough layers to fit the magnetic component windings entirely.

- Windings on PCB (PCB winding)

Copper cladded PCB is used to form the printed circuit board windings. The two sided boards are usually used with 1oz-2oz copper thickness. This makes it easier to easy connection of layers in a multiple winding layer, this enables easy winding interleaving that is difficult in a traditional transformer. It has advantages of simple assembly process, low cost high volume production and high winding surface area required for high frequency application. (Gunewardena., 1997). At present it is limited to low-power applications. The major drawbacks of this winding technology is the decreased copper fill due to the high substratum area. (Ropoteanu et al., 2016).

The drawbacks of PCBs is that due to a typical inter-turn spacing of 300 μm and minimum dielectric thickness of 200 μm, the window utilization factor can be very low (usually 0.25 compared to 0.4 for traditional magnetic cores).

The design of their windings is the main difference between the two kinds of transformer. Instead of litz wire, the windings are built on the PCB as per requirement. On the basis of the windings' current carrying capacity, there are two types of traces. If more current needs to be carry by the board, so the copper winding on the board must be thicker and is named as high current trace as seen in Figure 3.7 It has a copper thickness of about 10,715 mm.

Figure 3.7. PCB windings- high current trace. Image by (Venkatanarayanan et al., 2019).

If less current needs to be carry by the board, the winding does not need to be thick, as seen in Figure 3.8, these types of traces are considered as low current traces. It has a copper thickness of 0.701mm. These traces may be known as the primary or secondary board of the transformer, depending on the specifications. If it is a step up transformer, it is possible to consider high current trace as primary and low current trace as secondary.

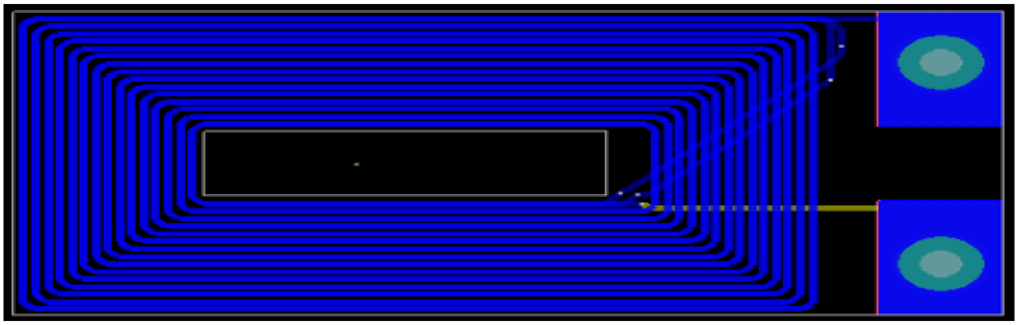

Figure 3.8. PCB windings- low current trace. Image by (Venkatanarayanan et al., 2019).

3.3. Loss Mechanisms in Magnetics

There are two types of loss in a magnetic component, one is a magnetic core loss, and the other is conduction or copper loss in the winding. The core loss has two parts, the loss of hysteresis and the loss of eddy current, while the loss of copper is often explained in the heat dissipated by the DC or AC loss in the windings. The high frequency magnetic part is subject to eddy current which increases copper losses.

Under operating conditions, core and copper losses in a transformer cause an increase in temperature. To prevent damage to the transformer or the rest of the circuit, this increase must remain below the highest permissible value. In thermal equilibrium the total losses in the transformer, Ptr, can be related to a temperature increase of the transformer ΔT with an analog of Ohm's law by:

$$P_{tr} = \frac{\Delta T}{R_{th}} \tag{3.17}$$

In this formula, Rth represents a transformer's thermal resistance. Ptr can be interpreted as the transformer's cooling capacity.

3.3.1. Transformer core loss

For planar E transformers, a relation has now been found, this relation can be used to approximate the temperature increase of the transformer as a function of the core flux density. It is advised to use the highest permitted flux densities in planar magnetic cores because of the small available winding area. With the assumption that half of the overall transformer loss is core loss, the maximum core loss density Pcore can be represented as a function of the transformer's permissible temperature rise ΔT as:

$$P_{core} = \frac{12\ .\ \Delta T}{\sqrt{\mathrm{Ve}\ (\mathrm{cm}^3)}} \qquad [\mathrm{mW/cm^3}] \tag{3.18}$$

The magnetic core exhibits magnetic field alternation. This varying magnetic field adds to the loss of hysteresis and eddy current. At low frequencies, the contribution of hysteresis loss to overall loss is important, whereas eddy current losses are important at higher frequencies (Roshen., 2007).

Power losses in our ferrites have been calculated in terms of frequency (fs in Hz), maximum flux density (B in T) and temperature (T in °C). To precisely determine the core loss resulting from hysteresis and eddy-current losses in magnetic cores. Will approximate the core loss density (3.18) by the following formula, which expresses core loss density as power law with a fixed frequency and flux density exponent,

$$P_{core} = C_m \,.\, f_s^{\,x} .\, B^{\,y}_{peak} .\, (ct_0 - ct_1 T + ct_2 T^2) \qquad (3.19)$$

$$= C_m \,.\, C_T \,.\, f_s^{\,x} .\, B^{\,y}_{peak} \qquad [\mathrm{mW/cm^3}]$$

In this formula C_m, x, y, ct_0, ct_1 and ct_2 are parameters discovered by curve fitting of the calculated power loss data. These parameter specifications are unique to a ferrite material. They are dimensioned in such a way that the C_T value is equal to 1 at 100 °C.

In table 3.2. Fit parameters are specified for many Ferroxcube power ferrites. Maximum permitted P_{core} is calculated with equation (3.18). This value is inserted in equation (3.19). Max-permitted flux density Bpeak can now be calculated by rewriting equation (3.19).

$$B_{peak} = \left[\frac{P_{core}}{C_m \,.\, C_T \cdot f_s^{\,x}}\right]^{1/y} \qquad [\mathrm{T}] \qquad (3.20)$$

The peak flux is inversely proportional to the frequency, so with increasing frequency, the core loss will decrease.

Table 3.2. Fit parameters to calculate the power loss density

Material	Freq min	Freq max	C_m	x	y	Ct_2	Ct_1	Ct_0
3C80	10000	100000	16.7	1.3	2.5	0.000117	0.02	1.83
	20000	100000	26.52000126	1.194999973	2.649999941	0.000267895	0.054329115	3.7539611
3C92	100000	200000	0.349247262	1.589999964	2.67499994	0.000150599	0.030541568	2.548162342
	200000	400001	0.000119	2.24499995	2.66499994	0.000208173	0.04371632	3.289902504
3C97	20000	150000	42.36588301	1.16	2.8	6.35519E-05	0.01100719	1.465
	150000	300000	0.003448693	1.99	2.935	7.85219E-05	0.0136	1.575
	300000	400001	0.000449188	2.055	2.415	8.74899E-05	0.01403339	1.528
3F3	20000	300000	0.25	1.6	2.5	0.000079	0.0105	1.26
	300000	500000	$2*10^{-2}$	1.8	2.5	0.000077	0.0105	1.28
	500000	1000000	$36*10^{-7}$	2.4	2.25	0.000067	0.0081	1.14

In other words, ferrites are typically good electrical conductors, as commonly used magnetic core materials in power ectronics systems. Therefore ac magnetic fields, cause electric eddy currents to circulate inside the core material itself, as seen in Figure 3.9. Eddy current losses add greatly at high frequencies to the overall core losses.

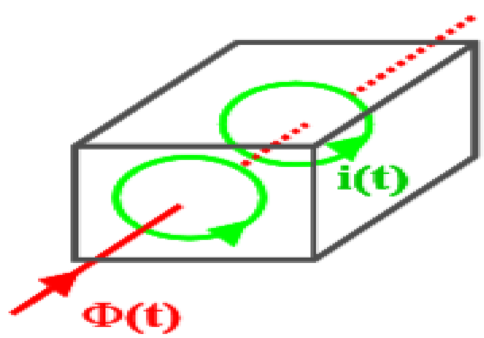

Figure 3.9. Eddy currents in a magnetic core.

It is obvious that core loss is proportional to core size.

$$P_{core(Watt)} = P_{core} * \mathrm{Ve} \quad (3.21)$$

Where Ve is core volume, P_{core} is the volumetric power losses in watts per cubic meter

3.3.2. Transformer copper loss

It is possible to quantify the DC or low frequency copper loss in the windings by

$$P_{Cu} = I^2 * R_{dc} \quad (3.22)$$

Where rms I is the RMS value of the current that flows through the windings, it is possible to express the dc resistance as

$$R_{dc} = \rho * \frac{\mathrm{l}}{\mathrm{A}} \quad (3.23)$$

Where A is the cross-sectional area of the wire, l is wire length and p is copper resistivity.

It is possible to make the windings thicker to decrease the copper loss. Resistance is inversely proportional to the square of the thickness, as we know, making the winding thicker reduces the resistance, which in turn reduces the loss of copper.

Copper or conduction loss in the winding, is often explained in the heat dissipated by the DC or AC loss in the windings. The high frequency magnetic part is subject to eddy current which increases copper losses.

With high frequency due to effects of eddy current, the winding losses in transformers significantly increase. For the design and optimization of transformers there is a need for a detailed prediction of the winding losses over a wide frequency range and for different winding arrangements. In high-frequency power conversion applications, Eddy current losses, including skin effect and proximity effect losses, greatly impair transformer performance, for flowing AC current in a conductor.

3.3.2.1. Skin effect

The alternating field in the conductor produces eddy currents in the conductor, which create a field tending to cancel the field generated by the original current, the trend of the alternating current distributes itself in the conductor such that the current density at the conductor's surface is greater than that at its center. This is known as skin effect, as shown in Figure 3.10. That causes the conductor's effective resistance to increase with the frequency of current. In the cross section of the conductor, both the skin effect and the proximity effect cause the current density to be non-uniform and hence cause greater winding resistance at a higher frequency. The ratio of ac resistance to dc resistance will represented the skin effect of an infinite foil conductor with sinusoidal excitation. As in (Nan and Sullivan., 2003).

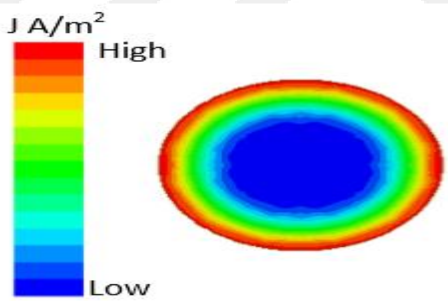

Figure 3.10. Skin effect in round conductor. Picture from (Gurusamy., 2018).

The decrease of the current conduction area results in an increase in resistance to current flow. This thin region is called the skin depth. This is provided by

$$\delta = \sqrt{\frac{\rho}{\pi * f_s * \mu}} \tag{3.24}$$

It is inversely proportional to the square root of the operational frequency. Figure 3.11 indicates the variation in skin depth with respect to frequency. To decrease this effect, the appropriate conductor dimension should be chosen. For a rectangular cross-section conductor, the current, as seen in Figure 3.12, appears to crowd at the edges of the conductor. The skin effect is the conductor's self-inductance action. That is due to a magnetic field that is self-induced.

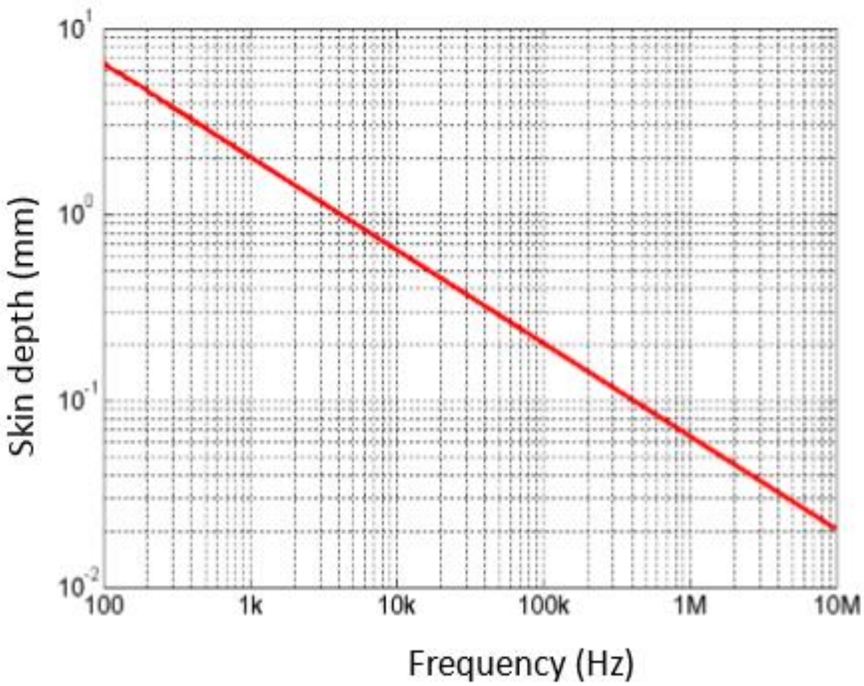

Figure 3.11. Variation of skin depth versus frequency. Picture from (Gurusamy., 2018).

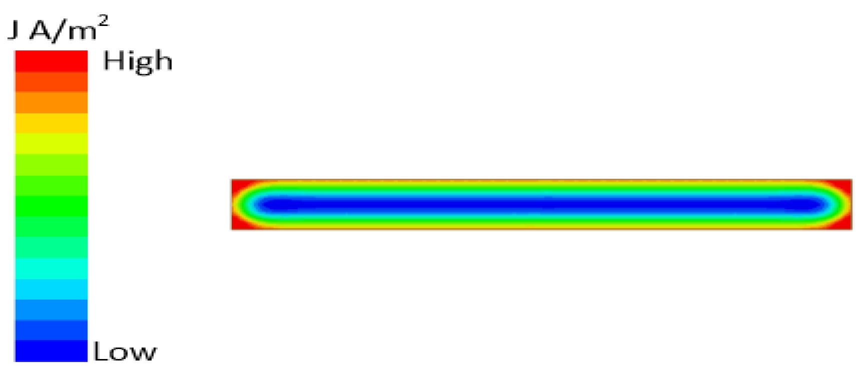

Figure 3.12. Skin effect in rectangular section conductor. Picture from (Gurusamy., 2018).

3.3.2.2. Proximity effect

The skin effect is caused by a self-induced magnetic field, because it takes place in free space in an isolated current carrying conductor, whereas the proximity effect is similar, but it is caused by the conductor carrying current in the vicinity. A time-varying field is induced by the current in the neighboring conductor and causes a circulating current within the conductor. In the cross section of the conductor, both the skin effect and the proximity effect causes the current density to be non-uniform and thus cause greater winding resistance at a higher frequency.

The proximity effect for a group of conductors is seen in Figure 3.13. For round conductors and as seen in figure 3.14. For conductors in rectangular shape. The current carrying in all conductors are in the same direction and current flowing away from the conductors' common center. This leads to greater resistance and higher losses.

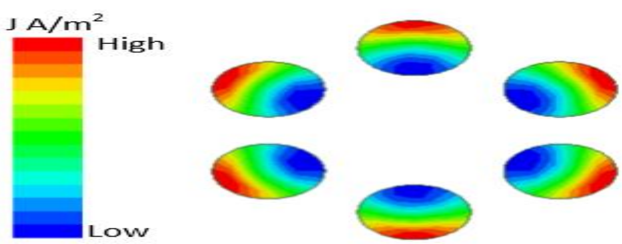

Figure 3.13. Proximity effect in round conductor. Picture from (Gurusamy., 2018).

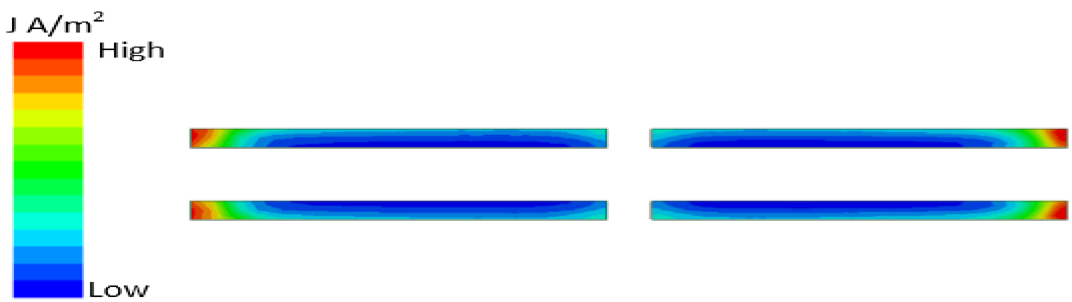

Figure 3.14. Proximity effect in rectangular section conductor. Picture from (Gurusamy., 2018).

The loss due to the proximity effect is usually greater than the skin effect of high frequency magnetic cores. With the rise in number of layers, the proximity loss increases, tackling the proximity effect is not an easy job since most planar magnetics have multilayer windings due to their decreased winding factor.

The transformer in the converter carries a high-frequency current that induces a high frequency loss due to the effects of skin and proximity. Increased resistance of the winding due to these effects is called resistance of the ac. The ac resistance of the winding is calculated by the well-known Dowell formula is given by (Saket et al., 2017), the expression for the ac resistance of the mth layer is derived as (Ferreira., 1994; Nan and Sullivan., 2003).

$$R_{ac} = R_{dc} * \frac{\Delta}{2}\ [\varepsilon_1 + (2m-1)^2\ \varepsilon_2] \tag{3.25}$$

Where $\Delta = \frac{t}{\delta}$ (3.26)

$$\varepsilon_1 = \frac{\sinh\Delta + sin\Delta}{\cosh\Delta - \cos\Delta} \tag{3.27}$$

$$\varepsilon_2 = \frac{\sinh\Delta - sin\Delta}{\cosh\Delta + \cos\Delta} \tag{3.28}$$

$$\mathrm{m} = \frac{\mathrm{F(t)}}{\mathrm{F(t)} - \mathrm{F(0)}} \tag{3.29}$$

Where m is the winding layers number, t is the conductor thickness and δ is skin depth at the switching frequency. Where F(t) and F(0) are the MMF at the limits of the layer at the boundary of the transformer conductors, The skin effect is associated with the first term ε1 and the next term is associated with the proximity effect. It can be seen that the proximity effect depends not only on the skin effect, but also on the number of layers, The MMF relies heavily on the winding arrangement and its transformer connection. As Figure

3.15 shows. The loss of proximity effect will strongly dominate over the loss of skin effect in a multilayer winding, depending on the value of m that is correlated with the winding arrangements.

Interleaving transformer windings, where the primary and secondary currents are in phase, will greatly minimize proximity loss. Figures 3.15. (a), (b) and (c) shows the distributions of MMF along the vertical direction for non interleaving arrangement, fully interleaving arrangement, Improved Interleaving arrangement $0.5\mathrm{P}-\mathrm{S}-\mathrm{P}-\mathrm{S}-\mathrm{P}-\mathrm{S}-\mathrm{P}-\mathrm{S}-0.5\mathrm{P}$ respectively. The value of m can be calculated according to (3.29), and quite different results are also shown in Figure 3.15. In order to further illustrate the eddy current effect in different arrangement.

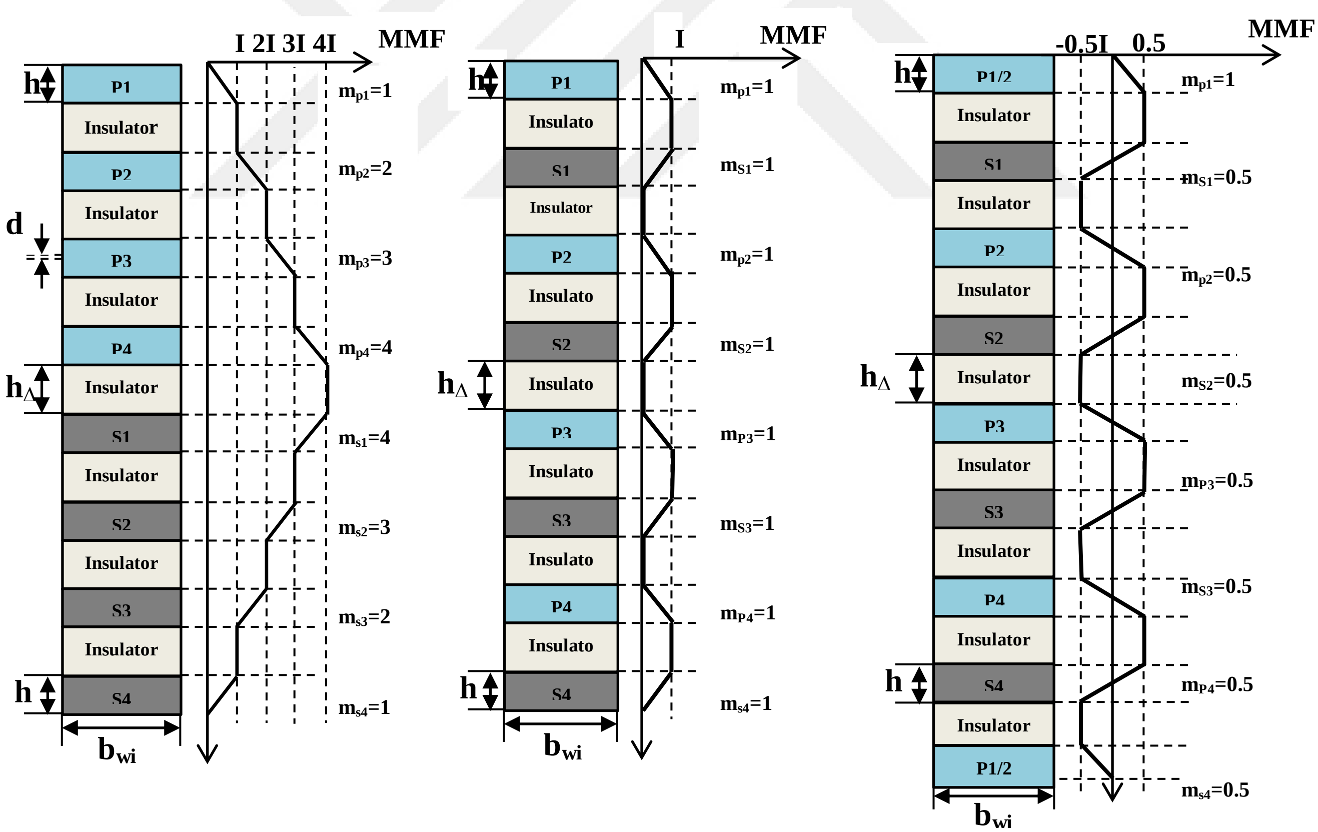

(a) (b) (c)

Figure 3.15. MMF distributions. (a) Noninterleaving arrangement. (b) Interleaving arrangement. (c)Improved Interleaving arrangement $0.5P-S-P-S-P-S-P-S-0.5P$ respectively.

At high frequencies, the eddy currents in the winding due to the skin effect and the proximity effect often induce power loss and typically contribute to a loss of copper considerably greater than DC or a loss of low frequency expressed above. Reducing the thickness of the conductor to the order of one skin depth is one way to minimize the high-frequency loss due to skin effect, so that the ac current can be expected to be uniformly distributed in the winding cross-sectional area. In the case of a planar magnetic structure, since the thickness of the conductor is typically equal to a single skin depth, the influence of the skin may be suppressed. For example, the thickness of 2-oz PCB is about 70 μm, while the depth of penetration (or depth of skin) for copper at 50 kHz is about 298 μm. From the circuit point of view, it is generally appropriate to ignore the impact of the skin when the thickness of copper is less than twice the depth of the skin. However, with most planar copper structures, the currents are uniformly spread at both ends rather than at the surface.

Figure 3.16. And 3.17. Separately represent current distributions for interleaving windings and non-interleaving windings, as the frequency goes high, the skin and proximity effects will further increase the non-uniform distribution of the current density. The color division of the current distribution is caused by the influence of the skin and proximity.

One way to minimize copper losses due to the proximity effect is to interleave the windings (especially for transformer design). Figures 3.16.And 3.17. Explain how to improve current delivery and thus reduce overall AC losses by interleaving both windings primary and secondary in power transformers.

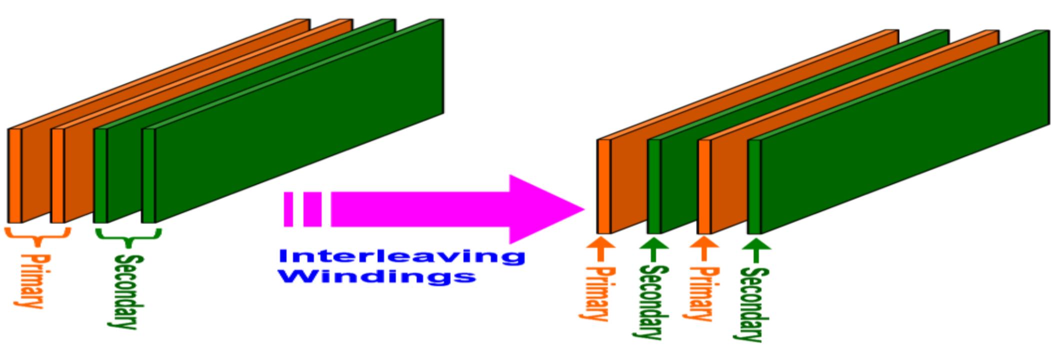

Figure 3.16. Interleaved windings. Picture from (Xiao., 2004).

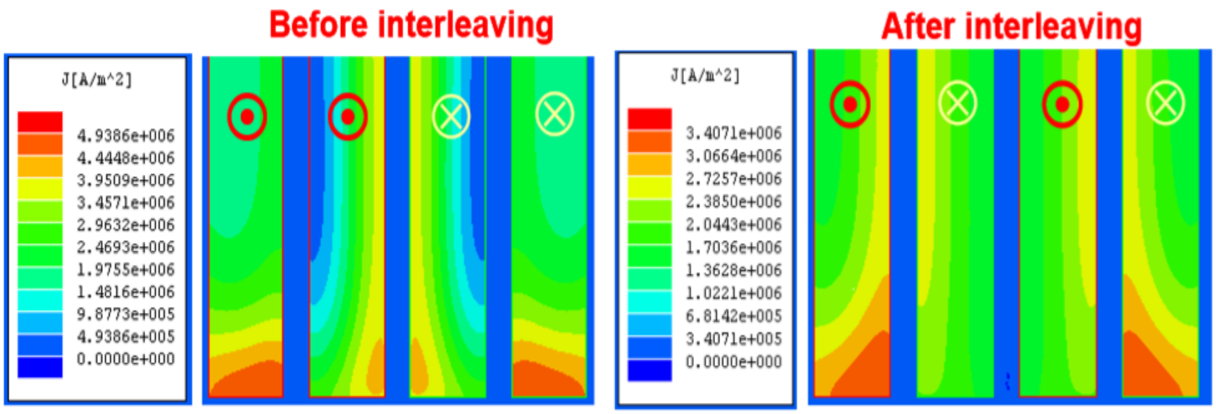

(a) (b)

Figure 3.17. Current distributions before and after interleaving. Picture from (Xiao., 2004).

Apparently, the current is distributed more equally after the primary and secondary windings are interleaved. As a consequence, the ac loss will be minimized.

For the non-interleaving arrangement in Figure 3.17. (a), Due to the greater proximity effect, the tendency of current density towards the conductor surface is improved. The greatest tendency towards the conductor surface occurs in the layer close to the interface between the primary and the secondary, and thus the region of color division becomes smaller, which means that a higher ac resistance will be generated.

As seen in 3.17. (b), the ac resistance is not only related to the MMF ratio m, but also to the ratio Δ. For a given frequency, the minimum ac resistance can be calculated by the layer thickness of the windings. The choice of thickness as a physical parameter was the key in optimizing PT.

3.4. Magneto Motive Force

3.4.1. MMF in a current carrying conductor

Consider a conductor carrying current of magnitude I, as it has one turn the maximal MMF is equal to the current at one turn. When the conductor's thickness (t) is less than the depth of the skin, the current distribution within the conductor is uniform, which allows the MMF to vary linearly across the conductor as seen in Figure 3.18. Where dx is the distance between the conductor. In a given region, the MMF is equal to the current enclosed by the region = NI = Hl.

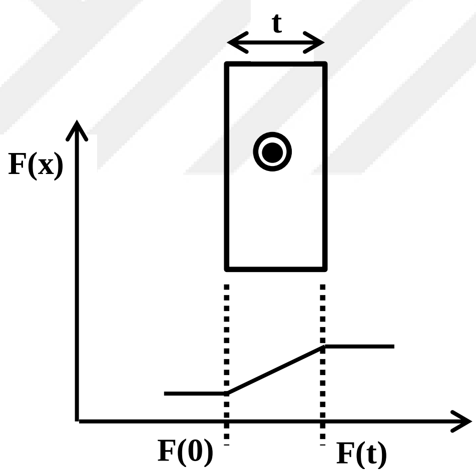

Figure 3.18. MMF across a conductor with uniform current density.

3.4.2. MMF in transformer windings

As seen in Figure 3.19, the MMF diagram for transformer windings is drawn on the basis of the MMF diagram for a single conductor. Consider that the transformer core has very high permeability, which makes zero MMF at the core. There are four layers of both primary and secondary windings. Each layer carries current of magnitude i, and so the cumulative MMF through the primary winding is 4i as all layers carry current in the same direction that allows the additive of the MMF. This is given in Figure 3.19. As the secondary winding carries current in the opposite direction. MMF begins to decrease when enclosing secondary windings. This MMF diagram is true when the layer thickness is smaller than the skin depth.

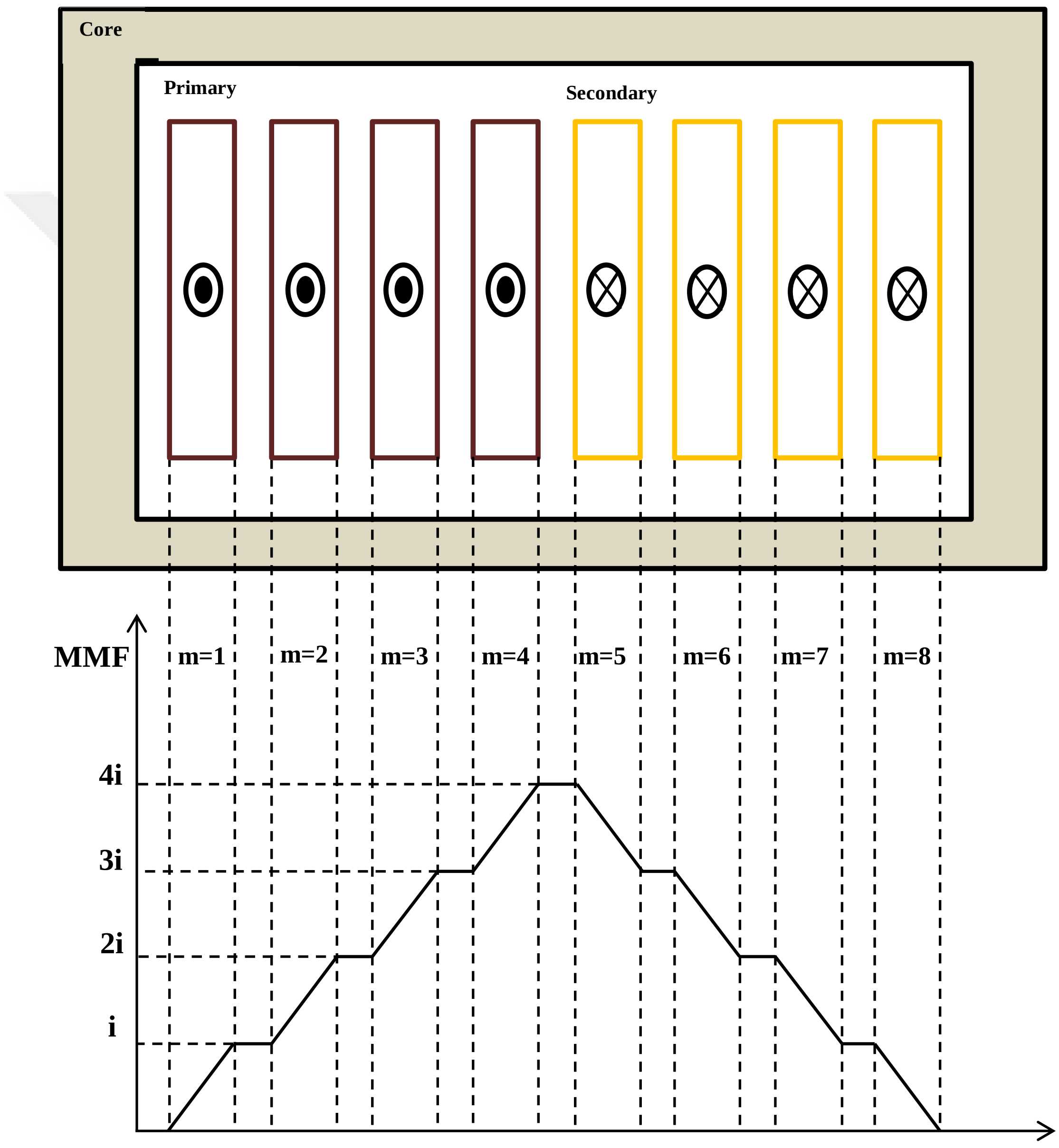

Figure 3.19. MMF in non interleaving transformer with multiple layer windings.

3.4.3. Reduction of copper loss due to proximity effect

Based on the previous discussion, MMF can be seen by winding raises as they are additive in nature, which occurs when windings carrying current in the same direction are positioned near each other. If we will reduce the MMF through the winding, so the loss can be minimized. To reduce the MMF, the primary and secondary winding layers may be placed next to each other. This principle is called the interleaving of the winding. The interleaving of the windings used in our design is discussed in this section.

- Interleaved windings

The winding of the transformer is initially partially interleaved and then fully interleaved. Figure 3.19 indicates the MMF over the winding of the transformer in a non-interleaved condition. The MMF is considerably higher reaching around 4i, which significantly increased the loss.

It can also be observed from the MMF plot that the current is not equally shared among the parallel windings, which also led to high losses. As stated there are 4 PCB boards per winding, and initially two boards are interleaved, meaning 2 primary boards followed by 2 secondary boards and so on. In Figure 3.20, the sectional image of the structural interleaving configuration of the core winding is seen.

Interleaving primary and secondary windings will significantly improve the distribution of current and thereby reduce the loss of AC copper. The MMF has been greatly reduced to i with Interleaving winding arrangement. From the MMF plot, it can be observed that the current is equally shared between all windings. Next, the configuration of the transformer is fully interleaved. As seen in Figure 3.20, the primary and secondary winding PCBs are placed next to each other,

The MMF decreased dramatically in its fully interleaved structure. The copper loss has reduced dramatically, and there is still a drawback in minimizing leakage inductance. As the winding MMF reduces, the leakage flux also decreases. This leads to a decrease in leakage inductance.

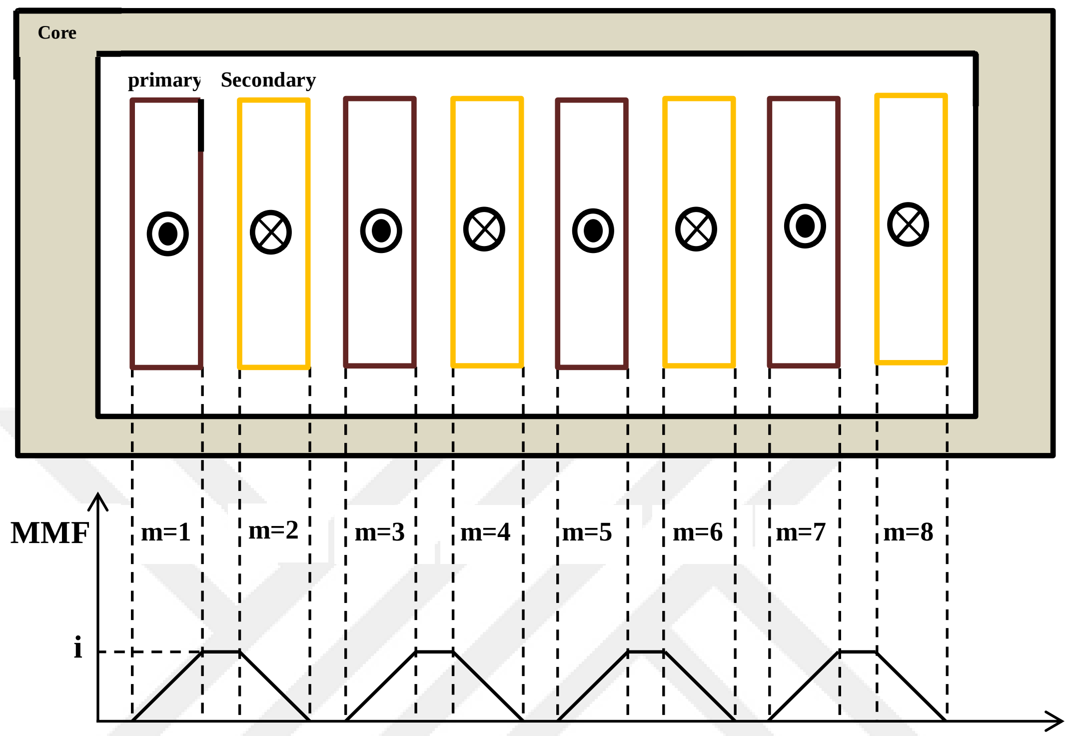

Figure 3.20. MMF of interleaving transformer.

3.5. Leakage Inductance

Leakage inductance is a parasitic factor in the design of the transformer due to the uncoupled portion of the windings between primary and secondary. Not all the magnetic flux produced on the primary side by AC current excitation follows the magnetic circuit and connects with the other windings. There is never a complete flux linkage between two windings or parts of the same winding. Some flux leaks from the core and returns to the air, insulator layers and winding layers, this flux creating incomplete coupling. It is seen from Figure 3.21. The mutual repulsion within the winding field allows the leakage flux to lay nearly parallel to the winding interface. The leakage inductance referred to the primary can be accessed by the energy stored in a magnetic field.

$$\mathrm{E}_{energy} = \frac{1}{2}\int \boldsymbol{B.H.dv} = \frac{1}{2}\mathrm{L}_{Llk.}\boldsymbol{I^2}_{P} \tag{3.30}$$

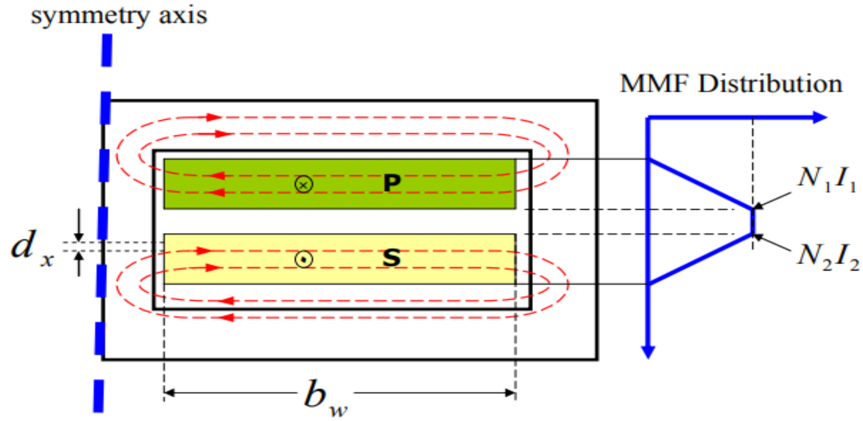

Figure 3.21.The leakage flux paths and magneto motive force variation (MMF).

A planar transformer is used as a solution to minimize the leakage inductance of the transformer. In (Li et al. 2009), a planar transformer is used to decrease the transformer's leakage inductance. As the transformer's flat configuration has a smaller magnetic path length through the air. The planar transformer results in a lower leakage inductance.

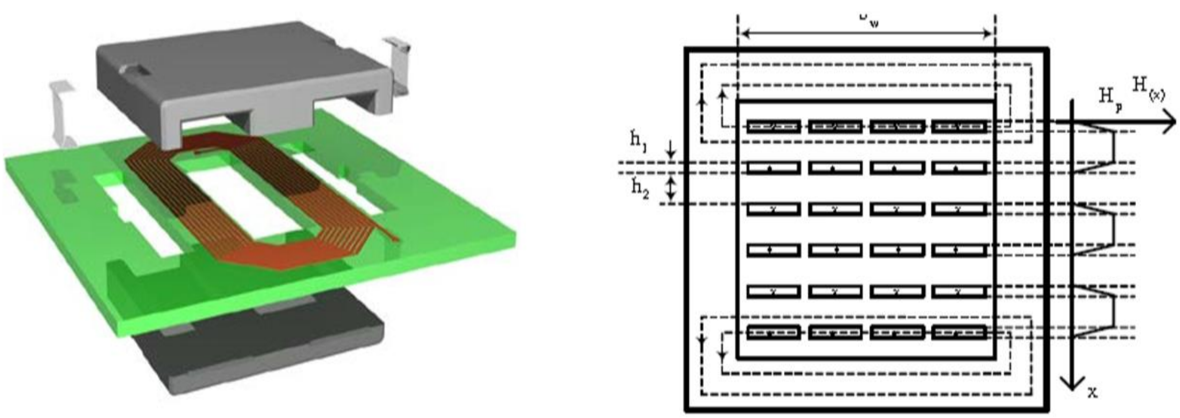

Figure 3.22. Planar transformer with winding window and MMF distribution (left picture from Wikipedia, righ picture from (Li et al., 2009).

The interleaving arrangement offers a major benefit in the reduction of leakage inductance. With printed circuit board (PCB) layers (Ouyang., 2011). PCB windings have a low-profile structure with high power density. For operation at high frequencies, the natural flatness of the winding cross section is more desirable as it is less sensible to the skin effect relative to conventional wires (Lu et al., 2003)., moreover, the leakage inductance can be significantly reduced by heavy interleaving (Carsten., 2001; Li et al., 2009; Cove et al., 2010; Ouyang et al., 2012) compared to conventional wounded components.

The most commonly used theoretical approach to calculating winding leakage inductance is the energy stored in the transformer winding. The generic expression of leakage inductance can be derived from the transformer winding as in (3.31) (Ouyang et al., 2012).

$$\boldsymbol{L_{lk}} = \boldsymbol{\mu_0} \frac{\boldsymbol{l_u}}{\boldsymbol{b_u}} \ \frac{\boldsymbol{N^2}}{\boldsymbol{M^2}} \left(\frac{\sum \boldsymbol{x}}{\boldsymbol{3}} + \sum \boldsymbol{x_\Delta}\right) \tag{3.31}$$

Where μ_0 is the permeability, $\boldsymbol{l}$u is the one turn length, $\boldsymbol{b}$u is the width of each turn, N is the number of turns on the winding on which the leakage inductance is to be applied, M is the number of section interfaces, $\sum$ x is the sum of all section layer heights (windings) and $\sum x_\Delta$ is the sum of all intersection layer heights (insulator). This method measures the leakage inductance on the basis of the linear magneto motive force (MMF) between the non-interleaved parts. Interleaving is a well-known method used to minimize leakage inductance and decrease high-frequency winding loss. It is seen in (Mohan et al., 2003; McLyman and McLyman., 2004; Doebbelin et al., 2007), leakage inductance decreases by M^2 times by sandwiching the windings, where M is the number of interfaces between primary and secondary (Mohan et al., 2003). Apparently, a complete interleaving arrangement has a major benefit in decreasing leakage inductance.

As a conclusion, besides winding structures, the leakage inductance in PT can be adjusted by changing certain physical parameters, including conductor thickness, conductor width, insulator thickness and number of turns. In addition, the energy stored in the leakage inductance contributes to the generation of voltage spikes on the main switch, which raises switching losses and decreases efficiency (Chen et al., 2003).

3.6. Stray Capacitance

In designing PT, stray capacitance cannot be ignored. This parasitic factor is generated by the potential between turns, winding layers and between windings and the core, the key aim of most papers on PT optimisation is to minimize leakage inductance, but stray capacitance was not taken into consideration seriously. Indeed, stray capacitances have a big effect on the performance of the magnetic component to distort the current waveform on the excitation side and reduce the overall efficiency of the converter. Stray capacitance between windings, which is subject to high voltage stresses, induces leakage currents (Lu et al., 2003).

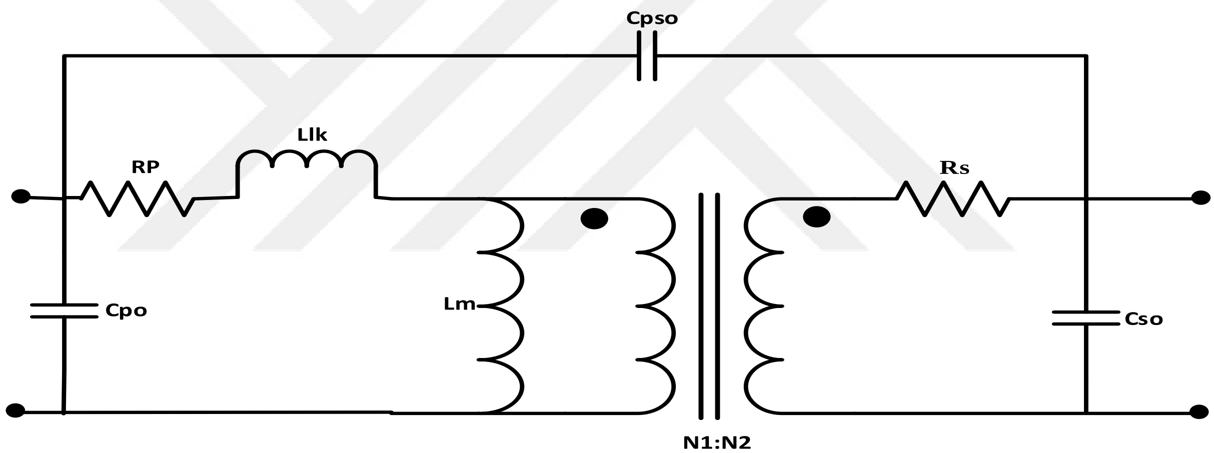

Figure 3.23. Equivalent circuit of the transformer model with self-capacitance and mutual capacitance.

Considering equivalent model of a two-winding PT as seen in Figure 3.23. Where the resistors of the primary and secondary windings are Rp and Rs. While Cpo, Cso and Cpso are used to account for the primary and secondary windings' self-capacitances and the mutual capacitance between the two windings, respectively. It is important to keep Cpso as minimal as possible.

The Cpso mutual capacitance due to the electrical coupling between the primary and secondary windings can be approximately determined by directly shorting of both the primary and secondary sides.

This makes it possible to easily measure the main stray parameters in a planar transformer. In planar transformers, the windings consist of flat and parallel conductors forming a parallel plane capacitance arrangement. In this kind of transformer, the intrawinding capacitance may also be ignored due to the dominant primary-secondary winding capacitance. This capacitance can be the key problem with common mode noise and can easily be calculated as (3.32) (Ouyang et al., 2012). In the case of PTs, as the windings consist of flat and parallel conductors, static layer capacitances can be measured easily. The formulation for the capacitance between two conductive parallel plates is given by,

$$\boldsymbol{C_i = \varepsilon o \varepsilon r \frac{(l + 4b.i)}{h_{\Delta}}} \qquad \boldsymbol{(i = 1, 2, 3 \ldots, u)} \tag{3.32}$$

Where εo is the free space permittivity, εr is the insulating material's relative permittivity, $\boldsymbol{l}$ is the length of the middle leg cross-section, b is the width of the conductor, $\boldsymbol{h_{\Delta}}$ is the distance between the conductive plates and u is the number of overlapping turns.

3.7. Flyback Conventional Transformer

3.7.1. Conventional transformer basic construction

The basic construction of a conventional transformer is it often involves core, windings and insulation. The core can be two halves, one at the top and the other at the bottom. Windings are placed in between these core halves, windings are built over the litze wire, the winding dimensions differ depending on the dimensions of the core of the transformer that we select. There are primary and secondary windings, based on the appropriate requirements, the number of turns will differ for each winding. If the winding turns higher on the secondary side, it is a step-up transformer and if it is vice versa, a step-down transformer. Insulation between the windings is also provided. Selection of materials based on our requirements is one of the transformer's greatest challenges.

Figure 3.24. Conventional transformer. Picture from Wikipedia.

3.7.2. Flyback conventional transformer design formulas

The transformer max-power dissipation per volume is calculated using equation (3.33):

$$Q_{\max dissapation} = \frac{T_s - T_a}{\mathrm{R}_{th} \,.\, (V_C + V_w)} \tag{3.33}$$

R_{th} is the transformer thermal resistance. V_c is the core volume and V_w is the winding volume. T_s is the (Max- allowable temperature) and T_a is the (max-ambient temperature)

$$V_c = 13.5 \text{ a}^3 \tag{3.34}$$

$$V_w = 12.3 \text{ a}^3 \tag{3.35}$$

Then calculating the max-windings current density by using equation (3.36).

$$Jrms = \sqrt{\frac{P_{max,diss}}{\rho_{cu} \cdot K_{cu}}} \tag{3.36}$$

The resistance of copper ρ_{cu} at 90°C is 17 * 10^{-9} Ωm. K_{cu} (Cu. fill factor) =0.67 for solid wire. K_{cu} =0.3 for Litze wire.

Then calculating the min-conductor size by using equation (3.37)

$$A_{pricu} = \frac{I_{prms}}{Jrms_{litze}} \tag{3.37}$$

$$A_{seccu} = \frac{I_{srms}}{Jrms_{litze}} \tag{3.38}$$

The needed winding area is calculated by using equation (3.39).

$$A_{wpri} = \frac{A_{pricu} * N_p}{K_{cu}} \tag{3.39}$$

$$A_{wsec} = \frac{A_{seccu} * N_s}{K_{cu}} \tag{3.40}$$

Then calculating total winding area needed

$$A_{wtotal} = A_{wpri} + A_{wsec} \tag{3.41}$$

The actual windings current density is calculated by using equation (3.42) and (3.43)

$$J_{prms} = \frac{I_{prms}}{A_{pricu}} \tag{3.42}$$

For the secondary winding

$$J_{srms} = \frac{I_{srms}}{A_{seccu}} \tag{3.43}$$

Then calculating the power loss density with using equation (3.44).

$$Q_{\text{pri}\,dissapation} = J_{prms}{}^{2} * \rho_{cu} * K_{cu} \tag{3.44}$$

For the secondary winding

$$Q_{\text{sec}\,dissapation} = J_{srms}{}^{2} * \rho_{cu} * K_{cu} \tag{3.45}$$

The power loss is calculated by using equation (3.46).

$$P_{pri\,cu} = Q_{\text{pri}\,dissapation} * \frac{A_{wpri}}{A_{w}} * V_{w} \tag{3.46}$$

Secondary winding power loss is calculated by using equation (3.47)

$$P_{\text{sec}\,cu} = Q_{\text{sec}\,dissapation} * \frac{A_{wsec}}{A_{w}} * V_{w} \tag{3.47}$$

The transformer total losses are calculated

$$P_{tr} = P_{pri\,cu} + P_{\text{sec}\,cu} + P_{core(watt)} \tag{3.48}$$

The transformer max-power dissipation is calculated by using equation (3.49)

$$P_{maxloss} = P_{\max dissapation} * (V_{C} + V_{W}) \tag{3.49}$$

3.8. Flyback Converter

Fly-back converter is the most widely used SMPS circuit for low-power applications. The key benefits of the flyback circuit are the expense, simplicity and convenience of adding multiple outputs.

Flyback topologies are practical and low costs for systems up to a 100W power level. The circuit can provide single or multiple isolated output voltages and can work over a wide range of input voltage variations. In terms of energy-efficiency, the widely used fly-back converter requires a single controllable switch like MOSFET and the normal switching frequency is in range of 50 kHz.

One of the most significant considerations in the design of the flyback converter is the design of the planar transformer. This converter uses a transformer with an airgap in the core. Magnetic energy is stored in the air gap while the switch is closed. When the switch is opened, the energy from the air gap is delivered to the output.

While we call it a transformer, it is not really a true transformer, but rather an energy storage device, where, during the cycle that the primary switch is on, the energy is stored in the air gap of the core, and during the off time of the primary switch, the energy is delivered to the outputs. Current flows either in the primary or secondary winding, but not both simultaneously. Therefore, it can be thought of somewhat like an inductor with additional secondary windings. In a flyback converter, the transformer performs three roles: energy storage and transmission, ratioing multiple output voltages and (if required) providing electrical insulation.

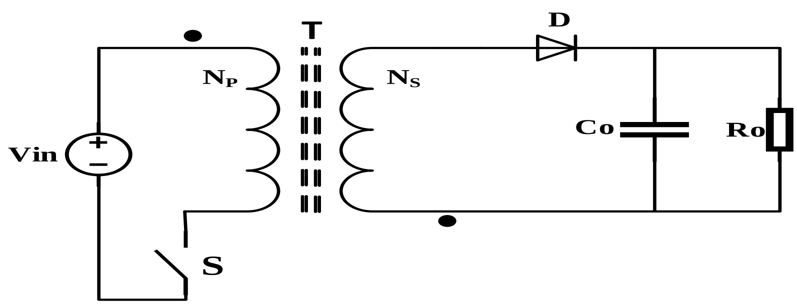

Figure 3.25. Flyback converter.

3.8.1. Principle of operation

In Figure 3.26, the basic operation of the flyback converter is explained. A simplified flyback transformer circuit diagram is presented. This is the initial state of the flyback converter, which assumes various circuit configurations during its operation. Any of these circuit configurations has been referred to here as circuit operating modes.

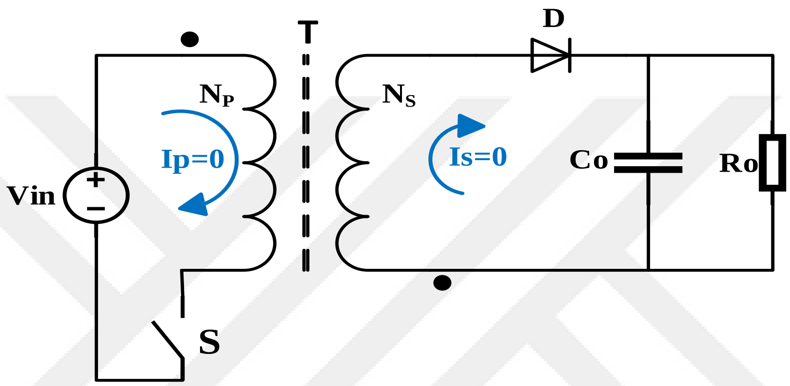

Figure 3.26. Flyback converter initial state.

3.8.1.1. Mode-1 of circuit operation

As can be seen in the circuit diagram in Figure 3.26. When the 'S' switch is on, the transformer primary winding is connected to the input supply with the dotted end connected to the positive side. At this time the diode 'D' connected in series to the secondary winding is set to reverse bias due to the induced voltage in the secondary winding (dotted end potential being higher). Thus, when switch 'S' is turned on, the primary winding is capable of carrying current, but the secondary winding current is interrupted due to the reverse bias diode. The flux formed in the core of the transformer and linking the windings is wholly due to the primary winding current. This circuit mode has been defined here as Mode-1 of circuit operation. At the end of the switch-conduction (i.e. the end of Mode-1) the stored energy contained in the magnetic field of the fly-back inductor-transformer is equal to L_{prim} $I_p{}^2{}_{peak}$, where I_{ppeak} represents the magnitude of the primary current at the end of the conduction cycle. Even if the secondary winding does not operate during this mode, the load is connected to the output capacitor receives uninterrupted current due to the previously charge stored on the capacitor.

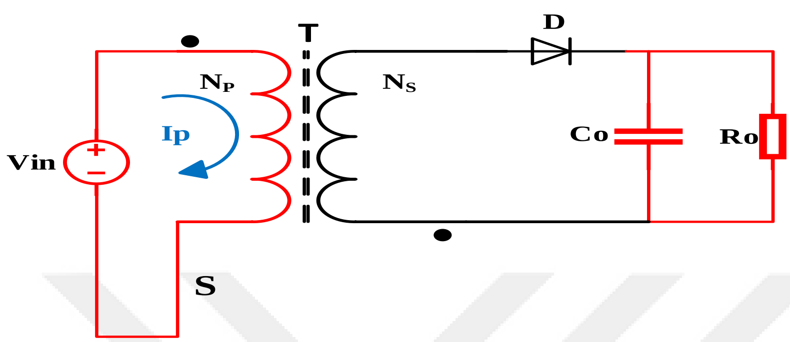

Figure 3.27. Flyback converter switch turned on

3.8.1.2. Mode-2 of circuit operation

Mode-2 of Circuit operation begins when the 'S' switch is cut off after some period of operation. The core's magnetic field begins to decrease, the primary winding current path is disrupted, and according to magnetic induction rules, the voltage polarities are reversed over the windings. Reversing in secondary current and voltage. The reversing of voltage polarities results in a forward bias of the diode in the secondary circuit. As seen in Figure 3.28. Then the secondary diode begins conducting and supplying the energy in the air gap to the output capacitor and the load. In mode-2, while the primary winding current is disrupted due to the switch 'S' being cut off, the secondary winding automatically begins to conduct so that the net MMF generated by the windings does not change suddenly. (MMF is the magneto motive force responsible for generating fluxes in the core.).

The secondary winding, when charging the output capacitor (and feeding the load), begins transmitting the energy from the flyback transformer's magnetic field to the output of the power supply. The secondary current gets enough time to decay to zero if the off cycle of the switch is kept high, and magnetic field energy is fully delivered to the output capacitor and load. The flux linked by the windings stays zero until the next switch-turn-on, and the circuit is operated in a discontinuous flux mode. Alternatively, if the switch's off time is short, until the secondary current decays to zero, the next turn on takes place. The circuit is then operated in a continuous flux mode.

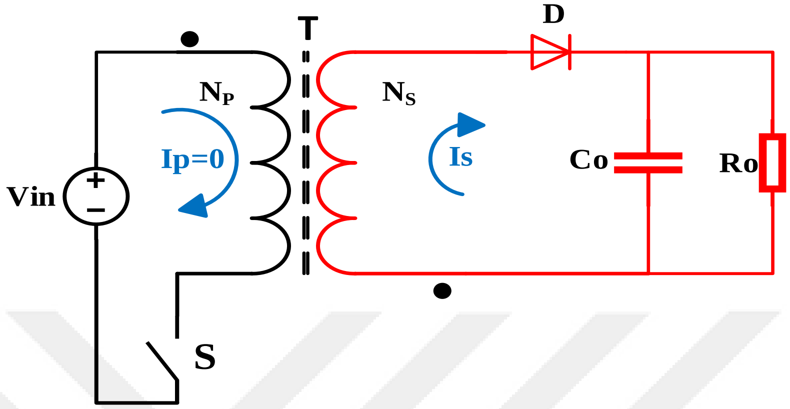

Figure 3.28. Flyback converter switch turned off.

3.8.1.3. Continuous versus discontinuous flux mode of operation

The flyback converter has two modes of operation, a continuous conduction mode (CCM) and a discontinuous conduction mode (DCM). Both CCM and DCM have their own benefits and drawbacks. In general, DCM provides better switching conditions for the rectifier diodes, since the diodes run at zero current only before reversing the bias. Using DCM, the transformer size can be decreased because the average stored energy relative to CCM is low. However, high RMS current is inherently caused by DCM, which raises the MOSFET's conduction loss and current tension on the output capacitors. DCM is also commonly recommended for the operation of high voltage and low output current. In the meanwhile, CCM continuous conduction means that not all the energy stored in the inductor is used for each cycle, so a greater volume of the transformer is required for higher overall energy. Since the current never falls to zero (it's continuous), the ripple of input and output is smaller. However, when non-zero current is switched twice as much, the quantity of switching noise is doubled. CCM is favored for applications with low voltage and high output current. KRP is the ripple factor in full load and minimum input voltage conditions as described in Figure 3.29. KRP = 1 for DCM operation and KRP < 1 for CCM operation. The ripple factor is directly related to the size of the transformer and the RMS value of the

MOSFET current. Even if the conduction loss in the MOSFET can be minimized by reducing the ripple factor, too small a ripple factor forces an increase in transformer size.

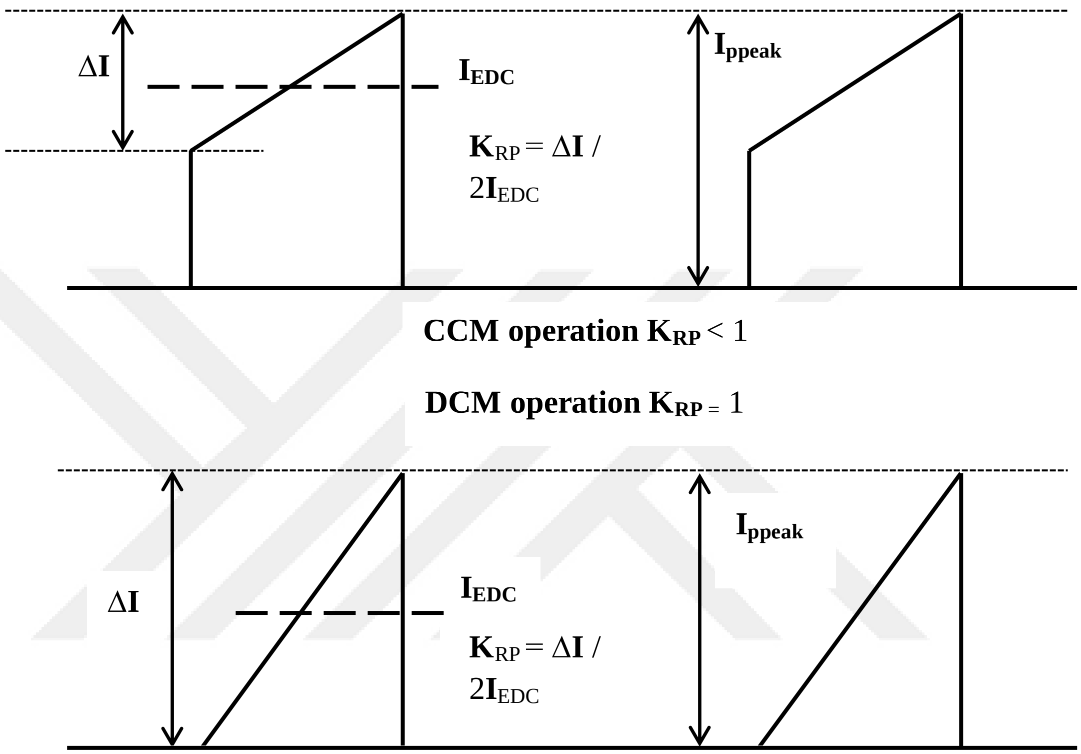

Figure 3.29. MOSFET drain current and ripple factor (K_{RP}).

3.8.2. Design the RCD snubber

As the power MOSFET is cut off, there is a high voltage surge on the drain due to the leakage inductance of the transformer. This excessive voltage on the MOSFET will lead to a breakdown of the avalanche and, finally a failure of the circuit.

Another concept is to design a snubber that absorbs the spikes of high voltages induced by the oscillation between the transformer's leakage inductance and the MOSFET's parasitic capacitance. Some snubber solutions are available in (Nozari., 2011) for transistor switching converters. A snubber with a resistor, capacitor and diode is the most common snubber used, also called the RCD snubber seen in Figure 3.30.

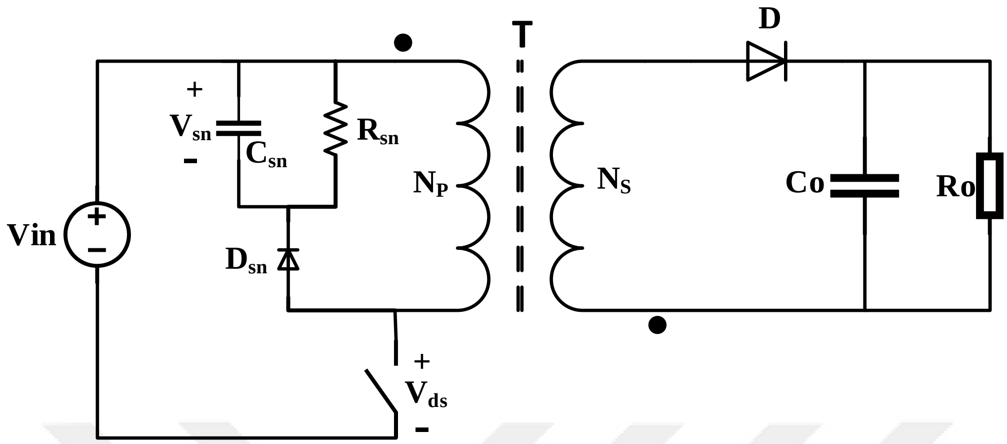

Figure 3.30. Flyback converter with RCD snubber.

To measure the values of the snubber circuit's resistor and capacitor, we derive some formulas.

A way to limit the MOSFET's voltage stresses is to reduce the transformer's leakage inductance, which decreases the oscillation magnitude and thus the MOSFET's voltage stress. In (Prieto et al., 1996), the winding technique for the transformer is addressed, since the MMF in the transformer is more homogeneous, the transformer leakage inductance is decreased. The MMF is more uniformly distributed, by interleaving the windings with each other, resulting in a higher physical coupling between both windings primary and secondary.

$$V_{RO} = \frac{\mathrm{D}_{max}}{(1 - \mathrm{D}_{max})} . Vin_{min} \tag{3.57}$$

n*vo = V_{RO} is the reflected output voltage on primary side.

The snubber circuit's dissipated power is calculated with:

$$P_{sn} = \frac{(V_{sn})^2}{\mathrm{R}_{sn}} = \frac{1}{2} . f_s . \mathrm{L}_{lk} . (I_{ppeak})^2 . \frac{\mathrm{V}_{sn}}{(\mathrm{V}_{sn} - \mathrm{V}_{RO})} \tag{3.58}$$

The voltage of the snubber capacitor V_{sn} should be greater than V_{RO}, and setting V_{sn} to be 2~2.5 times V_{RO} is common. As seen in the equation (3.58), too small a V_{sn} results in a serious loss of the snubber network, fs is the switching frequency, the maximum ripple of the snubber capacitor voltage is gained. Generally 5~10 percent ripple is acceptable.

The leakage inductance is calculated to be 3% of the primary inductance, and then leakage inductance becomes 49.83µH. The snubber circuit power dissipation is calculated by using equation (3.58).

$$P_{sn} = \frac{(V_{sn})^2}{\mathrm{R}_{sn}} \tag{3.59}$$

The snubber capacitor is determined using the equation (3.60) that sets the snubber capacitor's maximal ripple voltage ΔVsn to 10 percent.

$$C_{sn} = \frac{\mathrm{V}_{sn}}{(\Delta \mathrm{V}_{sn} . \mathrm{R}_{sn} . f_s)} \tag{3.60}$$

4. RESULTS AND DISCUSSION

4.1. Flyback Planar Transformer Design Procedure

According to Table 3.1. Was given in section 3.2.3. Planar Cores and according to Appendex 1. Planar EE Core. It seems for me for the rounded primary turns number, E-PLT38 core combinations seem to be the most suitable option, rounding of N_p, N_s results in 44, 4 respectively.

First calculating the total losses in the transformer described in section 3.3. Loss Mechanisms in Magnetics, P_{tr}, by assuming ΔT = 40 °C and E-PLT38 core combination are used P_{tr} is calculated using equation 3.17.

$$R_{th} = \frac{0.06}{\sqrt{\mathrm{Ve}\ (\mathrm{cm}^3)}}$$

$$R_{th} = \frac{0.06}{\sqrt{8460 * 10^{-9}}} = 20.6284$$

$$P_{tr} = \frac{\Delta \mathrm{T}}{R_{th}} = \frac{40}{20.6284} = 1.939\ Watt$$

Calculation of the P_{core} (max-core loss density) with respect to the permissible temperature increase ΔT of the transformer as described in section 3.3.1. Transformer core loss and P_{core} is calculated using equation 3.18.

$$P_{core} = \frac{12 * \ \ 40}{\sqrt{8460 * 10^{-9}}} = 165027.399 \frac{\mathrm{W}}{\mathrm{m3}}$$

$$P_{core(Watt)} = P_{core} * \mathrm{Ve} = 165027.399 * 8460 * 10^{-9} = 1.396\ \mathrm{Watt}$$

B_{peak} (peak flux density) is calculated using equation 3.20.

In this design using 3C97 Ferroxcube power ferrite described in section 3.2.4. Planar core material With its fit parameter listed in table 3.2. And operating frequency 50kHz.

$$B_{peak} = \left[\frac{165027.399}{42.36588301 * 1 * 50000^{1.16}}\right]^{1/2.8}$$

$$B_{peak} = [\ 0.0137954]^{1/2.8} \ = 0.218\ T$$

4.1.1. Flyback planar transformer design

First calculating primary, secondary number of turns according to section 3.2.1. Formulas for flyback transformers using equation (3.1 to 3.3)

When Vin =311 V D_{max}=0.3 V_o=12 V f_s=50000 Hz P_o =50 Watt

$$N_p = \frac{310 * \ 0.3}{50000 * 0.218 * \ 194 \ * 10^{-6}} = 44\ turn$$

Calculating turn ratio (n)**:**

$$\mathrm{n} = \frac{310}{12} * \frac{0.3}{(1 - \ 0.3)} = 11.07 \simeq 11$$

Calculating secondary turn (Ns):

$$\mathrm{Ns} = \frac{44}{11} = 4\ turn$$

Average primary current I_{av} is calculated using equation (3.4) by estimating $\eta = 96\%$

$$I_{av} = \frac{50}{0.96 * \ \ 310} = 0.168\ A$$

Primay peak current I_{ppeak} is calculated using equation (3.5)

$$I_{ppeak} = \frac{0.168}{0.5 * \ 0.3} = 1.12\ A$$

Primary self-inductance L_{pri} is calculated using equation (3.6)

$$L_{pri} = \frac{2 * \frac{50}{0.96}}{50000 * 1.12^2} = 0.001661\ H$$

Air gap length G is calculated using equation (3.7)

$$\mathrm{G} = \frac{44^2 * 4 * 3.14 * 10^{-7} * 194 * 10^{-6}}{0.001661} = 0.000284 \text{ m} = 0.284 \text{ mm}$$

Primary rms current I_{prms} is calculated using equation (3.9**)**

$$I_{prms=} \sqrt{0.3 * \frac{(1.12)^2}{3}} = 0.35417\ A$$

Secondary peak current I_{speak} is calculated using equation (3.10)

$$I_{speak} = 1.12 * \ 11 = 12.32\ A$$

Secondary average current I_{sav} is calculated using equation (3.12)

$$I_{sav} = \frac{50}{12} = 4.16667\ A$$

D_s is calculated using equation (3.13)

$$\mathrm{D}_s = \frac{4.16667}{0.5 * 12.32} = 0.676$$

Secondary rms current I_{srms} is calculated using equation (3.14)

$$I_{srms= 12.32*}\sqrt{\frac{0.676}{3}} = 5.848\ A$$

4.1.2. Turns distribution in the winding area

The symbols N_t and sp are used to denote the number of turns per layer and the spacing between the turns. Then the track width w_{track} can be determined by using equation 4.1. For the available winding width b_{wi}.

$$\mathrm{w}_{track} = \frac{[\mathrm{b}_{wi} - (\mathrm{N}_t + 1).\,\mathrm{sp}]}{\mathrm{N}_t} \tag{4.1}$$

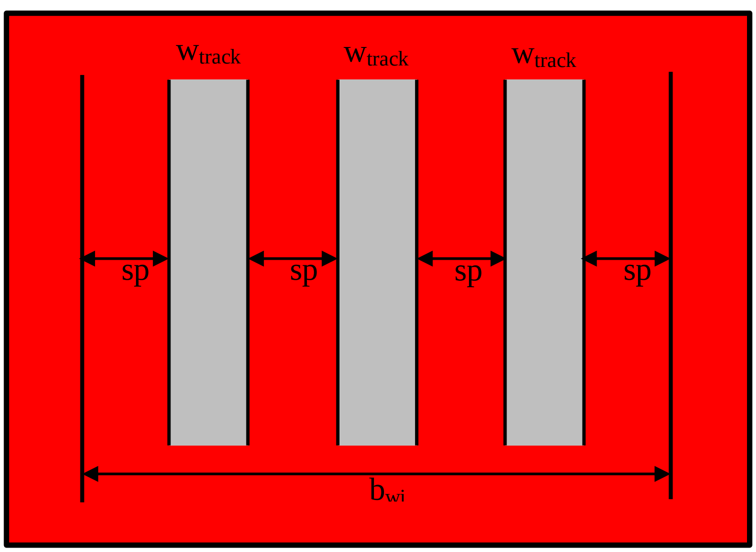

Figure 4.1. Winding width b_{wi}, Track width w_{track} and spacing sp.

It has to be decided how to divide the windings into the existing layers, the currents in the tracks will cause the PCB to overheat, for the reason of thermal expansion in the winding, it is better to distribute the outer layers turns symmetrically with respect to the inner layers turns. The optimum solution is to interleave both layers primary and secondary, this will decrease the proximity effect, as described in detail in Section 3.3.2.2 Proximity effect. In addition, the PCBs winding height and the rounded number of turns will not every time allow for a perfect design.

For cost-price reasons, it is better to use 35 or 70 micrometer thickness for cupper layers, choosing layers thickness have a significant role of the windings temperature increase created by the currents.

Possibility of choosing between 35 or 70 µm copper layers depends on the heat produced by the currents, for the main insulation a distance of 400 µm between both layers is necessary, a 200 µm distance is sufficient between the winding layers and should consider a 50 µm solder mask layer in up and down of the PCB. .

The winding track width depends on the current and the max-current density that is permitted, according to the rule of thumb the w_{track} and sp must greater than 150 µm for a 35 µm layer, and must greater than 200 µm for 70 µm layers.

In this design we used the Ferroxcube power ferrite 3C97 and a Core EPLT38 described in section 3.2.3 Planar Cores and in table 3.1. Standard planar EE cores for industrial use and according to Appendex 1. Planar EE Core, the available winding width for E-E38& EPLT38 cores is 11.315mm by using equation (3.1 to 3.3)

$N_p = 44\ turn$ and $N_s = 4\ turn$

The 44 turns in the primary winding is symmetrically divided by using 4 layers, the winding width exist of the EPLT-38 is 11.315mm as seen in table 3.1. Standard planar EE cores for industrial use, so the choice is made for primary winding 4 layers, each containing 11 turns, the smaller layers number in the PCB will bring down the cost-price.

Therefore for four turns in the secondary winding, two layers each containing 2 turns are chosen, in table 4.1. The construction of the six-layer design is presented.

For an economical design, we assumed 300 µm spacing between the tracks, so 4 layers with 11 turns each are chosen for the primary winding.

$I_{prms} = 0.35417\ A$ $\qquad$ *calculated* using equation(3.9)

For the turns in the primary winding the track widths is calculated using equation 4.1. And is about. 701.36 µm, this value does not make any overheating by 0.35417 A of primary RMS current, the spacing between tracks =300 µm.

$$\mathrm{w}_{track} = \frac{[11315 - (11+1).300]}{11} = 701.36\ \mu\mathrm{m}$$

So for the secondary winding 2 layers with 2 turns each are used, according to figure 4.2 using the calculated secondary RMS current with equation (3.11) of 5.848 A

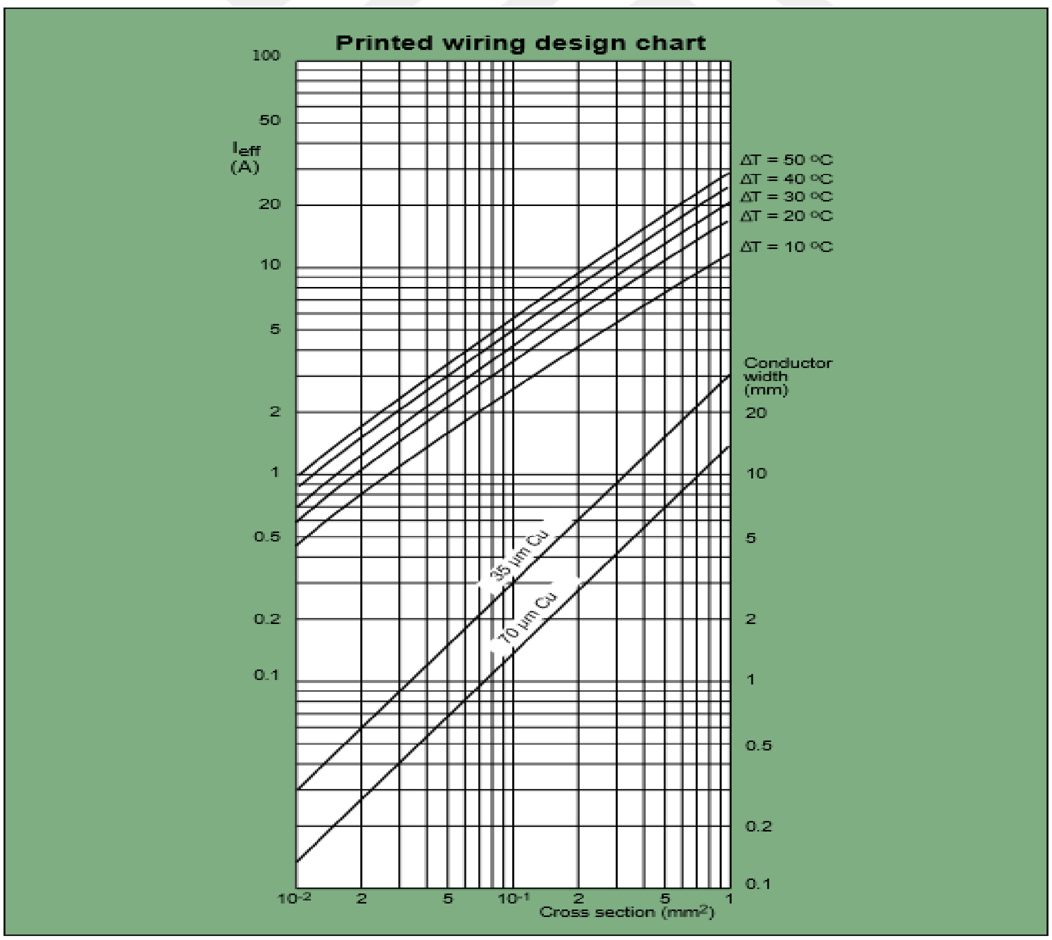

Figure 4.2. Relations between temperature increase, PCB tracks dimensions and current.

Using the calculated secondary RMS current of 5.848 A, and according to figure 4.2. By choosing 70 µm thickness layer design with temperature rise ΔT = 40 °C the width of tracks should be≥ 1750 µm.

The secondary winding track width (w_{track}) is calculated by using equation **(**4.1**)** returns 5.2075 mm, inclusive mains insulation.

$w_{\mathrm{track}} = \frac{[11315-(2+1).300]}{2} = 5207.5\ \mu\mathrm{m}$ Which is beggar than 1750 µm

Table 4.1. Six layers design of PCB winding . S.M. = Solder mask P. =primary winding S. =secondary winding I. =insulation.

Layers arrangement	No. of Turns	µm
S.M.		50
P.	11	70
I.		200
P.	11	70
I.		400
S.	2	70
I.		200
S.	2	70
I.		400
P.	11	70
I.		200
P.	11	70
S.M.		50
TOTAL		1920

This 6-layer of 70µm tracks design should work according to specifications. The thickness of the printed circuit board is about 1920µm, it means that we can use the standard planar E-PLT38 combination with 4.22 mm winding window. However, its winding window is large, so a more proper solution would be a core with 2 mm winding window.

In practical cases, the eddy current effects in the conductor will not result only from its current alternating field (skin effect) but also from the fields of other conductor in the adjacent, this called the proximity effect, this effect will severely reduce when interleaving arrangement between both layers primary and secondary are used (Maswood, and Song., 2003), described in section 3.4.3. Reduction of copper loss due to proximity effect, this is because secondary and primary currents not flow in same directions but in opposite directions, so their magnetic fields will be canceled.

For reducing losses interleaving technique is used between primary and secondary winding of the transformer, so interleaving winding as shown below, can greatly decrease proximity loss described in section 3.4.3 Interleaved winding.

The secondary winding track width (w_{track}) is calculated by using equation (4.1) when choosing 4 layers with 1 turn each for secondary winding so track width returns 10.715mm, inclusive mains insulation

$w_{track} = \frac{[11315-(1+1).300]}{1} = 10715\ \mu m$ Which is beggar than calculated width 1750 µm

So using 4 layers with 11 turn each for primary winding and 4 layers with 1 turn for secondary winding, the layer arrangement is shown below.

Table 4.2 Eight layers design of PCB winding (interleaving) S.M. = solder mask
P. =primary winding S. =secondary winding I. =insulation.

Layers Arrangement	No. of Turns	µm
S.M.		50
P.	11	70
I.		400
S.	1	70
I.		400
P.	11	70
I.		400
S.	1	70
Ins.		400
P.	11	70
I.		400
S.	1	70
I.		400
P.	11	70
I.		400
S.	1	70
S.M.		50
TOTAL		3460

This 8-layer of 70 µm tracks design should work according to specifications, the thickness of the printed circuit board is about 3460 µm; it means that we can use the standard planar E-PLT38 combination with 4.22 mm winding window. However, its winding window is a bit large, so a more proper solution would be a core with 3.5 mm winding window.

4.1.3. Losses in flyback planar transformer for the above core calculated with:

Dimensions reference to figure 3.4 (b), typical planar core shapes EE and EPLT and table 3.1. Standard planar EE cores for industrial use and according to Appendex 1. Planar EE Core

$$\mathrm{G} = (E - F)/4 \tag{4.2}$$

$$\mathrm{MLT} = 2(F + C) + 2 * 3.14 * G = 2(7.6 + 25.4) + 2 * 3.14 * 5.6575 = 101.5 \tag{4.3}$$

$$\mathrm{R}_{dc} = \frac{\rho * \mathrm{l}}{\mathrm{A}} \tag{4.4}$$

The resistivity of copper ρ at 100 °C is assumed to be $17*10^{-6}$mm

Primary cupper loss**:**

$$\mathrm{R}_{dc} = MLT * \mathrm{N}_p * \frac{\rho_{\mathbf{cu}}}{\mathrm{A}} \tag{4.5}$$

$$\mathrm{R}_{dc\ pri} = 101.5 * 44 * \frac{1.7*10^{-5}}{701.36*10^{-3}*0.0712} = 1.52\ ohm$$

$$\mathrm{P}_{pri\ cu} = I_{prms}\ ^{2} * \mathrm{R}_{dc\ pri} \tag{4.6}$$

$$\mathrm{P}_{pri\ cu} = 0.35417^2 * 1.52 = 0.1907\ watt$$

Secondary cupper loss:

$$\mathrm{R}_{dc} = MLT * \mathrm{N}_s * \frac{\rho_{cu}}{\mathrm{A}}$$

$$\mathrm{R}_{dc\ sec} = 101.5 * 4 * \frac{1.7 * 10^{-5}}{10715 * 10^{-3} * 0.0712} = 0.009047\ ohm$$

$$\mathrm{P}_{\sec\ cu} = I_{secrms}{}^{2} * \mathrm{R}_{dc\ sec} \tag{4.7}$$

$$\mathrm{P}_{\sec cu} = 5.848^2 * 0.009047 = 0.3094\ watt$$

Total Cupper loss:

$$\mathrm{P}_{\mathrm{Tt\ Cu}} = \mathrm{P}_{pri\ cu} + \mathrm{P}_{\sec cu} = 0.1907 + 0.3094 = 0.5\ \mathrm{watt} \tag{4.8}$$

Then P_{core} (max-core loss density) is calculated as a function to the permissible temperature increase ΔT, as detailed in section 3.3.1. Transformer core loss and using equation 3.18.

$$P_{core} = \frac{12\ .\ 40}{\sqrt{8460 * 10^{-9}}} = 165027.3994\ \ \mathrm{W/m3}$$

Core loss is calculated by using equation 3.21.

$$P_{core(Watt)} = P_{core} * \mathrm{Ve}\ = 165027.3994 * 8460 * 10^{-9} = 1.396\ \mathrm{Watt}$$

Total loss in Transformer is calculated

$$P_{\mathrm{tr}} = \mathrm{P}_{\mathrm{Tt\ Cu}} + P_{core(Watt)}\ = 0.5 + 1.3961 = 1.896\ \mathrm{watt} \tag{4.9}$$

Transformer efficiency is calculated using equation 3.16

$$\eta = \frac{P_o}{P_0 + P_{\text{tr}}} \cdot 100\% = \frac{50}{51.896} * \ 100\% = 96.35\%$$

The layers arrangement is shown below, and we use half primary layer in up and down of winding layer arrangement, this represents an improved (enhanced) interleaving arrangement. That makes the up and down layers parallel with each other and in series with other primary layer turns, lower MMF value is obtained, as described in section 3.4.3. Interleaved windings for Reduction of copper loss due to proximity effect.

Table 4.3 Eight layers design (improved interleaved arrangement) S.M. = solder mask P. =primary winding S. =secondary winding I. =insulation.

Layers arrangement	No. of Turns	µm
S.M.		50
½ P.	11	70
I.		400
S.	1	70
I.		400
P.	11	70
I.		400
S.	1	70
I.		400
P.	11	70
I.		400
S.	1	70
I.		400
P.	11	70
I.		400
S.	1	70
I.		400
½ P.	11	70
S.M.		50
TOTAL		3930

This 8-layer of 70 µm tracks design should work according to specifications, the thickness of the printed circuit board is about 3930 µm, it means that we can use the standard planar E-PLT38 combination with 4.22 mm winding window. And its winding window is proper solution.

4.2. Snubber Calculations

The Snubber circuit is seen in figure 4.3.

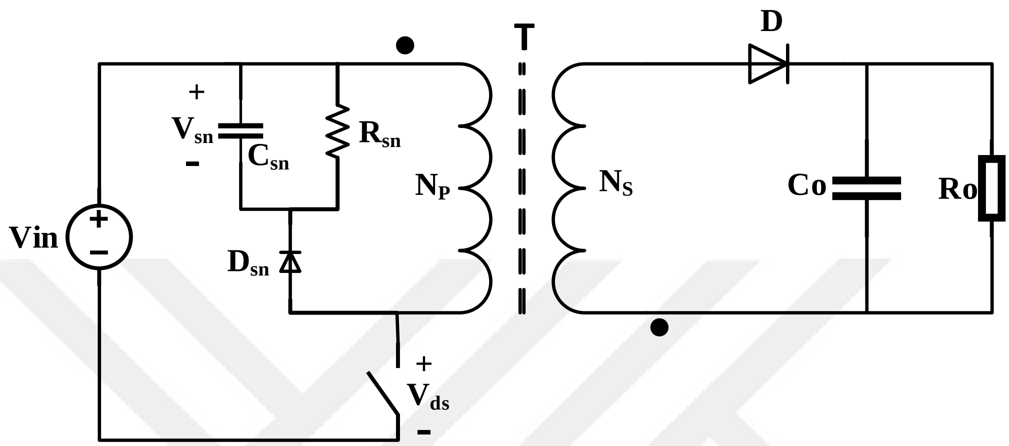

Figure 4.3. Flyback converter with RCD snubber.

We derive some formulas for calculating the values of capacitor and resistance of a snubber circuit, the voltage loop for the snubber circuit is calculated using equation (3.57).

$$V_{RO} = \frac{0.3}{(1-\ 0.3)} * 310 = 132.857 \text{ volt}$$

n*vo = V_{RO} is the primary side reflected output voltage

The leakage inductance is estimated to be 3% of the primary inductance then leakage inductance becomes 49.83µH, the snubber circuit power dissipation is calculated by using equation (3.58). And it becomes:

$$V_{sn} = 2.5 * \mathrm{V}_{RO} = 2.5 * 132.857 = 332\ volt$$

$$\mathrm{L}_{lk} = 0.03 * L_{pri} = 0.03 * 0.001661\ = 49.83\ \mu H$$

$$P_{sn} = \frac{(V_{sn})^2}{\mathrm{R}_{sn}} = \frac{1}{2} * 50000 * 49.83 * 10^{-6} * (1.12)^2 * \frac{332}{(332 - 132.857)}$$

$$= 2.605w$$

Then calculating the snubber resistor by using equation (3.59)

$$R_{sn} = \frac{(V_{sn})^2}{\mathrm{P}_{sn}} = \frac{(332)^2}{2.605} = 42.312k\Omega$$

The capacitor for the snubber is calculated using equation (3.60), by assuming ΔV_{sn} (max-ripple voltage) of the capacitor to 10%, then the value of the capacitance:

$$C_{sn} = \frac{332}{(33.2 * 42.312 * (10)^3 * 50000)} = 4.727\ nF$$

4.3. Flyback Conventional Transformer Design

First calculating primary, secondary number of turns according to section 3.2.1. Formulas for flyback transformers using equation (3.1 to 3.3)

When Vin =311 V D_{max}=0.3 V_o=12 V f_s=50000 Hz P_o =50 Watt

and using core type EE 40/16/12 , 3C92 B=0.190 T

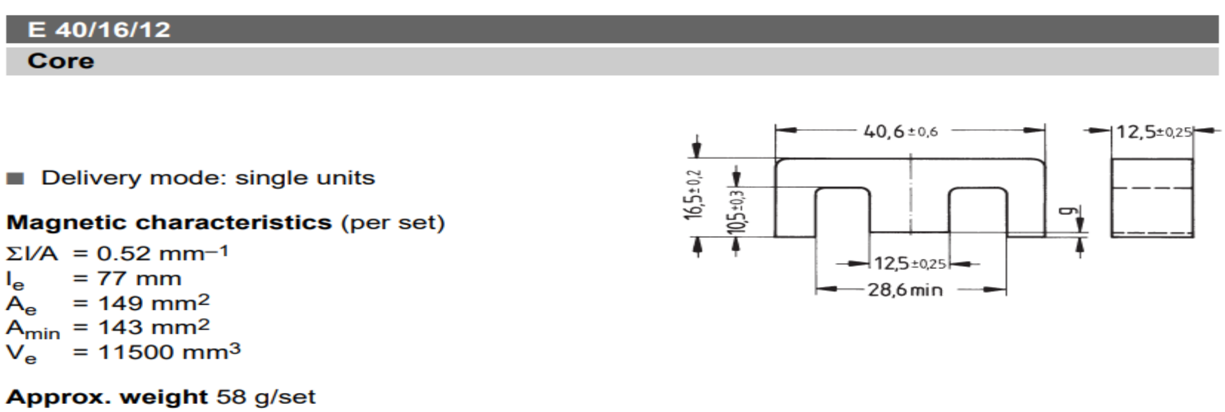

Figure 4.4. E40/16/12 core half.

$$N_p = \frac{310 * \ 0.3}{50000 * 0.190 * \ 149 \ * 10^{-6}} = 65.7 \ turn \simeq 66 \ turn$$

Calculating turn ratio (n)**:**

$$\text{n} = \frac{310}{12} * \frac{0.3}{(1 - \ 0.3)} = 11.07 \simeq 11$$

Calculating secondary turn (Ns):

$$\text{Ns} = \frac{66}{11} = 6 \ turn$$

Average primary current I_{av} is calculated using equation (3.4) by estimating $\eta = 88\%$

$$I_{av} = \frac{50}{0.88 * \ \ 310} = 0.1833 \ A$$

Primay peak current I_{ppeak} is calculated using equation (3.5)

$$I_{ppeak} = \frac{0.1833}{0.5 * \ 0.3} = 1.222 \ A$$

Primary self-inductance L_{pri} is calculated using equation (3.6)

$$L_{pri} = \frac{2 * \frac{50}{0.88}}{50000 * 1.222^2} = 0.001522 \ H$$

Air gap length G is calculated using equation (3.7)

$$G = \frac{66^2 * 4 * 3.14 * 10^{-7} * 149 * 10^{-6}}{0.001522} = 0.0005356 \text{ m} = 0.5356 \text{ mm}$$

Primary rms current I_{prms} is calculated using equation (3.9**)**

$$I_{prms=} \sqrt{0.3 * \frac{(1.222)^2}{3}} = 0.3864\, A$$

Secondary peak current I_{speak} is calculated using equation (3.10)

$$I_{speak} = 1.222 * 11 = 13.442\, A$$

Secondary average current I_{sav} is calculated using equation (3.12)

$$I_{sav} = \frac{50}{12} = 4.16667\, A$$

D_s is calculated using equation (3.13)

$$\mathrm{D}_s = \frac{4.16667}{0.5 * 13.442} = 0.620$$

Secondary rms current I_{srms} is calculated using equation (3.14)

$$I_{srms= 13.442*} \sqrt{\frac{0.620}{3}} = 6.11\, A$$

The transformer max-power dissipation per volume is calculated using equation (3.33):

$$V_c = 13.5 * 12.5^3 * \ 10^{-9} = 2.6367 * 10^{-5} \ \text{m}^3$$

$$V_w = 12.3 * 12.5^3 * \ 10^{-9} = 2.4 * 10^{-5} \ \text{m}^3$$

By assuming Ts (max-allowable temperature) = 90°C and Ta (max-ambient temperature) = 50°C. Rth (thermal resistance) = 20 Δ°C/W from datasheet.

$$Q_{\max dissapation} = \frac{90 - \ 50}{20\,.(2.6367 * 10^{-5} + 2.4 * 10^{-5}\,)} = 39708.539 \ w/\text{m}^3$$

Then calculating the max-windings current density by using equation (3.36). The resistance of copper ρ_{cu} at 90°C is $17*10^{-9}$ Ωm. K_{cu} (Cu. fill factor) =0.67 for solid wire, K_{cu} =0.3 for litze wire.

$$Jrms_{\ solid} = \sqrt{\frac{39708.539}{17 * 10^{-9} * \ 0.67}} = \ 1867153.797 \ \frac{A}{\text{m}^2} = 1.867 \ \frac{A}{\text{mm}^2}$$

$$Jrms_{\ litze} = \sqrt{\frac{39708.539}{17 * 10^{-9} * \ 0.3}} = \ 2790338.338 \ \frac{A}{\text{m}^2} = 2.79 \frac{A}{\text{mm}^2}$$

Calculating the min-conductor size by using equation (3.37)

$$A_{\ pricu} = \frac{0.3864}{2.79} = \ 0.13849 \ \text{mm}^2$$

$$A_{\ seccu} = \frac{6.11}{2.79} = \ 2.19 \ \text{mm}^2$$

The needed winding area is calculated by using equation (3.39).

$$A_{wpri} = \frac{0.13849 * 10^{-6} * 66}{0.3} = 30.4678 \text{ mm}^2$$

$$A_{wsec} = \frac{2.19 * 10^{-6} * 6}{0.3} = 43.8 \text{ mm}^2$$

Then calculating total winding area needed

$$A_{wtotal} = 30.4678 + 43.8 = 74.268 \text{ mm}^2$$

For this transformer Aw (total-winding Area) is 217 mm^2 this will be in the limit, the actual windings current density is calculated by using equation (3.42) and (3.43)

$$J_{prms} = \frac{0.3864}{0.13849 * 10^{-6}} = 2.79 \frac{A}{\text{mm}^2}$$

$$J_{srms} = \frac{6.11}{2.19 * 10^{-6}} = 2.79 \frac{A}{\text{mm}^2}$$

Calculating the power loss density with using equation (3.44).

$$Q_{\text{pri}\,dissapation} = 2.79^2 * 17 * 10^{-9} * 0.3 = 39.699 \text{ kw/m}^3$$

Calculating the power loss density for the secondary winding

$$Q_{\text{sec}\,dissapation} = 2.79^2 * 17 * 10^{-9} * 0.3 = 39.699 \text{ kw/m}^3$$

The power loss is calculated by using equation (3.46).

$$P_{pri\,cu} = 39.699 * 10^3 * \frac{30.4678}{217} * 2.4 * 10^{-5} = 133.774mw$$

Secondary winding power loss is calculated by using equation (3.47)

$$P_{sec\ cu} = 39.699 * 10^3 * \frac{43.8}{217} * 2.4 * 10^{-5} = 192.3\ mw$$

The transformer total loss is calculated with assuming core loss of 1.62 W

$$P_{tr} = 133.774mw + 192.3mw + 1.62 = 1.946\ w$$

The transformer max-power dissipation is calculated by using equation (3.47)

$$P_{maxloss} = 39708.539 * (2.6367 * 10^{-5} + 2.4 * 10^{-5}) = 2\ w$$

Summary

Primary turns Number: 66

Secondary turns Number: 6

Conductor size for the Primary winding: 0.13849 mm^2 (using litze wire)

Conductor size for the Secondary winding: 2.19 mm^2 (using litze wire)

Inductance of the primary winding: 0.001522 H

Length of the air gap: 0.536 mm

Table 4.4. Comparision difference between planar and conventional transformer in flyback converter

	Planar transformer	Conventional transformer
Core weight (gram)	18	58
Core dimension (mm)	38.1*25.4*12.07	40.6*12.5*33
Core height (mm)	12.07	33
Area (mm^2)	967.74	507.5
Core volume (m^3)	$0.05926*10^{-4}$	$0.26367*10^{-4}$
Winding volume (m^3)	$0.05399 *10^{-4}$	$0.24*10^{-4}$
losses	1.896 watt	1.946 watt

4.4. Simulation Study

For this thesis, the simulation was performed in the Matlab / Simulink software, the flyback SMPS simulation is performed using the specification of the calculated parameters according to table 4.5 employing the improved PT has been designed, this circuit power value was set according to the required input and output voltages specification of the flyback converter showed in table 4.5.

Table 4.5. Specifications of flyback converter

Description	Value
Input voltage (Vin)	311 V
Output voltage (V_o)	12 V
Output power (P_o)	50 W
Transformer primary inductance (L_{pri})	1.661 mH
Transformer secondary inductance (L_{sec})	13.727μH
Switching frequency ($f_{s)}$	50 KHZ
Transformer turn ratio (n)	11
Primary winding turns number (N_p)	44
Secondary winding turns number (N_s)	4

The fly-back switch mode power supplies have a closed loop control for regulation and control of output voltage, this is by adding a controller circuit (feedback) to the flyback converter, this controller modifies the switch operating ratio to keep output voltage within an acceptable low range of ripple voltage around the required value of the output, by comparing reference value of +12 V with the measured output voltage of the flyback circuit, the general scheme of the simulation study is given in Fig.4.5

One of the most important conditions in the applied circuit is to adjust output voltage at +12 V constant, from the simulation study the circuit was controlled by a PI controller, for controlling the circuit a PWM signal must be generate to operate the switch, for this purpose the PWM manufacturer has been used, the switching frequency of the circuit is processed in the PI block by comparing the output voltage of the circuit with the desired voltage, the switching frequency of 50 kHz is used for our practical work.

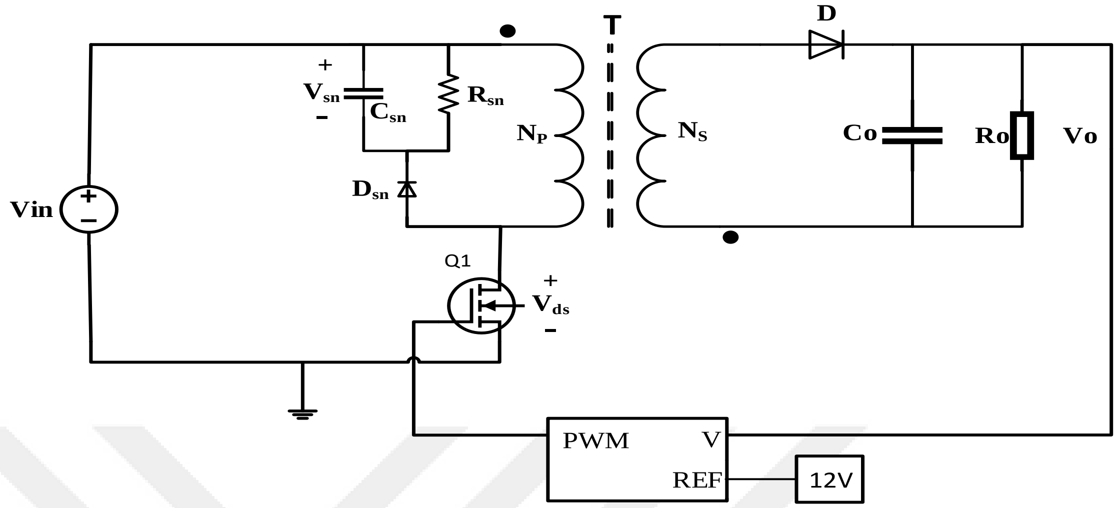

Figure 4.5. Simulation study general diagram of flyback converter.

The PWM signal is generated by the system at which the duty ratio and frequency are calculated and this generated signal is applied to the end of the switch gate.

When the switch is in transition, it begins to store energy in the transformer and current does not flow through the output diode since the output of the transformer is reverse polarized to its input, then the load is fed through the parallel capacitor. When the switch enters the cut-off, the current starts to increase in the secondary and the diode becomes forward biased, then it begins to transfer the stored energy to the output, the graph of output voltage is seen in figure 4.6.

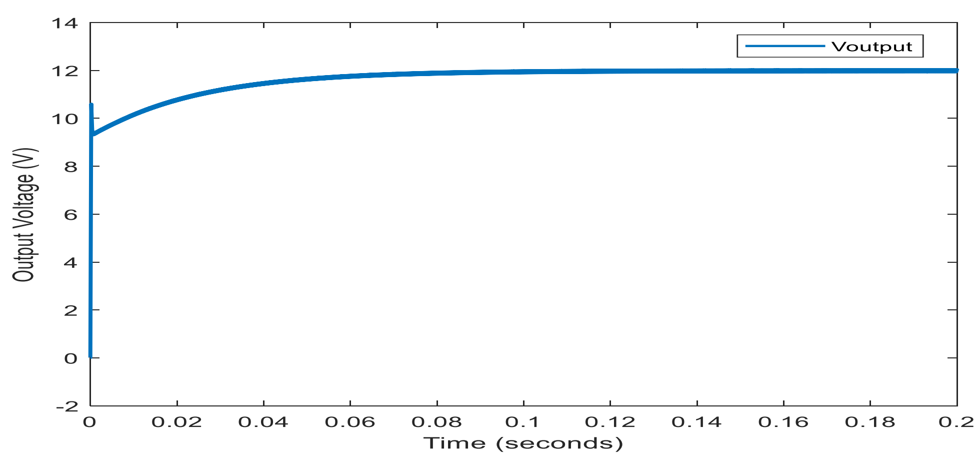

Figure 4.6. Output voltage graph.

With the feedback block controller, it provides constant output voltage of +12V the controller unit corrects the output voltage and adjusts the voltage that it receives from the output, this was done by comparing the receiving voltage from the output with the desired voltage, this is essential for applications where flyback converters are widely used, if these devices are not supplied with the desired voltage, damage or malfunction occurs, the operating output power of the circuit is given in Figure 4.7.

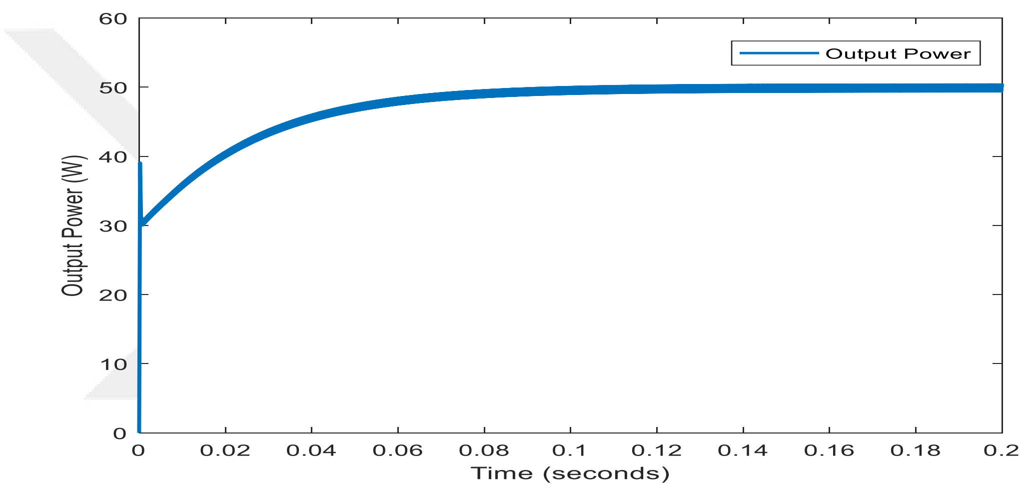

Figure 4.7. Output power graph.

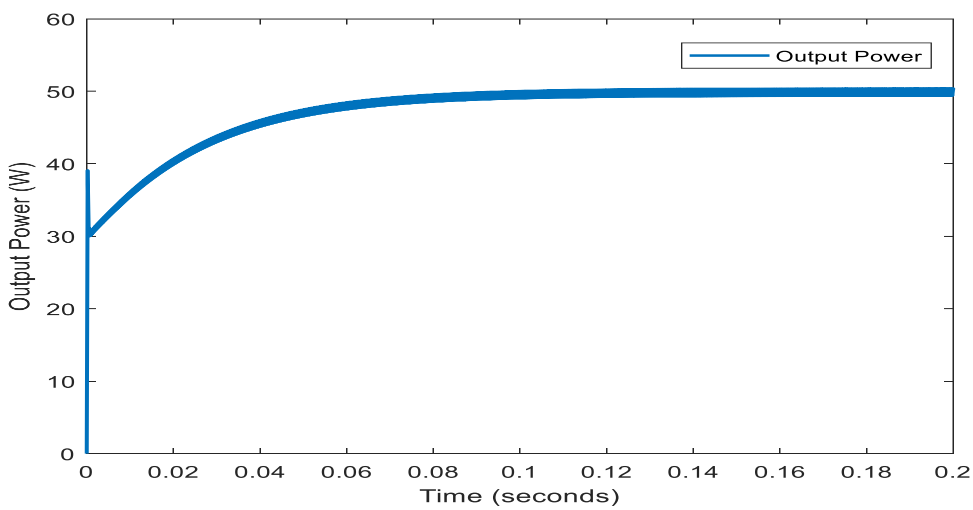

(a)

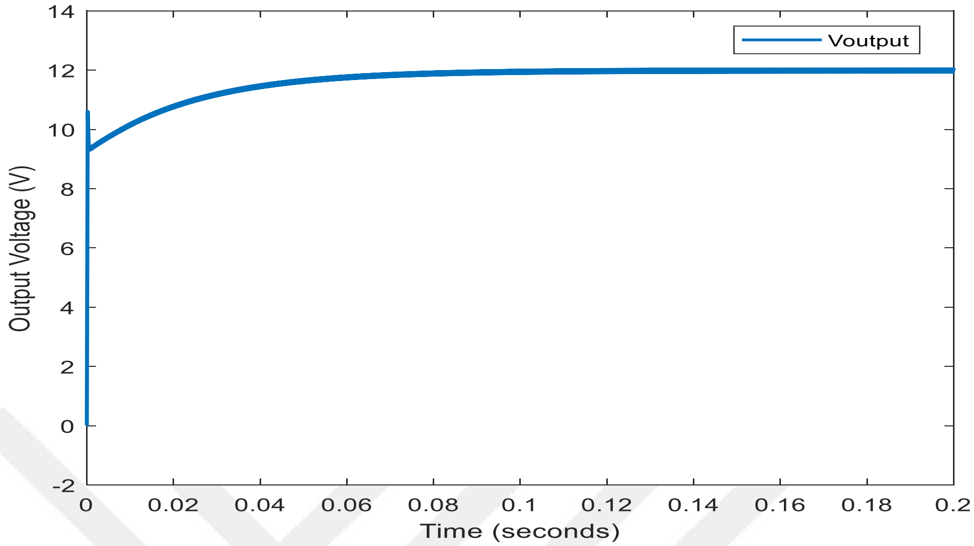

(b)

Figure 4.8. Output power and output voltage graph.

The proposed circuit was operated at output power of 50W, when the effect of output power on output voltage is examined, the controller used successfully keeps the output voltage constant with output power of 50 W, and the controller keeps the output voltage constant by using the switching frequency of 50 kHz.

Another important parameter of the study is the primary side current of the transformer, in figure 4.9 the primary current graph is given.

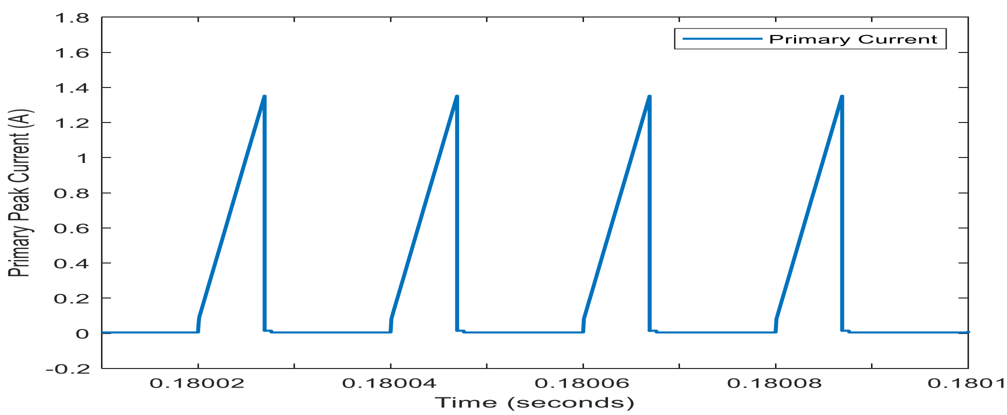

Figure 4.9. Primary current graph.

The primary current given in figure 4.9. As seen the circuit primary current decreases to zero at certain intervals it has a triangle wave shape, also this value is the current passing through the switch and this current value is an important parameter for choosing a switch, this current has a peak value of about 1.4 Amps.

The suppression cell is connected in parallel to the ends of the used transformer; it is used to reduce the Voltage stress on the switch (Nozari., 2011), the suppressor cell was explained in detail in section 3.8.3. Design The RCD Snubber**,** the capacitor and resistance values of the suppressor cell are calculated in chapter 4.2. Snubber Calculations**,** calculated values are used in the simulation if the suppressor cell was not used the voltage on the switch would be very high, considering that the switch we are using can withstand a maximum voltage of 440 volts, it is imperative to use a suppressor cells for the flyback circuit, the suppressor cell protects the switch by capturing the voltage produced by the leakage inductance of the transformer the switch voltage graph is given in figure 4.10.

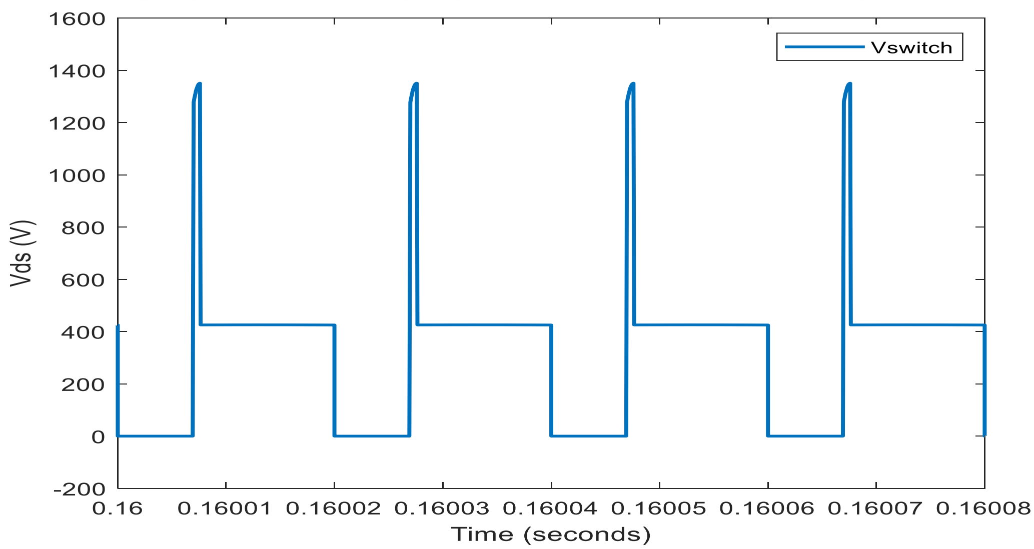

Figure 4.10. Switch voltage signal.

In order to easily compare the simulation study of the proposal circuit with calculation results, the primary voltage-current and secondary voltage-current graph are given in figure 4.11 and in figure. 4.12.

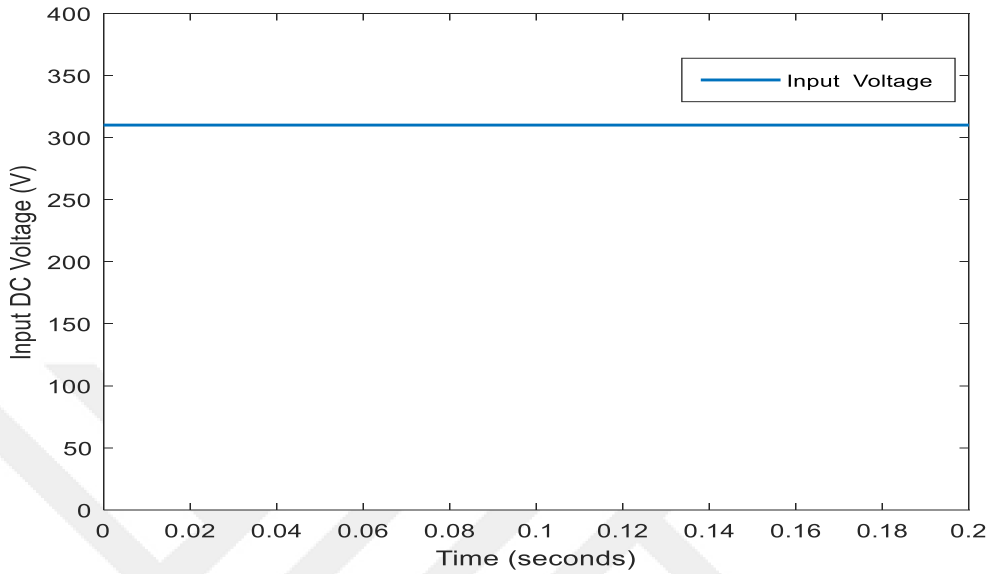

(a)

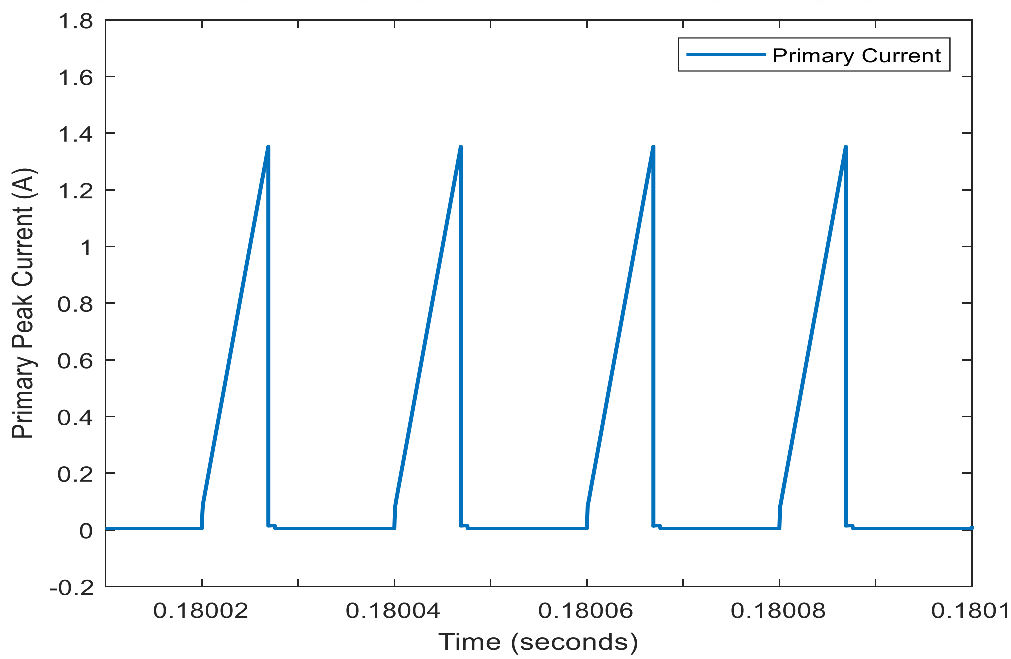

(b)

Figure 4.11. Primary voltage current signal.

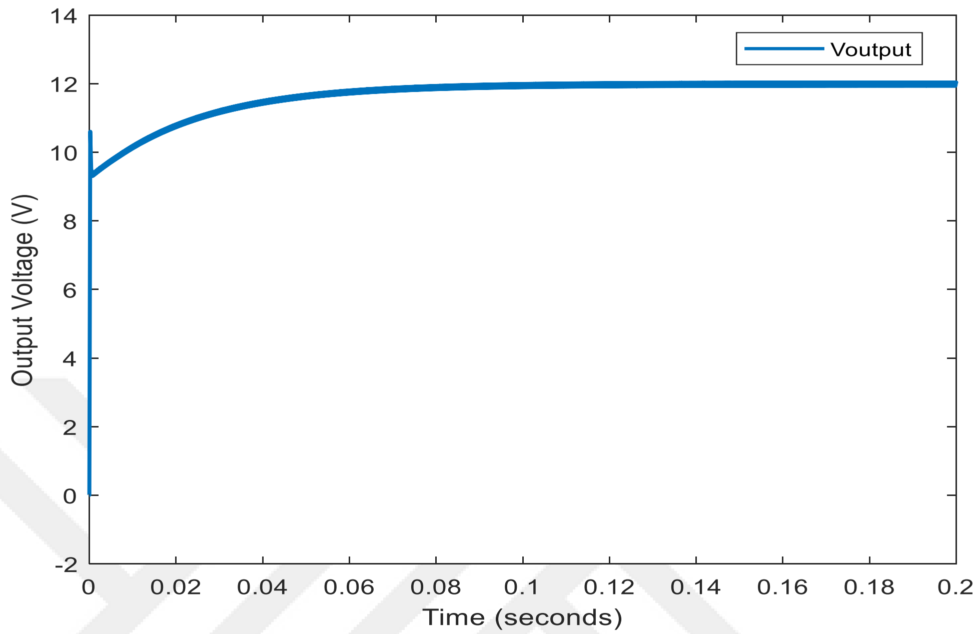

(a)

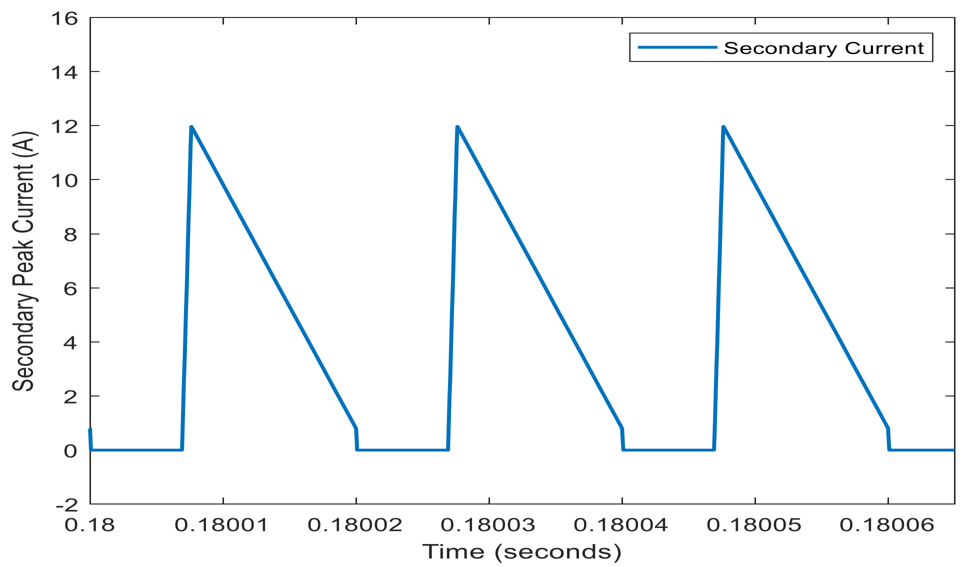

(b)

Figure 4.12. Secondary voltage current signal.

The PWM signal necessary for the circuit operation, and the PWM signal sent to the end of the switch gate is shown in figure 4.13.

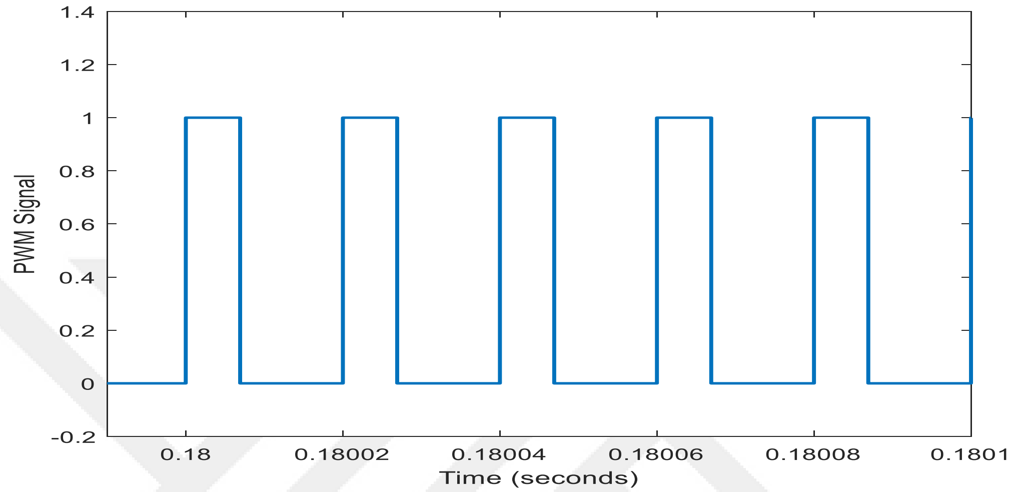

Figure 4.13. PWM signal.

In figure 4.13 the circuit frequency was very high while the frequency was 50 kHz, also when we look at the PWM signals in fixed frequency switching in fig 4.13, the periods do not change when the output load is 50 watts and a constant load is observed.

In addition, the input current signal and PWM signal are shown in fig 4.14 in the same time interval.

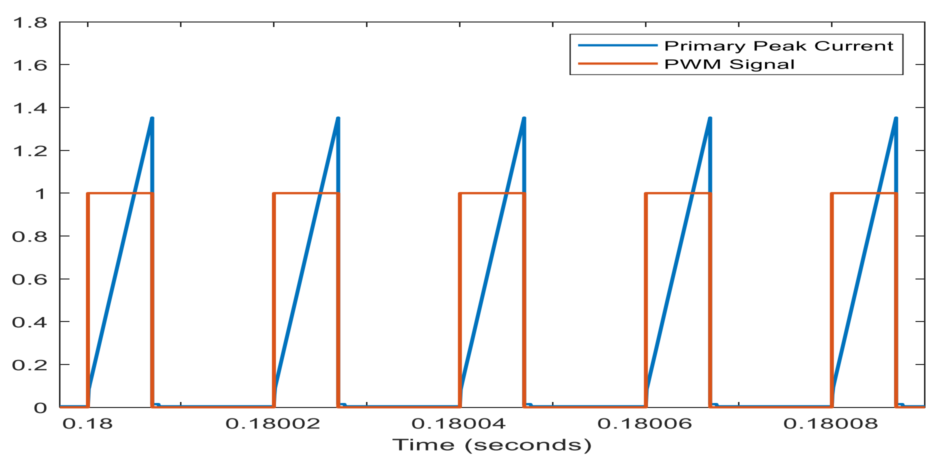

Figure 4.14. Primary current and PWM signal.

As seen in figure 4.14 the primary current increases during the time the switch is in transmission, when the switch breaks in the transmission the PWM signal is "0" and the input current decreases to zero, this input current is zero while the switch is in the cut-off position, during this time, the transformer energy is transferred to the output and current begins to flow from the output.

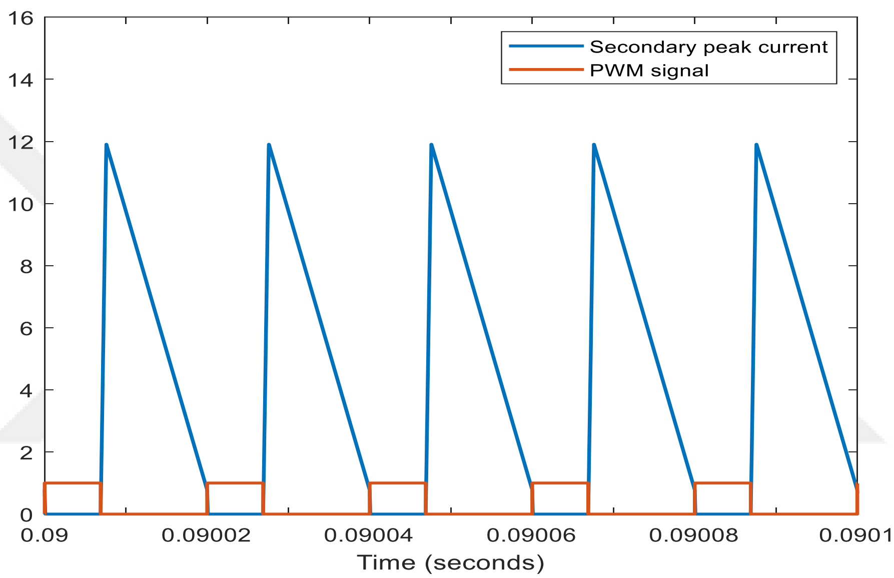

Figure 4.15. Secondary current and PWM signal.

A comparison of secondary current with a PWM signal in the same range is shown in figure 4.15.

As shown in figure 4.15, the current flowing in the secondary is zero while the switch is in transmission, since the transformer is reverse polarized and there is a diode at the output the current does not flow, when the switch turns off current begins to flow on the secondary and the secondary current increases individually; the secondary current feeds the output load and the output capacitor they are fed after secondary current passes through diode. Output current is given in Figure 4.16.

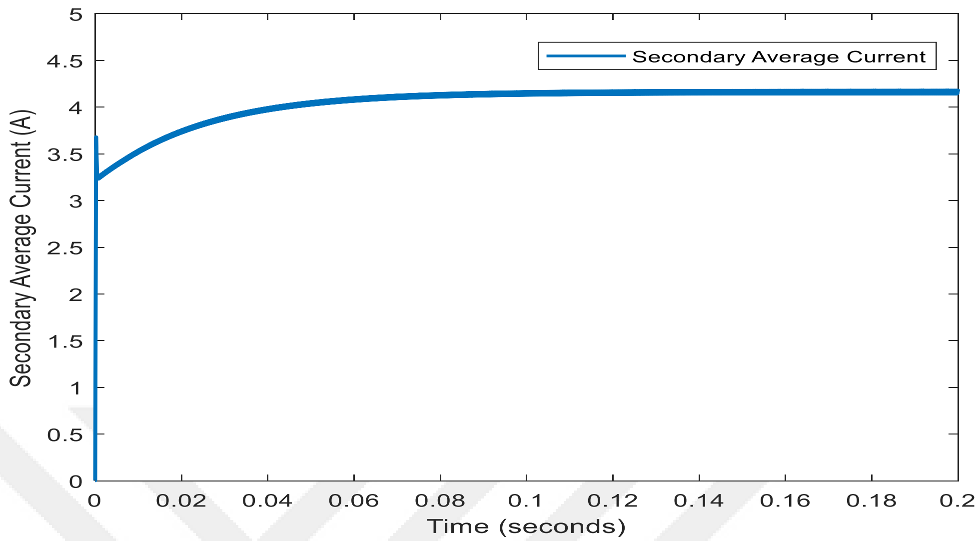

Figure 4.16. Flyback converter output current graph.

Losses in the flyback planar transformer are measured and the results are given in figures 4.17, 4.18 and 4.19 it seems that the results are closely identical with calculation results.

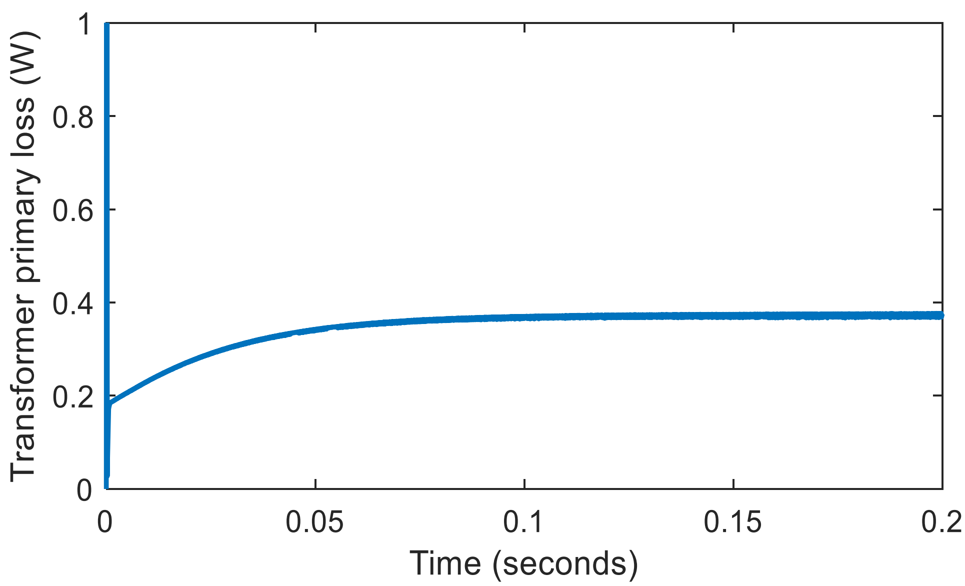

Figure 4.17. Flyback planar transformer primary loss graph.

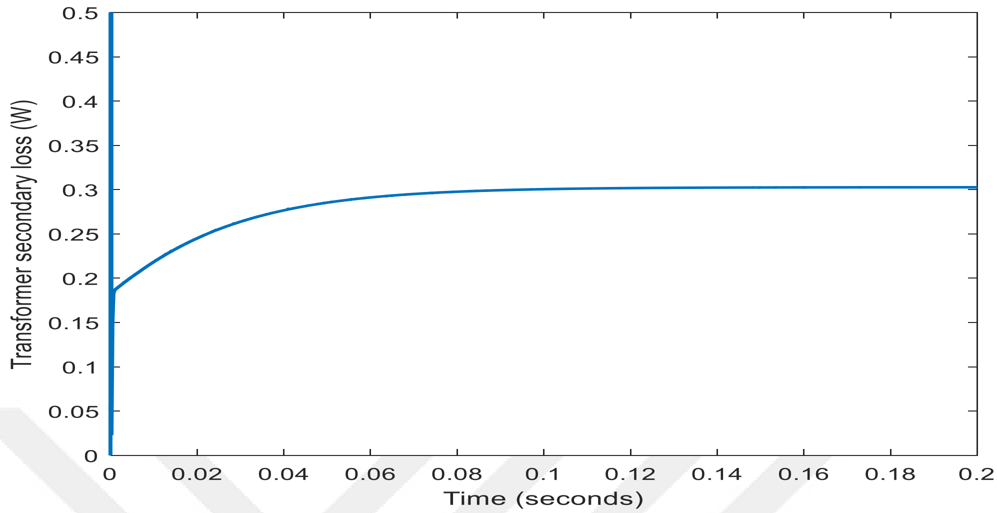

Figure 4.18. Flyback planar transformer secondary loss graph

.

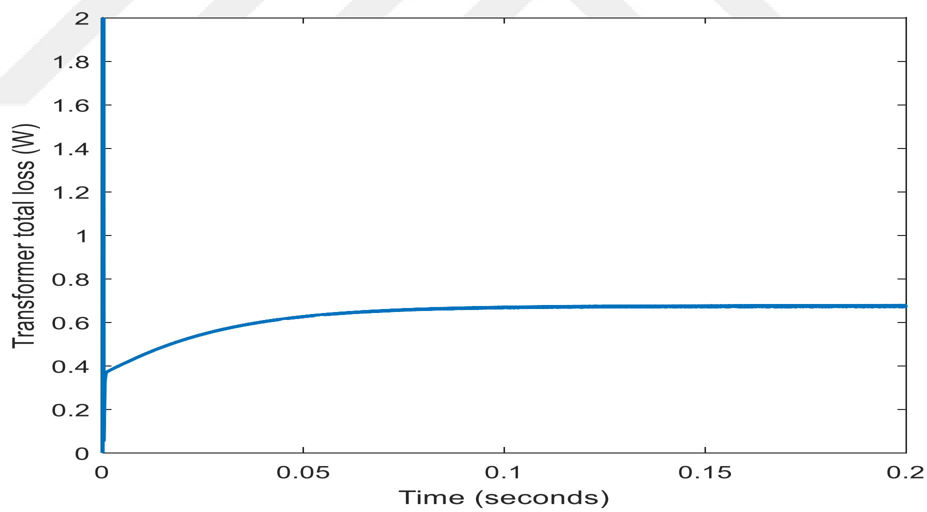

Figure 4.19. Flyback planar transformer total winding loss graph.

The flyback converter is operated under constant switching frequency of 50 kHz, 50 Watt output power the system efficiency obtained is more than 64%. The graph is given in (Figure. 4.20). According to (Taneri et al., 2019). If the variable switching frequency controlled flyback converter is more effective than the constant frequency operated flyback converter.

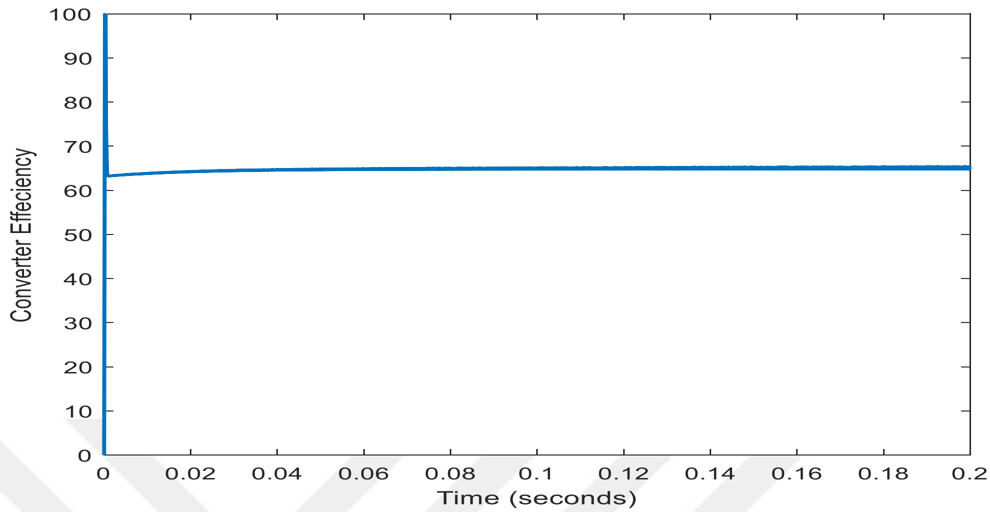

Figure 4.20. Flyback converter efficiency graph with constant frequency operation.

And the efficiency of the flyback transformer more than 98% is achieved at 50 kHz, 50 W output power the graph is given in (Figure 4.21.).

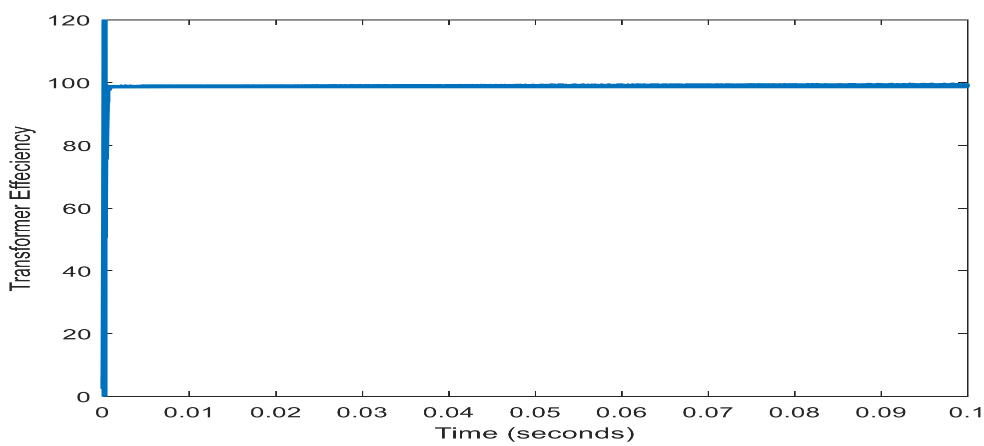

Figure 4.21. Transformer efficiency graph with constant frequency operation.

As seen in Figure 4.16, output current in a 50 W system is approximately 4.16 A since the output load is connected in parallel with the capacitor, the output current does not decrease to zero, as seen in Figure 4.8. Output voltage at this current remains constant at 12 volts.

5. CONCLUSION

In this thesis a detailed design methodology for flyback planar transformer with details on the printed circuit board (PCB) layer is presented and simulation for flyback converter with calculated parameters are performed employing PT has been designed, the transformer is an essential element of any power supply design, planar transformers have been shown to be more suitable over traditional wire wound transformer. Because the planar magnetic cores provides greater efficiency, super repeatability, smaller in size and lighter in weight. Planar transformers provide more options for modifying and utilizing parasitic parameters than conventional models, PCB transformers have been shown to be mostly used to miniaturize power converters and with thinner conductors, planar PCB transformers are also used to reduce high frequency effects, interleaving of the primary and secondary winding can greatly improve the distribution of current then it reduces leakage inductance and winding losses (AC losses) in PCB transformers due to the low proximity effects with low leakage inductance improving the coupling between the windings, this is difficult to explain with traditional methods of design.

In this thesis design of RCD clamping is presented, the effect of leakage inductance voltage was reduced using an RCD suppressor cell. An RCD snubber with a PWM flyback converter single switch was used to reduce the voltage spikes and power losses, with suppressor cell the voltage tension on the switch is minimized and circuit works properly

Results of the simulation are closely identical with the design calculation results, using the improved PT has been designed more than 98% transformer efficiency was obtained, the flyback converter is operated under constant switching frequency of 50 kHz, more than 64% system efficiency is achieved, and if the variable switching frequency controlled flyback converter is more effective than the constant frequency operated flyback converter.

Results of the simulation show that flyback converter is worked properly and recommended flyback converter is a best candidate for high-frequency isolated low power DC-DC converters.

REFERENCES

A. Razak, A. R., Rahman, A., Zhafran, M., Hashim, U., Hassan, S., 2016. A system conceptual design of flyback converter with split-planar transformer style for single photovoltaic module. ***ARPN Journal of Engineering and Applied Sciences***, **11**(18): 10888-10892.

Adams, J., 2001. Flyback Transformer Design for the IRIS40xx Series. ***www.irf.com***: 1-18.

Ahmad, J., Sonar, S., 2020. Design of flyback converter for DC-DC application. ***International Journal of Innovative Technology and Exploring Engineering (IJITEE),*** **9**(3): 2239-2243.

Al-Jubory, R. T., Al-Khafaf, H. M. A., 2008. An Algorithm for designing an inductor-transformer of a flyback converter with optimal copper/core loss ratio. ***The Iraqi Journal for Mechanical and Material Engineering, Special issue,*** **9**: 858-878.

Arshak, K.1 and Almukhtar, B., 2000. ***The Design and Development of a Novel Flyback Planar Transformer for High Frequency Switch Mode DC-DC Converter Applications***. International conference on microelectronic**,** 2: 14-17.

Barnwell, P. G., Jackson, T. J., 1991. ***High Frequency Transformers Using Thick Film Technology.*** 8th European hybrid microelectronics conference: 211-218.

Barnwell, P. G., Jackson, T. J., 1993. Low profile high frequency power supplies using thick film planar transformers. ***EPE***: 93-97.

Butler, P. A., 2001. ***Designing with Planar Ferrite Cores***. Magnetics. Technical bulletin: 1-12.

Carsten, B. W., 2001. ***The Low Leakage Inductance of Planar Transformers***. Applied power electronics conference and exposition sixteenth annual Ieee, 2: 1184-1188

Chen, R. G., Strydom, J. T., van Wyk, J. D., 2003. Design of planar integrated passive module for zero-voltage-switched asymmetrical half-bridge PWM converter. ***IEEE Trans. on Ind. Appl.***, **39**(36): 1648-1655.

Chen, W., Yan, Y., Hu, Y., Lu, Q., 2003. Model and design of PCB parallel winding for planar transformer. ***IEEE Transactions on Magnetics***, **39**(5): 3202-3204.

Choi, H. S., 2003. Design guidelines for off-line flyback converters using fairchild power switch (FPS). ***www.onsemi.com***: 1-19.

Cove, S. R., Ordonez, M., Quaicoe, J. E., 2010. ***Modeling of Planar Transformer Parasitics using Design of Experiment Methodology***. 23rd Canadian conference on electrical and computer engineering, (CCECE): 1-5.

Dai, N., Lotfi, A. W., Skutt, G., Tabisz, W., Lee, F. C., 1994. A comparative study of high frequency low profile planar transformer technologies. ***IEEE Apec.,*** **4**: 153-161.

Dekker, M., 2004. Planar transformers. ***https://www.worldcat.org/title/transformer-and-inductor-design-handbook/oclc/54994421***: 1-19.

Derkaoui, M., Hamid, A., Lebey, T., Melati, R., 2013. Design and modeling of an integrated microtransformer in a flyback converter. ***Telkomnika***, **11**(4): 669-682.

Dixon, L., 2007. ***Designing Planar Magnetics***. Texas instruments

Doebbelin, R., Herms, R., Teichert, C., Schaetzing, W., Lindemann, A., 2007. ***Analysis Methods and Design of Transformers with Low Leakage Inductance for Pulsed***

Power Applications. In proceedings of the European conference on power electronics and applications: 1–7.

Ebert, C. L., 2008. ***Design of the Planar Magnetic Device used in Switching Power Supply Aiming Reduction of Power Losses***. Ph.D thesis. Universidade federal de Santa Catarina.

Estrov, A., 1986. Power transformer design for 1MHz resonant converter. ***High Frequency Power Conversion Proceeding***s, **7**: 36-54.

Ferreira, J., 1994. Improved analytical modeling of conductive losses in magnetic components. ***IEEE Trans. on Power Electron***, **9**(1): 127-131.

Design of Planar Power Transformers. Ferroxcube yageo company: 1-15

Ferroxcube, D. B., 2013. ***Soft Ferrites and Accessories***. Taipei, Taiwan.

Fu Keung, W., 2004. ***High Frequency Transformer for Switching Mode Power Supplies***. Ph.D thesis. Griffith university, Brisbane, Australia.

Gradski, P. M., Lee, F. C., 1988. Design of high frequency hybrid power transformer. ***IEEE Apec., 2***: 183-191.

Gunewardena, T. R., 1997. ***Manufacturing Design Considerations for Planar Magnetics, Proceedings***. Electrical insulation conference and electrical manufacturing and coil winding conference: 309-311

Gurusamy, V., 2018. ***Design and Analysis of Integrated Planar Transformer for LLc Converter***. Master thesis. University of Texas, Dallas.

Huljak, R. J., Thottuvelil, V. J., Marsh, A. J., Miller, B. A., 2000. Where are power supplies headed. ***IEEE Apec.,*** **5**: 10-17.

Hurley, W., Wölfle, W. H., Ebrary, I., Wiley, J., 2013. ***Transformers and Inductors for Power Electronics: Theory, Design and Applications***. John Wiley & Sons., Galway, Ireland.

Kasikowski, R., Gołaszewski, J., Więcek, B., Farrer, M., 2015. Thermal characterization of high-frequency flyback power transformer. ***Measurement Automation Monitoring,*** **61**(6): 237-241.

Kumar, N. V., Satpathy, S., Lakshminarasamma, N., 2016. Analysis and design methodology for planar transformer with low self-capacitance used in high voltage flyback charging circuit. ***IEEE.,*** **1**: 1-5.

Kumar, S., Shinde, T., Vasambekar, P., 2015. Engineering high permeability Mn-Zn and Ni-Zn ferrites. ***Int J Appl Ceram Technol.***, **12**: 851-859.

Li, J., Hu, C., Pang, X., 2009. ***Analysis of the Leakage Inductance of Planar Transformer***. 9th International conference on electronic measurement & instruments, ICEMI: 273-276.

Li, J., Shi, Y., Niu, Z., Zhou, D., 2002. Modeling, Simulation and Optimization Design of PCB Planar Transformer: 1736-1739.

Lu, H. Y., Zhu, J. G., Hui, S. Y. R., 2003. Experimental determination of stray capacitances in high frequency transformers. ***IEEE Trans. on Power Electron,*** **18**(5): 1105-1112.

Magambo, J. S., 2017. Planar magnetic components in more electric aircraft: review of technology and key parameters for DC–DC power electronic converter. ***IEEE Transactions on Transportation Electrification,*** **3**(4): 831-842.

Magambo, J. S. N. T., Bakri, R., Margueron, X., Moigne, P., Mahe, A., Guguen, S., Bensalah, T., 2018. Review of technology and key parameters for DC–DC power electronic converter. ***https://hal.archives-ouvertes.fr/hal-01886549***: 1-13.

Maswood, A. I., Song, L. K., 2003. Design aspects of planar and conventional SMPS transformer: a cost benefit analysis**.** ***IEEE Transactions on Industrial Electronics***, **50**(3): 571-577.

McLyman, W. T., McLyman, C. W. T., 2004. ***Transformer and Inductor Design Handbook***. Marcel Dekker., New York, NY, USA.

Miyan, H., Tavade, C. M., Deshpande, L. M., Prashanth, R. S., 2013. Design and implementation of high frequency transformer for SMPS based flyback DC-DC converter. ***International Journal of Engineering and Technology***, **4**(6): 494-499.

Mohan, N., Undeland, T. M., Robbins, W. P., 2003. ***Power Electronics Converters, Applications, and Design***. John Wiley & Sons., New York, NY, USA.

Nan, X., Sullivan, C. R., 2003. An improved calculation of proximity-effect loss in high-frequency windings of round conductors. ***IEEE pesc***: 853-860.

Ngo, K. D., Lai, R. S., 1992. Effect of height on power density in spiral-wound power-pot-core transformers. ***. IEEE Trans. Power Elec.***, **7**(3): 352-367.

Nozari, F., 2011. Selection of snubbers and clamps to optimize the design of transistor switching converters. Industry Applications, ***IEEE Transactions.***, **2**: 513-523.

Oosterom, J. V., 2012. ***Auxiliary Power Supply for HISPEM***. Master thesis. Delft university of technology.

Ouyang, Z., Andersen, M. A. E., 2014. Overview of planar magnetic technology fundamental properties. ***IEEE Trans. Power Electron***, **29**(9): 4888-4900.

Ouyang, Z., 2011. ***Advances in Planar and Integrated-Magnetics***. Ph.D thesis. Danish technical university.

Ouyang, Z. W., Thomsen, O. C., Andersen, M. A. E., 2012. Optimal design and tradeoff analysis of planar transformer in high-power DC–DC converters**,** ***IEEE Transactions on Industrial Electronics***, **59**(7): 2800-2810.

Ouyang, Z. W., Thomsen, O. C., Andersen, M. A. E., 2009. The analysis and comparison of leakage inductance in different winding arrangements for planar transformer. ***IEEE Peds.,*** **6**: 1143-1148.

Philip. M. C., 1997. ***Planar E Cores***. Application note, Netherlands.

Prieto, R., Garcia, O., Asensi, R., Cobos, J. A., Uceda, J., 1996. Optimizing the performance of planar transformers. ***IEEE Apec.***, **1**: 415-421.

Prieto, R., Cobos, J. A., Garcia, O., Asensi, R., Uceda, J., 1996. ***Optimizing the Winding Strategy of the Transformer in a Flyback Converter.*** Power electronics specialists conference PESC '96 record 27th annual Ieee, 2: 1456-1462.

Quinn, C., Rinne, K., O'Donnell, T., Duffy, M., Mathuna, C. O., 2001. A review of planar magnetic techniques and technologies. ***IEEE Apec.,*** **2**: 1175-1183.

Quirke, M. T., Barret, J. J., Hayes, M., 1992. Planar magnetic component technology- a review. ***IEEE Trans Comp. Hybrids, and Man.,*** **7*:*** 884-892.

Ramachandran, R., 2016. ***Ultra-high Efficiency DC-DC Converter using GaN Devices***. Ph.D thesis. University of Southern Denmark.

Rascon, M., Ara, J., Madsen, R., Navas, J., Perez, M., San Miguel, F., 2001. Thermal analysis and modelling of planar magnetic components. ***IEEE Apec.***, **1**: 97-101.

Ropoteanu, C., Codreanu, N. D., Ionescu, C., 2016. ***Thermal Investigation of a Planar Core Power Transformer***. Proc. 39th int. spring seminar electron. technol. (ISSE): 112-115.

Ropoteanu, C., Svasta, P., Ionescu, C., 2017. A study of losses in planar transformers with different layer structure. ***IEEE23rd International Symposium for Design and Technology in Electronic Packaging*** **(SIITME)., 5**: 255-258.

Roshen, W. A., 2007. High-frequency tunneling magnetic loss in soft ferrites. ***IEEE Transactions on Magnetics***, **43**(3): 968-973.

Saket, M. A., Ordonez, M., Shafiei, N., 2017. Planar transformers with near zero common mode noise for flyback and forward converters. ***IEEE Transactions on Power Electronics.,*** **9**: 1-18.

Saket, M. A., Shafiei, A., Ordonez, M., 2017. LLC converters with planar transformers: issues and mitigation. ***IEEE Transactions on Power Electronics***, **32**(6): 4524-4542.

Sharafat Ali, M. A., Mehmood, K. K., Kim, C. H., 2017. ***Transient and Steady-State Analysis of Flyback Converter with Non-Dissipative LC Snubber***. International conference on power systems transients (IPST) in seoul, republic of korea: 1-7.

Skutt, G., Lee, F. C., Ridley, R., Nicol, D., 1994. Leakage inductance and termination effects in a high-power planar magnetic structure. ***IEEE Apec.,*** **2**: 295-301**.**

Špánik, P., Feo, I., Kácsor, G., 2003. Using planar transformers in soft switching dc/dc power converters. ***Electrotechnical Research and Projecting Institute****: 59-65.*

Taneri, M. C., Genc, N., Mamizadeh, A., 2019. ***Analyzing and Comparing of Variable and Constant Switching Frequency Flyback DC-DC Converter.*** The 4th international conference on power electronics and their applications (ICPEA): 1-5.

Tria, L. A. R., 2017. ***Modelling and Design of Planar PCB Transformers for High-frequency DC-DC Converters***. Ph.D thesis. University of new South Wales.

Venkatanarayanan, A., 2019. ***High Frequency LTCC based Planar Transformer***. Master thesis. University of Arkansas, Fayetteville.

Wallace, K., 1982. Multiple output planar transformer. ***IBM Technical Disclosure Bulletin***, **2**4(8): 523-532.

Xiao, S., 2004. ***Planar Magnetics Design for Low-Voltage Dc-Dc Converters***. Master thesis, university of Central Florida.

Zhang, J., Ouyang, Z., Duffy, M., Andersen, M. A. E., Hurley, W. G., 2013. Leakage inductance calculation for planar transformers with a magnetic shunt. ***IEEE.,*** **4**: 1-6.

Zhou, H., 1997. ***Magnetics Design for High Current Low Voltage Dc/Dc Converter***. Ph.D thesis. Xi'an Jiaotong university.

EXTENDED TURKISH SUMMARY
(GENİŞLETİLMİŞ TÜRKÇE ÖZET)

DÜZLEMSEL TİP FLYBACK TRANSFORMATÖR TASARIMI VE UYGULAMASI

MUSTAFA, Bestoon Ahmed
Yüksek Lisans Tezi, Elektrik Elektronik Mühendisliği Bölümü
Danışman: Dr. Öğr. Üyesi Ali MAMIZADEH
Şubat 2021, 99 sayfa

ÖZ

Flyback dönüştürücüler, kullanım kolaylığı ve ihtiyaç duydukları az sayıda devre elemanlarından dolayı giderek daha popüler hale gelmektedirler. Flyback dönüştürücülerin tasarımında karşılaşılan temel zorluklardan biri, dönüştürücünün çalışması için hayati önem taşıyan düzlemsel transformatörün tasarımıdır. Transformatör, anahtarlama elemanı iletim halinde olduğunda birincil sargıda enerji depolar, kapalı durumda olduğunda ise depolanan enerji ikincil sargıya aktarılır.

Düzlemsel transformatörün en önemli kısmı, faklı şekilleri ve ebatları olan nüvesidir. Optimize edilmiş düzlemsel bir nüve, benzer özelliklere sahip geleneksel bir nüveye kıyasla daha iyi özellikler sergiler. Düzlemsel trafonun sargılarında farklı konfigürasyonlar mevcuttur ve optimum konfigürasyon ile transformatör kayıpları verimli bir şekilde azaltılabilir.

Manyetik bileşenler için, yüksek frekanslarda çalışma, yüzeysel ve yakınlık etkilerinden kaynaklanan iletken kayıplarını artırır. Düzlemsel transformatörlerin baskılı devre kartlarında (PCB) kullanılması bu sorunu hafifletebilir. Daha geniş yüzey alanlarına sahip düzlemsel transformatörler ayrıca geleneksel sargılı manyetik nüveden daha iyi termal performans sağlar. Katmanların düzlemsel transformatördeki en etkili uygulaması, her iki sargıyı serpiştirmektir. Birincil ve ikincil sargının serpiştirilmesi, akımın dağıtımını büyük ölçüde geliştirebilir, böylece katmanlar arasında akan girdap akımlarının neden olduğu kaçak manyetik akı etkili bir şekilde iptal edilebilir, bu da düşük kaçak endüktanslı düşük yakınlık etkileri nedeniyle, sargılar arasındaki bağlantıyı iyileştirerek PCB

transformatörlerinde kaçak endüktansı ve AC sargı kayıplarını azaltacaktır. Bu durumu geleneksel tasarım yöntemleriyle açıklamak zordur. Bu tez çalışmasında, Flyback düzlemsel transformatör (DT) tasarımını için gerekli olan temel denklemler ve Snubber RCD devresinin detaylı analiz sunulduktan sonra 50 W güce sahip Flyback DT tasarımı yapılmıştır. Yapılan tasarımın, MATLAB/Simulink ortamında benzetim çalışmaları gerçekleştirilmiştir. Yapılan benzetim çalışmalarının sonucunda önerilen topolojinin verimini %98 'ün üzerinde olduğu görülmüştür.

Anahtar Kelimeler: Düzlemsel trafo (DT), Flyback dönüştürücü, Trafo kayıpları.

1. GİRİŞ

Düşük maliyetleri ve kullanım kolaylığına sahip olan Flyback dönüştürücüler, düşük güçlü uygulamalarda daha popüler hale gelmektedir. Bu dönüştürücülerin tasarımını ve çalışmasını kontrol eden iki ana faktör mevcuttur; birincisi, statik elektrik anahtarı için darbeleri (modülasyon teknikleri) üreten kontrol devresi ve ikincisi, düzlemsel transformatör tasarımıdır. Bu dönüştürücüler için indüktör-transformatör, anahtarın iletimde ve kesimde olduğu süreçte önemli bir rol oynar. Enerji işleme kapasitesi, bu dönüştürücülerin performans davranışında belirleyici bir faktördür, bu nedenle, indüktör-transformatörün tasarımı, dönüştürücünün genel tasarımının aktif bir parçasıdır. (Al-Jubory ve Al-Khafaf., 2008).

Günümüzde, anahtarlama yapmak için kullanılan yüksek frekans temelli uygulamalar daha popüler hale gelmiştir. Yüksek frekanslı transformatör uygulamalarında, yüksek güç yoğunlukları için faydalı olacak daha küçük boyutlara elde edilebilir. Yüksek frekanslı anahtarlama işlemleri için geleneksel tel sargılı manyetik malzemeler uygun olamadığı için düzlemsel manyetik nüve teknolojisine geçiş yapılmıştır (Venkatanarayanan., 2019). Düzlemsel manyetikler, geleneksel tel sargılı manyetiklere kıyasla daha küçük boyutta olması ve tasarım kolaylığının yanında daha yüksek performansa sahip olmasının nedeni sargıların tekrarlanabilir olmasıdır (Rascon ve ark, 2001).

Düzlemsel manyetik nüve bileşeninin boyutu, yüksekliği (z-ekseni) daha küçüktür ve geleneksel manyetik nüve bileşeninden daha fazla yüzey alanına sahiptir. Düzlemsel sargılar z-ekseninde üst üste istiflenirken, geleneksel sargılarda ise düşük frekanslı güç transformatörüne benzer bir şekilde nüve etrafına sarılır. Nüve geometrisi ve sargısındaki bu farklılıklar, güç yoğunluğu, üretim kolaylığı ve manyetik cihazın parametrelerinin tekrarlanabilirliği gibi birçok faktörde geleneksel teknolojiye göre üstünlük sağlar.

Bu tezde düzlemsel transformatör tasarım konuları, PCB üzerinde sargı tasarımı, nüve seçimleri, sargı düzenlemeleri, Flyback DT için temel denklemler sunulmakta ve birincil ve ikincil sargı özelliklerinin hesaplanması yapılmaktadır. Bakır ve nüve kayıplarında kayıp mekanizması dahil olmak üzere, verimlilik, hava boşluğu uzunluğu, nüvenin her iki tarafındaki dönüş sayısı gösterilmektedir. Geliştirilmiş DT yapısının kullanıldığı 50 W'lık Flyback dönüştürücü devre için benzetim çalışmaları yapılmış ve tartışılmıştır. Yapılan çalışmalar sonucunda, %98'ün üzerinde verime sahip tasarımı gerçekleştirilmiştir

2. MATERYAL VE YÖNTEM

Bu tez çalışmasında hem DT hem de DT'li Flyback dönüştürücü tasarımı ve benzetim çalışmaları yapıldı. Yapılan çalışmanın ilk kısmını; DT yapısı, özellikleri, malzemeleri ve Flyback dönüştürücünün anahtarlama elemanının iletimde ve kesimde olma durumunun yanında RCD snubber'ın tasarımı ve bunların teorik altyapısından meydana gelmektedir. Tasarımı gerçekleştirilen sistemin benzetim çalışmaları MATLAB/Simulink ortamında gerçekleştirildi.

Düzlemsel bir transformatörün temel yapısı, geleneksel transformatörünkine çok benzer. Transformatördeki temel çalışması mantığı DT için de geçerli olduğundan, yapıları ve bileşenleri bakımından klasik ve düzlemsel transformatörler oldukça benzer hale gelmektedir. Klasik bir transformatörde olduğu gibi DT'de de nüve, sargılar ve yalıtım vardır. Nüve, biri üstte diğeri altta olmak üzere iki yarımdan oluşabilir. DT nüveleri çoğunlukla Ferroxcube tarafından üretilmektedir (Ferroxcube., 2013). Muhtemelen en popüler olanı düzlemsel EE ve EPLT nüveleridir. Bu nüve yarımlarının arasına sargılar yerleştirilir. Sargılar, Litz teli yerine baskılı devre kartının (PCB) üzerinden tasarlanmıştır. Bir PCB sargıları, bakır kaplı bir PCB tarafından oluşturulur. İki taraflı levhalar için normalde 1 oz – 2 oz kalınlığında bakır kullanılır. Bu, katmanların çok katmanlı bir sarıma kolayca bağlanmasına izin verir ve bu durum klasik bir transformatörde yapılması zor olan sargıların kolay serpiştirilme işini oldukça kolaylaştırır. PCB Sargıları şekil (2.1) 'de gösterilmiştir. PCB'nin boyutları, seçtiğimiz trafo nüve boyutlarına göre değişir. Sargılar arasında da izolasyon sağlanmıştır (Venkatanarayanan., 2019)

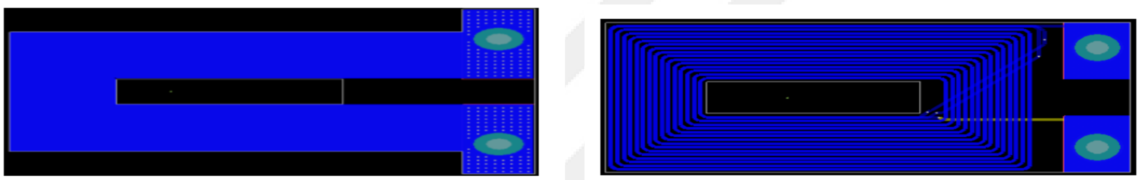

Şekil 2.1 a) Yüksek akım ve b) alçak için PCB sargıları.

DT'nin en önemli özelliklerinden biri sahip olduğu küçük ebattır. Bu özellik, yerleşik dönüştürücülerde DT'lerin kullanımını neredeyse gerekli kılar. Küçük ebat (düşük profil) terimi genellikle DT'leri tanımlamak için kullanılır. Düşük profilli olan DT'ler, güç kaynaklarının minyatürleşmesine katkıda bulunur. DT bileşenin yüksekliği, eşdeğer tel sargılı bileşeninden %25-50 daha azdır (Ouyang ve Andersen., 2014). Bu özellik onları, hacim ve ağırlığın önemli olduğu uygulamalarda cazip kılar. DT, azaltılmış kübik hacme sahip daha fazla yüzey alanı sayesinde geleneksel yapılara göre düşük profil yapısına sahiptir. Bu, daha yüksek hacimsel verimlilik sağlar. Daha önce belirtildiği gibi, DT'ler, sahip oldukları düşük profil nüve yapıları, transformatörün hacimsel olarak daha etkili bir şekilde kullanılmasına imkan sağlamanın yanında daha yüksek güç yoğunluğunun elde edilebilmesi için daha yüksek frekanslarda anahtarlama yapılan uygulamaların da temel elemanı olmuştur.

DT'lerin bir başka avantajı, hacim oranı nedeniyle sahip oldukları daha büyük yüzey alanı sayesinde soğutucu ile temas için daha fazla alanı sağlar ve böylece termal performans geliştirilmiş olur. Bu, geleneksel nüvelere göre düzlemsel nüveler için belirtilen daha küçük termal direnç değerinde demektir (Philip., 1997).

3. BULGULAR VE TARTIŞMA

Bu tez kapsamında tasarlanan transformatörün özellikleri aşağıda verilmiştir. Giriş voltajı (Vin_{min}) 311 Vdc, Çıkış voltajı (V_o) 12 Vdc, anahtarın maksimum görev çarpanı (D_{max}) 0.3, çalışma frekansı (F_s) 50 KHz 'de sabit ve çıkış gücü (P_o) 50 W'tır.

İlk önce tablo 3.1'de listelenen değerleri hesapladı

B_{peak} = 0,218 T ve tahmini verim Ƞ =% 96, ΔT = 40 ° C

Tablo 3.1 Flyback düzlemsel trafo tasarımı için hesaplanan değerler

N_p	n	N_s	I_{ppeak}	L_{pri}	G	I_{prms}	I_{sav}	I_{srms}	I_{speak}
44	11	4	1.12 A	0.001661 H	0.284mm	0.35417 A	4.167 A	5.848 A	12.32 A

B_{peak} (tepe akı yoğunluğu), n (Sarım Oranı), I_{av} (Birincil Ortalama Akım), G (Hava Boşluğu Uzunluğu), I_{prms} (Birincil rms Akımı), I_{srms} (İkincil Çıkış Akımı), I_{sav} (İkincil Ortalama Akım) ve Ƞ (Transformatörün Verimliliği).

Birincil tarafta (N_p) 44 ve ikincil tarafta (N_s) 4 sarım mevcuttur. E-PLT38 nüve kombinasyonları en uygun seçenek gibi görünüyor. Bu tasarımda 3C97 Ferroxcube power ferrit Core malzemesi ile E-PLT38 çekirdek kombinasyonu kullanılmıştır.

Katman başına dönüş sayısı ve dönüşler arasındaki boşluk sırasıyla N ve sp sembolleri ile belirtilmiştir. Daha sonra mevcut bir sarma genişliği b_{wi} için, iz genişliği w_{track} denklem (3.1) ile hesaplanabilir.

$$\mathrm{w}_{track} = \frac{[\mathrm{b}_{wa} - (\mathrm{N} + 1).\mathrm{sp}]}{\mathrm{N}} \tag{3.1}$$

Akımların ürettiği ısıya bağlı olarak 35 veya 70 µm bakır tabakalar arasından seçim yapmak mümkündür. Şebeke yalıtımı için birincil ve ikincil katmanlar arasında 400 µm'lik bir mesafe gereklidir. Şebeke yalıtımı gerekmiyorsa, sargı katmanları arasında 200 µm'lik bir mesafe yeterlidir. Ek olarak, PCB'nin üstünde ve altında yaklaşık 50 µm'lik bir lehim maskesi tabakası düşünülmelidir. EPLT-38 çekirdeklerinin mevcut sarım genişliği 11.315 mm'dir

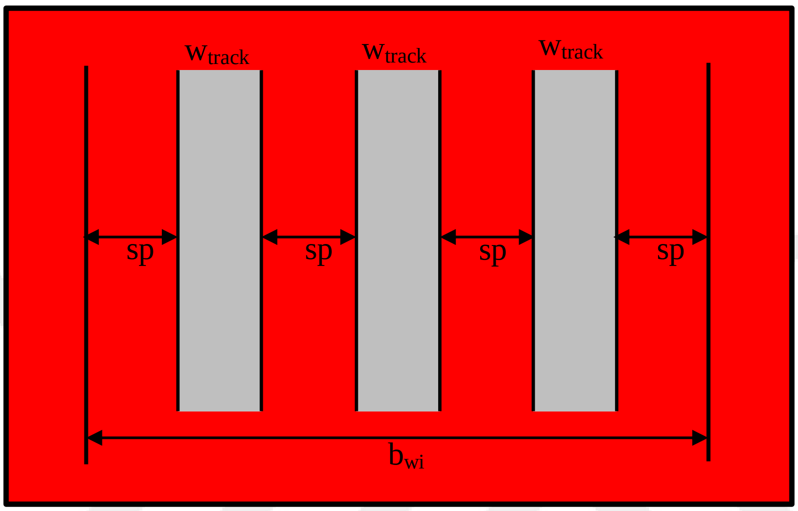

Şekil 3.1. İz genişliği w_{track} ,aralığı sp ve sarma genişliği $b_{wi.}$

Bu nedenle, her biri 11 tur içeren 4 katlı birincil sargı için seçim yapılır. Çok katmanlı PCB'deki daha düşük katman sayısı, maliyet fiyatını düşürecektir.

Birincil sargı dönüşleri için iz genişlikleri denklem (3.1) 'e göre hesaplanır ve yaklaşık 701.36 um'dir. Bu iz genişliği, 0,35417 A birincil RMS akımı kadar aşırı ısınmaya neden olmaz. Parçalar arasındaki boşluk = 300 µm'dir. İkincil sargı için her biri 1 dönüşlü 4 katman seçerken ikincil sargı için iz genişliği 10.715 mm olarak hesaplanır, şebeke yalıtımı dahil. 5.848 A olarak hesaplanan ikincil RMS akımını kullanarak sıcaklık artışı $\Delta T = 40\ °C$ olan 70 µm kalınlıktaki katman tasarımını için seçilen hatların genişliği 1750 µm den daha büyük olmalıdır. Bu nedenle, birincil sargı için her biri 11 dönüşlü 4 katman ve ikincil sargı için 1 dönüşlü 4 katman kullanılmaktadır.

Bakır (Cu) yolların kalınlığı 70 µm olan bu 8 katmanlı P-S-P-S-P-S-P-S tasarımı, özelliklerine göre çalışmalıdır. Baskılı devre kartının nominal kalınlığı yaklaşık 3460 µm olacaktır, bu da standart düzlemsel E-PLT38 kombinasyonunun kullanabileceği anlamına gelir. Ve sarma tabakası düzenlemesinde yukarı ve aşağı yarım birincil tabaka kullanılıyorsa. Bu, üst katmanı alt katmanla paralel olarak ve ardından birincil katmanın diğer dönüşleriyle seri olarak oluşturan geliştirilmiş bir serpiştirme düzenlemesi olan 0.5P-S-P-S-P-S-P-S-0.5P'yi temsil eder, böylece MMK oranı (m) düşürülebilir. Baskılı devre kartının nominal kalınlığı yaklaşık 3930 µm olacaktır, bu da standart düzlemsel E-PLT38 kombinasyonunu 4.22 mm sarım penceresi ile kullanabileceği anlamına gelir, bu onun sarma penceresi için uygun bir çözümdür.

Bu tezde, Flyback dönüştürücü için DT tasarlanmıştır, önerilen DT'li Flyback dönüştürücü devresi, 50 kHz' lik sabit anahtarlama frekansı için benzetim çalışmaları yapılmıştır, MATLAB/Simulink ortamında .

Devrenin çalışma çıkış voltajı, çıkış akımı, trafo verimi ve dönüştürücü verimi grafiği Şekil 3.2'de verilmiştir.

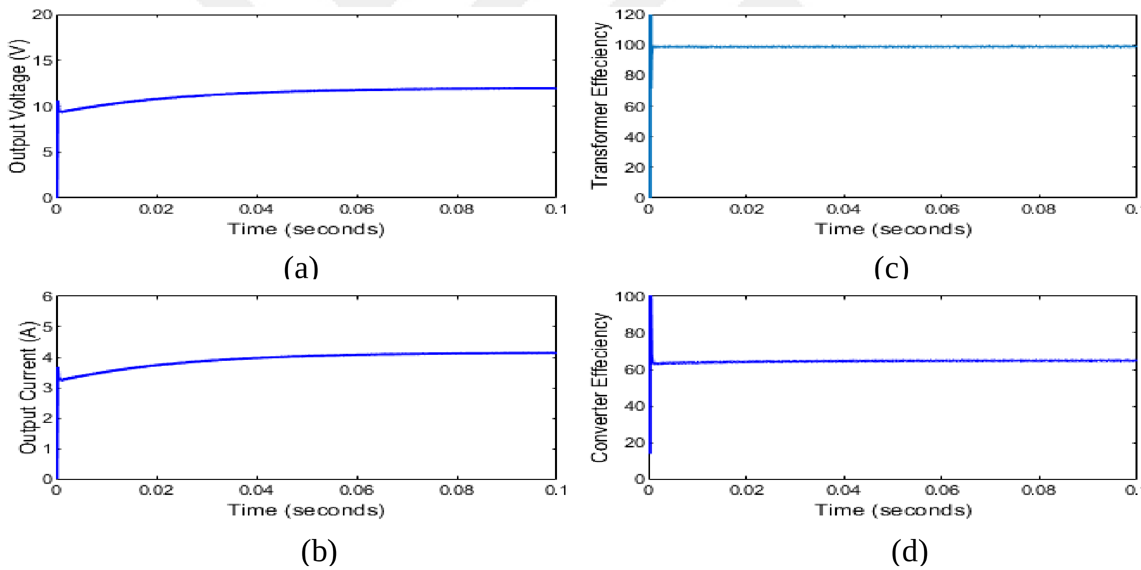

Şekil 3.2. (a) çıkış voltajı, (b) çıkış akımı, (c) trafo verimi ve (d) dönüştürücü verimlilik grafiği.

Şekil 3.2'de görüldüğü gibi. 50W'lık bir sistemde çıkış akımı yaklaşık olarak 4,16 A'dır. Kapasitör çıkış yüküne paralel olduğu için çıkış akımı sıfıra düşmez. Bu akımdaki çıkış voltajı 12 voltta sabit kalır.

Flyback dönüştürücü 50 KHZ'lik sabit anahtarlama frekansı altında çalıştırılır, sistemin verimliliği% 64'ün üzerindedir ve% 98'ün üzerinde trafo verimliliği elde edilir.

4. SONUÇ

Bu tezde, PCB katmanındaki detaylarla birlikte DT'li Flyback için detaylı bir tasarım metodolojisi sunulmuş ve Flyback dönüştürücü için hesaplanan parametrelerle simülasyon çalışmaları yapıldı. Transformatör, herhangi bir güç kaynağı tasarımının önemli bir unsurudur. Düzlemsel transformatörlerin, geleneksel tel sargılı transformatörlere (klasik modeller) göre yumuşak anahtarlamalı güç kaynağı tasarımları için daha uygundur, çünkü DT daha fazla verimlilik, daha fazla güvenilirlik, Güç yoğunluğunda yüksek performans, süper tekrarlanabilirlik ve mükemmel ısı dağılımı sağlar. Boyut olarak daha küçük ve geleneksel bir transformatörün yaklaşık yarısı ağırlığından daha hafiftir. DT'ler, geleneksel modellere göre parazitik parametreleri değiştirilmesi ve kullanması için daha fazla seçenek sunar. PCB transformatörlerinin çoğunlukla güç dönüştürücülerini küçültmek için kullanıldığı gösterilmiştir ve daha ince iletkenlerle düzlemsel PCB transformatörleri de yüksek frekans etkilerini azaltmak için kullanılır. AC kayıplarının, yüksek frekans transformatörleri için nüvelerin tasarımında baskın bir rol oynadığı gösterilmiştir. Katmanların en etkili uygulaması, birincil ve ikincil katmanların "sandviç" olarak adlandırılan sırayla istiflenmesidir (Maswood ve Song., 2003). Birincil ve ikincil sargının serpiştirilmesi, akımın dağıtımını büyük ölçüde iyileştirebilir. Daha sonra, düşük kaçak endüktans ile düşük yakınlık etkileri nedeniyle PCB transformatörlerinde kaçak endüktansı ve sargı kayıplarını (AC kayıpları) azaltır ve sargılar arasındaki bağlantıyı iyileştirir. Bunu geleneksel tasarım yöntemleriyle açıklamak zordur.

Yapılan hesaplamalar sonucunda elde değerlere göre yapılan tasarımdan alınan benzetim sonuçları, hesaplamalara uygunluk göstermiştir. Tasarlanan DT'nin verimi %98 'in üzerinde olduğu görülmüştür. Sabit 50 kHz anahtarlama frekasına sahip DT'nin kullanıldığı Flyback dönüştürücü devresinin verimi ise %64 'ün üzerinde olduğu görülmüştür. (Taneri ve ark., 2019) tarafından yapılan çalışmada, değişken anahtarlama frekansı ile kontrol edilen Flyback dönüştürücünün verimi sabit frekanslıya göre daha verimliği olduğu gösterilmiştir. Elde edilen benzetim sonuçları, önerilen DT'li Flyback dönüştürücünün düzgün çalıştığını ve düşük güç uygulamalarına sahip yüksek frekanslı izole DC-DC dönüştürücüler için mükemmel bir aday olduğunu göstermiştir.

LIST OF APPENDIX

APPENDIX 1. Planar EE core

Cores	I_c (mm)	A_c (mm^2)	Volume (mm^3)	Height (mm)	Window width(mm)	Window Height(mm)
EE 14/3.5/5	20.7	14.3	300	7	4	4
E 14/3.5/5 PLT14/5/1.5	16.7	14.5	240	5	4	2
EE 18/4/10	24.3	39.3	960	8	5	4
E 18/4/10 PLT18/10/2	20.3	39.5	800	6	5	2
EE 22/6/16	32.5	78.3	2550	11.4	5.9	6.4
E 22/6/16 PLT22/16/2.5	26.1	78.5	2040	8.2	5.9	3.2
EE 32/6/20	41.4	130	5380	12.7	9.275	6.36
E 32/6/20 PLT32/20/3.2	35.1	130	4560	10.16	9.275	3.18
EE 38/8/25	52.4	194	10200	16.52	11.315	8.9
E 38/8/25 PLT38/25/3.8	43.7	194	8460	12.07	11.315	4.45
EE 43/10/28	66.1	229	13900	19	13.3	10.8
E 43/10/28 PLT43/28/4.1	50.4	229	11500	13.6	13.3	5.4
EE 58/11/38	80.6	308	24600	21	20.95	13
E 58/11/38 PLT58/38/4	67.7	310	20800	14.6	20.95	6.5
EE 64/10/50	79.9	519	40700	20.4	21.8	10.2
E 64/10/50 PLT64/50/5	69.7	519	35500	15.28	21.8	5.1

CURRICULUM VITAE

Bestoon Ahmed MUSTAFA was born in Erbil, Iraq in 1977. He completed his primary and secondary education in Erbil, Iraq. He started learning from Salahaddin University Bachelor of Engineering, Electrical Department in Erbil/Iraq and he graduated in 2001. With the rank 5 of 17. He is working as an electrical engineer in the directorate of electricity distribution in Erbil, Iraq. He started his graduated studies M.Sc. degree programme at Van Yüzüncü Yıl University Electrical and Electronics Engineering Department in 2019.

UNIVERSITY OF VAN YUZUNCU YIL
THE ISTITUTE OF NATURAL AND APPLIED SCIENCES
THESIS ORIGINALITY REPORT

Date: 06 / 02 / 2021

Thesis Title: **DESIGN AND APPLICATION OF PLANAR TYPE FLYBACK TRANSFORMER**

The title of the mentioned thesis, above having total 99 pages with cover page, introduction, main parts and conclusion, has been checked for originality by Turnitin computer program on the date of 13/1/2021 and its detected similar rate was 2% according to the following specified filtering

Originality report rules:

- Excluding the Cover page,
- Excluding the Thanks,
- Excluding the Contents,
- Excluding the Symbols and Abbreviations,
- Excluding the Materials and Methods
- Excluding the Bibliography,
- Excluding the Citations,
- Excluding the publications obtained from the thesis,
- Excluding the text parts less than 7 words (Limit match size to 7 words)

I read the Thesis Originality Report Guidelines of Yuzuncu Yil University for Obtaining and Using Similarity Rate for the thesis, and I declare the accuracy of the information I have given above and my thesis does not contain any plagiarism; otherwise I accept legal responsibility for any dispute arising in situations which are likely to be detected.

Sincerely yours,

Bestoon Ahmed MUSTAFA
06/02/2021

Name and Surname: Bestoon Ahmed MUSTAFA

Student ID#: 18910001408

Science: The Institute of Natural and Applied Sciences

Program: Electrical Electronics Engineering

Statute: M. Sc. X Ph.D. ☐

APPROVAL OF SUPERVISOR	**APPROVAL OF THE INSTITUTE**
SUITABLE	SUITABLE
Asst. Prof. Dr. Ali MAMIZADEH	
(Title, Name-Surname, Signature)	(Title, Name-Surname, Signature)